AD

USAAVLABS TECHNICAL REPORT 67-76

HIGH TEMPERATURE SENSORS FOR SMALL GAS TURBINES

By

A. Marshall Gaylord

William A. Compton

April 1968

U. S. ARMY AVIATION MATERIEL LABORATORIES
FORT EUSTIS, VIRGINIA

CONTRACT DA 44-177-AMC-380(T)

SOLAR DIVISION OF INTERNATIONAL HARVESTER COMPANY

SAN DIEGO, CALIFORNIA

Disclaimers

The findings in this report are not to be construed as an official Department of the Army position unless so designated by other authorized documents.

When Government drawings, specifications, or other data are used for any purpose other than in connection with a definitely related Government procurement operation, the United States Government thereby incurs no responsibility nor any obligation whatsoever; and the fact that the Government may have formulated, furnished, or in any way supplied the said drawings, specifications, or other data is not to be regarded by implication or otherwise as in any manner licensing the holder or any other person or corporation, or conveying any rights or permission, to manufacture, use, or sell any patented invention that may in any way be related thereto.

Trade names cited in this report do not constitute an official endorsement or approval of the use of such commercial hardware or software.

Disposition Instructions

Destroy this report when no longer needed. Do not return it to originator.

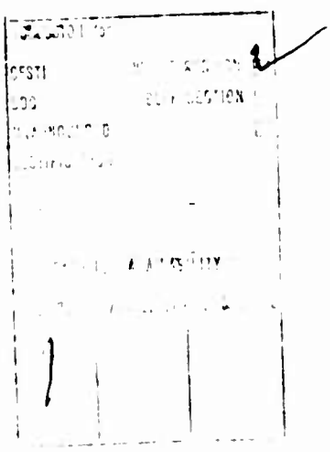

DEPARTMENT OF THE ARMY
U. S. ARMY AVIATION MATERIEL LABORATORIES
FORT EUSTIS, VIRGINIA 23604

This Command has reviewed this report and concurs in the conclusions contained herein. The findings and recommendations of this report will be used to guide future programs of temperature sensor development.

Task 1M121401D14416
Contract DA 44-177-AMC-380(T)
USAAVLABS Technical Report 67-76
April 1968

HIGH TEMPERATURE SENSORS FOR SMALL GAS TURBINES

Final Report

By

A. Marshall Gaylord
William A. Compton

Prepared by

Solar Division of International Harvester Company
2200 Pacific Highway
San Diego, California 92112

for

U. S. ARMY AVIATION MATERIEL LABORATORIES
FORT EUSTIS, VIRGINIA

ABSTRACT

This report describes an experimental program performed to generate technology on high temperature sensor concepts for small gas turbines. Major emphasis was placed on the definition of material systems needed for transducers with long life, good reliability, and fast response for sensing turbine inlet temperatures in the range of 2200° to 2500°F with transients to 3000°F. The technology related to three types of sensors was considered: thermocouples, resistive devices, and radiation pyrometers. Inherent material problems with resistive devices at temperatures above 1600°F limited the experimental program on this concept. Thermocouple and radiation sensors were studied extensively, resulting in several promising approaches to meet program goals.

Several material systems were identified and experimentally shown capable of sensing air temperatures at 2500°F with transients to 3000°F. Since thermocouples measure temperature at one point in the flow path, a large number of junctions are necessary to obtain proper averaging due to burner streaking (the T-56 uses 16 junctions). A method of determining the effect of gas blockage on engine cycle efficiency is presented and shown to be significant. A proposed protected thermocouple junction offers best reliability and durability, but has relatively slow response to changes in gas temperature. A suggested exposed junction has greatly improved response rate, however, the reliability and durability are much less than the protected junction.

Five commercial radiation pyrometers were evaluated and one concept chosen as having, by far, the greatest potential for application to turbine engines. Detailed experiments on environmental effects on all materials led to the design and purchase of a miniaturized model especially for this program. The sensor consists of a sapphire window, a quartz lens and a silicon p-n junction detector which must sight on an emissive body in the gas stream. Thus, hardware, rather than air temperature, is measured. The rotating buckets are chosen since they will register close to average temperature. The sensor tested demonstrated microsecond response, good accuracy, and good reliability as long as the environmental temperature for the silicon chip was kept below 250°F and the window was maintained clean. A unique gas-collimator lens (gcl) system was devised which acts as an interface between the turbine gas path and the sensor head window. An experimental gas-collimator lens operating on a simulated turbine rig was able to keep the sensor head window perfectly clean after many hours of operation interfaced with a high soot-laden gas stream.

Recommendations are included for continued development of three approaches which have potential value to the high temperature advanced gas turbines: the protected thermocouple junction which employs advanced high temperature material systems, including a TNV-7 coated tantalum alloy sheath, diffusion bonded to a W-Re junction; the bare PT-RN thermocouple, using in-series junctions, to give the fastest possible response rate; the radiation pyrometer, in conjunction with the gas-collimator lens devised to measure individual bucket temperatures.

TABLE OF CONTENTS

LIST OF ILLUSTRATIONS

LIST OF TABLES

LIST OF SYMBOLS

A	effective heat transfer area
C_D	drag coefficient
C_p	heat capacity at constant pressure
d	diameter
emf	electromotive force
g	gravitational constant
h	coefficient of heat transfer
J	mechanical equivalent of heat
K	thermal conductivity
M	Mach number
N_μ	Nusselt number
P	total pressure
p	static pressure
P_r	Pradtl number
Q	heat energy
q	dynamic pressure
r	recovery factor
T	stagnation temperature
t	free stream static temperature
t_{ad}	adiabatic temperature
t_g	gas temperature
t_{wl}	surface temperature
T_{ss}	steady state temperature

T_θ	temperature at time θ
V	gas velocity
v	volume
W	mass
α	isentropic index
γ	ratio of specific heats
Δ	recovery error ratio
Δ_t	instantaneous transient temperature error
ϵ	emissivity
μ	viscosity
σ	Stefan-Boltzmann constant
ρ	density
τ	time constant

INTRODUCTION

The gas temperature of most gas turbines is determined by inserting thermocouple probes at the turbine outlet. In most cases, it is possible to extrapolate from the turbine outlet to obtain turbine inlet temperature (TIT) with sufficient accuracy to operate the gas turbine. If extrapolation is not possible, calibration of the engine is used to measure the difference of turbine outlet and turbine inlet temperatures for subsequent control by measuring only the turbine outlet temperature.

When gas is measured at the turbine outlet, the temperature is averaged by the turbine wheel and is at the lowest possible temperature in the engine. Equilibrium temperature of the probe is not influenced by direct radiation from the burner flame and rarely exceeds 1400°F at the junction. In these systems, the extrapolated TIT is not used in a closed-loop control system, so response rate of the sensor is not critical.

Advanced gas turbines, however, bring about drastic changes to the above concept. Programs are under way to prove feasibility of turbine designs with inlet temperatures of 2300° to 2500°F. Since air cooling of the blades and vanes will be used, extrapolation from turbine outlet to TIT is not possible due to the mixing of cooling gases with turbine gas. The higher turbine inlet temperatures give greater specific power, thus less airflow for the same horsepower. Conventional temperature probes may cause excessive gas blockage in the smaller engines. In addition, control systems must employ direct sensing of critical temperatures for optimum performance and component protection. This can be accomplished only by measuring gas temperature at the TIT position, which introduces additional problems and requirements for consideration:

- Streaking or temperature maldistribution caused by burner hot spots necessitates the use of from 12 to 24 sensors to obtain the proper temperature averaging.
- Temperatures are much higher at the TIT position in the engine (2500°F with transients to 3000°F).
- Gas passages are the smallest inthe high temperature zone, meaning that blockage and pressure drop are critical.
- Temperature errors due to radiation are most severe at this position in the cycle. The probes can view the hot flame as well as the cold wall.
- At the TIT position, dynamic loads are higher than at any point in the hot gas cycle.

- The need to include direct sensing in the control system and instrument indications means that response rate, linearity and reliability become very critical factors.

- Particulate matter entrained in the gas stream is most severe at the TIT position.

To meet these requirements, a set of goals was established for a sensor transducer to measure the turbine inlet temperature of small gas turbines. They were as follows:

- The sensor must be capable of measuring average and/or individual temperatures of 2500°F with excursions up to 3000°F and transients of 2000°F per second in an atmosphere of air and/or gas at pressures up to 250 psia and gas velocities up to 700 ft/sec.

- The sensor must record the true gas temperature within ±15°F throughout the range from ambient to 3000°F.

- Response times of 10 milliseconds (for 90% of a step change in temperature) shall be the target for all sensors.

- The signal generated should be linear with temperature to simplify control problems.

- The sensor should be reliable, durable and rugged to withstand the stress of the high dynamic environment in the engine.

The foregoing suggests that sensing of such gases is a formidable problem. However, a number of approaches can be considered to effect a solution. The most direct approaches which were considered are:

- The thermocouple or thermoelectric type sensor, where a junction is projected into the gas stream. The junction approaches the temperature of the gas stream and yields a millivolt signal proportional to its temperature. Major problems include: oxidation resistance of materials up to 3000°F, selection of protective sheathing, electrical insulation and thermocouple materials which are stable up to these temperatures, and reduction of the response time.

- The resistive type sensor, where a conductor is projected into the gas stream. The conductor also approaches the temperature of the gas stream and exhibits a resistivity change proportional to temperature. Major problems are similar to the problems outlined for the thermocouple sensor.

- The radiation type sensor, where a nozzle vane or element submerged in the gas stream is viewed by an optical detector. The emissive power of the viewed part is proportional to temperature. Major problems include: sooting of the viewing lens or gas stream interface, and the design of an optical pyrometer rugged enough to operate in the gas turbine temperature and dynamic environment.

Each of these approaches has certain desirable features which make its consideration necessary for TIT sensing. A redefinition of the limitation of each of these proven concepts employing the most advanced materials system available today is necessary to meet the requirements of advanced gas turbine engines.

There are several second-generation temperature sensing methods, which were not a part of this program, that could have been considered. Probably the most popular concept of those not considered is the pure fluids system device. In this method, a fluid oscillator extracts turbine inlet gases and yields a frequency which is proportional to sonic velocity or square root of the absolute temperature of the gases in the resonant cavity of the oscillator. Many of the same problems outlined above must be solved for this method to be a practical candidate for temperature sensing.

This report outlines the results of the program conducted to advance the temperature transducer technology in the three areas mentioned specifically for small gas turbines. The program recognizes the temperature streaking which occurs at the turbine inlet and the need for multiple sensors to obtain proper averaging. The program also reviews the special considerations of gas flow blockage problems, unique with the 2 to 5 lb/sec flow gas turbines. Small sensor probes with fast response and minimum gas blockage were considered in the thermocouple task. Emphasis was placed on laboratory experiments that would yield data which would allow design of workable systems for sensing turbine inlet gases in the temperature ranges outlined. Emphasis was also placed on reviewing the potential of radiation sensors applied to small gas turbines.

The program concentrated on the transducer, that is, the element that actually produces a signal proportional to the measured temperature. The processing of this signal was not specifically dealt with except in general terms. The program was divided into three tasks, each one concentrated on one of the three transducers outlined above: thermoelectric, resistive, and radiation sensors. Resistive type sensors appear to offer the least potential for turbine application and received relatively little emphasis, although most of the work done on the materials problems of thermoelectric sensors is directly applicable to resistive devices.

TASK I
THERMOELECTRIC DEVICES

Thermoelectric devices (thermocouples) have many features that make them attractive as temperature sensors for small gas turbines. Among these are: nearly linear thermoelectric output versus temperature, small size, availability, simplicity, wide acceptance, and ease with which they may be integrated into engine controls. Placing the thermocouples at the turbine inlet, however, presents new problems that must be overcome in order to adapt the thermocouple to the new conditions and requirements. The thermocouple probe is immersed in the moving gas and an emf is produced proportional to the temperature of the hot junction, which is in equilibrium with the gas immediately surrounding the probe. To function properly, the probe must reach a temperature very nearly equal to the gas temperature. In addition, it must respond rapidly to a change in the gas temperature. The immersed probe is subjected to very high temperatures, oxidation, erosion, contamination, and mechanical loading. Designing a probe to be accurate and reliable over a long period of time under these conditions often is contrary to design criteria aimed at reducing response time.

Response rates are maximum for a thermocouple probe with an exposed hot junction. The exposed junction, however, is susceptible to reactions with the gas, contamination, erosion, and mechanical failure. The performance of the probe must not be affected by these conditions over the required lifetime. The reliability requirement is easily satisfied by using a junction surrounded by a protective sheathing. The rate of heat transfer through the sheathing and insulation, however, is reduced, slowing the response. Compromises and trade-offs have to be made between opposing requirements to enable a thermocouple probe to best fit a given application.

The possibility of using materials other than metallic materials for thermocouples has been extensively studied in both England and the United States. A comprehensive review of such materials is given in Reference (1), where a great many materials were reviewed for possible thermopile generator applications. Included in this study were: metals versus transition metal hydrides; metals versus refractory borides, carbides, nitrides and silicides; metals versus oxides and some semiconductor studies. In some cases, high Seebeck voltages were obtained, but they were mostly nonlinear. The most serious restriction in using nonmetallic thermoelectric pairs is the difficulty in fabricating small high-response thermocouples from hard, brittle materials. Also, the poor thermal shock resistance of many of these materials would probably result in early failure during transient engine operations.

Since alloy development for thermoelectric materials is such a broad field and is constantly being explored by thermocouple manufacturers, no new materials were developed during this program. Instead, emphasis was placed on currently available high-temperature (melting points greater than 3000°F) thermocouple materials

and the development of high-response thermocouples that will not be "short-lived" in the turbine inlet.

THERMODYNAMIC AND ANALYTICAL CONSIDERATIONS

Sensor Errors During Steady-State Conditions

The purpose of placing a temperature sensor or probe into a gas stream is to obtain a measurement of the total (stagnation) temperature of the gas. Neglecting the influence of read-out circuits and indicators, a sensor would be considered to be perfect if that part of the sensor which gives the measured effect (e.g., the hot junction of a thermocouple) were at all times equal in temperature to the stagnation temperature of the gas.

It is well known that when an object is immersed in a moving gas, thermal equilibrium will be obtained with some surface temperature other than that of the stagnation temperature of the gas. Figure 1 illustrates the temperature gradient in the gas film close to the surface of an immersed body. At great distances from the body surface, the temperature of the gas is called the free-stream static temperature.

As the surface is approached, the gas temperature increases because of reduction in velocity with consequent recovery of kinetic energy by conversion to heat. This "aerodynamic heating" effect will follow a curve of type 1 or 2 in Figure 1, depending upon the boundary conditions at the surface of the body.

In considering curve 2, which is the case of an ideal, perfectly insulated, non-radiating body, there is no heat transfer into or out of the body, and the surface temperature achieved is called the adiabatic temperature. It should be noted that even in this case the probe is not "perfect" as defined above, because the adiabatic temperature will always be less than the theoretical stagnation temperature of the gas. This is because, as the gas velocity reduces through the boundary layer, the gas heats up and loses heat by conduction, convection and radiation to cooler parts of the gas further away from the surface. These losses ensure that the adiabatic temperature, t_{ad}, is always less than the stagnation temperature T, and so a recovery factor, r, may be introduced, where

$$r = \frac{t_{ad} - t}{T - t} \qquad (1)$$

where t = the free-stream static temperature of the gas.

Since by definition

$$T = t + \frac{V^2}{2gJC_p}$$

then

$$t_{ad} = t + r\left(\frac{V^2}{2gJC_p}\right)$$

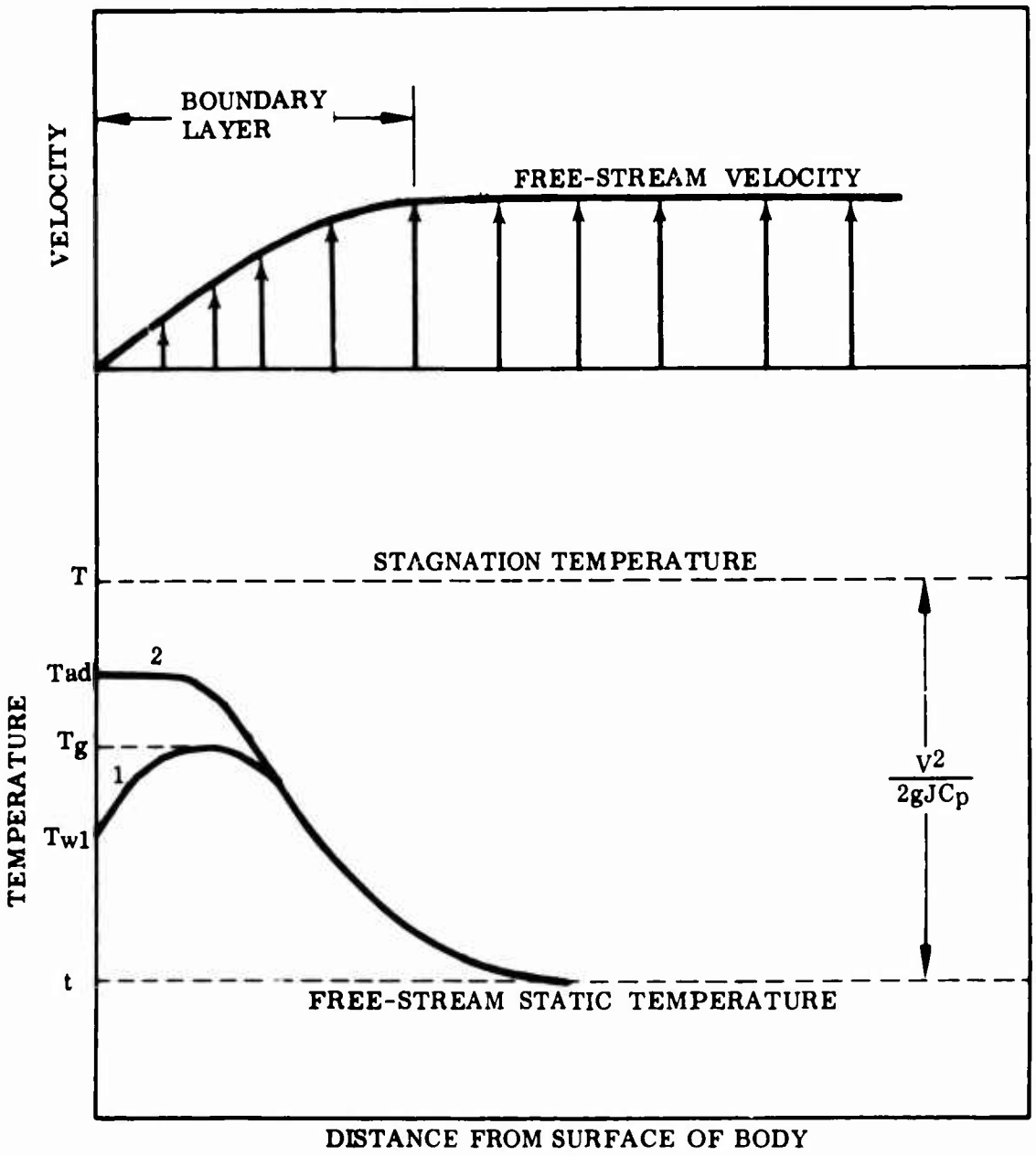

Figure 1. Temperature and Velocity Distribution Near an Immersed Body.

From this, it is clear that the recovery factor is that fraction of the kinetic energy of the gas which is recovered by conversion to heat at the surface of the immersed body.

The recovery error ratio Δ, given by

$$\Delta = \frac{T - t_{ad}}{T} \tag{2}$$

is more convenient than the recovery factor in the temperature sensor analysis. The relationship between the two is

$$\Delta = (1 - r) \frac{V^2}{2gJC_p T} \tag{3}$$

or

$$\Delta = \frac{(1 - r) \frac{\gamma - 1}{2} M^2}{1 + \frac{\gamma - 1}{2} M^2} \tag{4}$$

where M is the free-stream Mach number. This equation indicates that the recovery error tends to zero (even for quite low recovery factors) as the free-stream velocity reduces to zero.

For example, with a recovery factor of only 80%, the recovery error ratio (with $\gamma = 1.4$) is given in Table I for various Mach numbers.

TABLE I. RECOVERY ERROR RATIO AS A FUNCTION OF VARIOUS MACH NUMBERS

Mach No.	0.25	0.5	1.0	1.5
(%)	0.247	0.87	3.33	6.2

From this table it is apparent that recovery errors become significant only at Mach numbers greater than 0.3. The steady-state heat transfer characteristics of a real temperature probe may be best expressed in terms of the heat energy balance on the probe

$$\text{Input} = \text{Output}$$

$$Q_{GR} + Q_{CV} = Q_R + Q_{CD} \tag{5}$$

where the subscripts are

GR = radiation from gas to probe

CV = forced convection from gas to probe

R = radiation from probe to surroundings

CD = conduction from probe to surroundings

Generally, apart from gases rich in water vapor or carbon dioxide, the gas radiation component may be neglected, since it is small in comparison to other components. The steady-state energy balance reduces to

$$\text{Input} = \text{Output}$$

$$Q_{CV} = Q_R + Q_{CD} \tag{6}$$

In Figure 1, the curve of type 1 is produced under these conditions where the immersed body is gaining heat by convection from the gas (at some effective gas temperature, t_g, in the boundary layer) and losing heat by conduction and radiation to its surroundings. The resulting surface temperature, t_{w1}, is less than t_g, which in turn is less than t_{ad} and T. The combined error ratio in this case is

$$= \frac{\Delta T - t_{w1}}{T}$$

This is the common steady-state case of a temperature sensor. The temperature, t_{ad}, loses significance and equation (5) can be written

$$\Delta = \frac{T - t_g}{T} + \frac{t_g - t_{w1}}{T} \tag{7}$$

$$= \Delta_1 + \Delta_2$$

where Δ_1 is the recovery error ratio based on gas temperature and Δ_2 is the combined radiation and conduction error ratio.

In most probe designs, it is possible to make the conduction component negligible compared to the gas to probe convection and probe to surroundings radiation. Equilibrium conditions are then given by

$$Q_{CV} = Q_R \tag{8}$$

Substitution and expansion yields probe temperature (t_p) as a function of (true) gas temperature (t_g)

$$t_g - t_p = (t_p - t_s)\frac{\dot{n}_r}{h_c} \tag{9}$$

where the previously unidentified variables are

t_s = temperature of surroundings

h_r = coefficient of heat transfer (radiation)

h_c = coefficient of convective heat transfer

The radiation conductance factor for this particular configuration reduces to

$$h_r = \frac{\epsilon_p \sigma \left[(t_p)^4 - (t_s)^4 \right]}{t_p - t_s} \tag{10}$$

where ϵ_p = probe emissivity

σ = Stefan-Boltzmann constant

Equation (9) establishes the magnitude of the radiation error when probe conduction and gas-probe radiation are negligible. Due to the nature of radiant transmission, the error becomes larger as the system gas temperature level is raised while driving through a fixed probe-surroundings potential. The error may be reduced by reducing the radiation conductance factor or increasing the convection coefficient.

Sensor Errors During Transient Conditions

When the gas temperature changes, there will be a time lag before the sensor reaches thermal equilibrium with the gas at its new temperature. This time lag will cause a transient error given by equating the heat transmitted from the gas to the heat absorbed by the sensor (neglecting all other effects) over a small interval of time; thus,

$$h_c(T_{ss} - T_\theta)\, A\, d\theta = WC_p \left(\frac{dT_\theta}{d\theta} \right) d\theta \tag{11}$$

$$\Delta_t = T_{ss} - T_\theta = \frac{WC_p}{hA} \cdot \left(\frac{dT_\theta}{d\theta} \right) \tag{12}$$

where

Δ_t = the instantaneous transient error

W = the mass of the sensor

T_{ss} = temperature at steady state

T_θ = temperature at time θ

A = the effective heat transfer area

θ = time

It is apparent from equation (12) that a transient error will exist until the time rate of temperature change of the sensor reduces to zero, i.e., until the new steady-state condition of thermal equilibrium is attained.

The above equation may be solved for the probe temperature as a function of time after a step change in the temperature of the surrounding gas. Assuming that the probe is at the same temperature as the gas before the change in temperature, then the fraction of the step change that is accomplished by the probe at time θ, after the step change ($\theta = 0$), is given by

$$\frac{T_\theta - T_o}{T_{ss} - T_o} = 1 - e^{-\theta/\tau} = \frac{\Delta T_\theta}{\Delta T_{ss}} \tag{13}$$

where

τ = time constant

ΔT_θ = temperature change at time θ

ΔT_{ss} = total temperature change at steady state

The time constant, τ, is equal to

$$\tau = \frac{WC_p}{h_c A} \tag{14}$$

Thus, the time constant is the parameter in the equation that reflects the physical size and shape of the probe as well as the convective heat transfer characteristics of the gas probe interface. It can be shown that when θ equals τ, the probe has reached 63.2% of its steady-state temperature. Thus, under given conditions, the way to reduce the transient error is to reduce the time constant.

The time constant may also be written

$$\tau = \frac{V\rho C_p}{hA}$$

where

V = volume of the body

ρ = density of the body

For the circular cylinder, the time constant reduces to

$$\tau cyl = \frac{\rho C_p d}{h_c 4} \tag{15}$$

where d = cylinder diameter.

The time constant may be minimized by:

1. Choosing a material wi minimum product of ρC_p
2. Minimizing diameter d
3. Maximizing the heat transfer coefficient h

When the heat transfer is based on forced convection to a cylinder in cross flow, as would be typical of a thermocouple, the convective heat transfer coefficient is given by

$$h_c = \frac{N_u K}{d} \tag{16}$$

where N_u is the Nusselt number, K is the thermal conductivity of the wire and d is the diameter of the wire. The Nusselt number is given in turn by

$$N_u = 0.478 \left(\frac{\rho V d}{u}\right)^{1/2} P_r^{0.3} \tag{17}$$

where V is the velocity of the gas, u is the viscosity (assumed to be constant) and P_r is the Pradtl number, a constant for a onstant viscosity. The heat transfer coefficient is then given by

$$h_c = 0.478 \sqrt{\frac{Vd/_u K P_r^{.03}}{d}} \tag{18}$$

or

$$= K \sqrt{\frac{V}{d}}$$

where K is a constant dependent on the physical properties of the thermocouple material; therefore,

$$\tau cylinder = \frac{C_p d}{4 h_c} = Q \frac{d^{3/2}}{V^{1/2}} \tag{19}$$

where Q is a given material constant.

A reduction in diameter reduces the time constant in two ways: by reducing the mass and by increasing the heat transfer coefficient. The time constant may also be reduced by increasing the velocity of the gas.

It is important to note that the procedure for minimizing the time constant, as applied to the forced convection coefficient, is identical to that applicable to minimizing the radiation error. Minimizing the diameter of a thermocouple probe, consistent with reasonable constraints as regards mechanical and fabrication properties, has now been established as the most important single feature in probe design.

The thermal response expression (Equation (13)) is really valid only for an "ideal" probe, where there is no net radiation between probe and surroundings (or gas), where the probe conduction component is zero, and where the gas stream temperature profile is uniform. None of these conditions exist in practice but, as previously noted, they can be approached with careful design with the possible exception of the radiation error. As previously noted, the only practical method of combating this problem is to add one or more reflecting shields. It is difficult to imagine how this can be accomplished without adding considerably to the time constant, which is entirely contrary to the subject design criteria. In addition, it should be noted that the time constant is not really a constant at all, as the forced convection coefficient is a function of mass flow rate and (to a lesser degree) gas temperature, both variables during an engine transient. The equation is important, however, in analyzing and comparing thermocouple response rates. Care must be taken not to try to compare response rates found under different conditions.

Multiple Junction Thermocouples

The response rate of a thermocouple is controlled by the value of the time constant which reflects the physical characteristics of the thermocouple and the surrounding medium. For fixed environmental conditions, a faster response rate, that is, a smaller constant, is obtained by reducing the mass and increasing the area of the hot junction. The severity of the environment and fabrication techniques limit the possible sizes and shapes of the hot junction due to erosion and mechanical loading. It may be assumed, then, that for a given set of conditions, an optimum thermocouple junction may be designed and built having a minimum size and thus a maximum response. The response of the junction would be described by equation (13) with the time constant equal to a minimum value τ_m. The response time of the thermocouple as a whole can still be further reduced by the use of multiple, in-series junctions, none of which are smaller than the optimum junction assumed above.

The multijunction thermocouple[2] is formed by making three junctions in series, as shown in Figure 2.

Junctions 1 and 2 produce additive potentials while junction 3 produces a counter, or bucking, potential. Under steady-state conditions (all three junctions at the same temperature), the total output is equal to that of a single-junction thermocouple. Under transient conditions, however, the total output will depend on the relative temperature of each junction. The temperature of each junction as a function of time depends upon its time constant. If junctions 1 and 2 have faster response (lower time constants) than junction 3, then the additive junctions will be at a

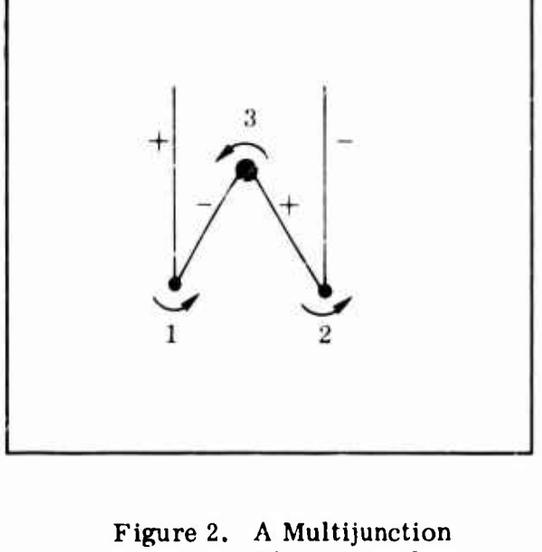

Figure 2. A Multijunction Thermocouple.

higher temperature than the bucking junction, creating a total voltage output that is larger than that for a single junction until the slower-responding bucking junction reaches the equilibrium temperatures at a later time. Thus, the overall output will rise faster than a single junction and will overshoot the steady-state value until the bucking junction reaches steady state. If the small additive junctions both possess the optimum time constant τ_m, then the total response is faster than would be possible with a single-junction thermocouple.

The total potential ($emf_{\theta-M}$) produced by the multijunction at time θ after a step change in temperature is given by

$$emf_{\theta-M} = emf_{\theta-1} + emf_{\theta-2} - emf_{\theta-3} \tag{20}$$

where

$emf_{\theta-x}$ = Electrical potential of junction x at time θ.

Since $\tau_1 = \tau_2$, $emf_{\theta-1} = emf_{\theta-2}$ at all θ. The steady-state potential emf_{ss} is equal for all three junctions. Using equation (13) together with (20) and assuming that emf is directly proportioned to T, then

$$\frac{emf_{\theta-M}}{emf_{ss}} = 1 - 2e^{-\theta/\tau_1} e^{-\theta/\tau_3} \tag{21}$$

The controlling factor in the response rate of the multijunction thermocouple will be the ratio τ_3/τ_1.

Calling this ratio k, the equation for the response of the multijunction can be written

$$\frac{emf_{\theta-M}}{emf_{ss}} = 1 - 2e^{-\theta/\tau_1} + e^{-\theta/k\tau_1} \tag{22}$$

The parameter k reflects the relationship between the response rates of the additive junctions and the opposing junction. Thus, for $k > 1$, the opposing junction responds more slowly and the total response is faster than that for a single junction with time constant τ_1. As k becomes larger, the response rate increases but the potential

overshoots its steady-state value by increasing amounts, requiring longer times to decay to the steady-state value.

The above equation was solved for several values of k using an electronic computer. The fractional change in potential is plotted against time in Figure 3. The time scale is given in multiples of the time constant, τ_1, of the additive junctions, allowing the use of this family of curves to predict the response of any thermocouple. The value of k is indicated for each curve. Curves for k = .25 and .5 show the negative potential created when the bucking junction responds more rapidly than the additive junctions. These curves are not of practical importance. The curve for k = 1 corresponds to a single junction with time constant τ_1. The curves for k > 1 show the decrease in response time as the time constant (τ_3) of the bucking junction becomes larger with respect to τ_1. The amount of overshoot also increases.

Figure 4 shows the decrease in the 90% response time as k increases. Nearly all the enhancement in the response time due to an in-series thermocouple configuration occurs for k < 3. From Figure 3, it can be seen that the amount of overshoot increases rapidly as k becomes large. If the maximum allowable overshoot is set at an arbitrary value of about 10%, the maximum practical value for k would be 2.

This analysis shows that the multiple-junction thermocouple is capable of decreasing the 90% response rate of an optimum single junction by up to 50%.

The characteristics of the multiple junction when subjected to a decrease in temperature are symmetrical to those discussed above for increasing temperature. The total output will decrease to a value less than that of the new steady-state condition before approaching its final value. The magnitude and duration of the undershoot will be equal in duration and magnitude to the overshoot observed with increasing temperature.

General Approaches to Reduce Sensor Errors

In summary, the errors of a temperature sensor can be enumerated as follows:

- Steady-state errors
  - recovery error
  - conduction error
  - radiation error
- Transient errors
  - response rate error

There are, in general, three approaches to the error problem:

1. Use the simplest possible sensor and correct the indicated temperature according to the environment.
2. Use a sensor which has a known constant correction factor over the range of environmental conditions to be expected in the application.

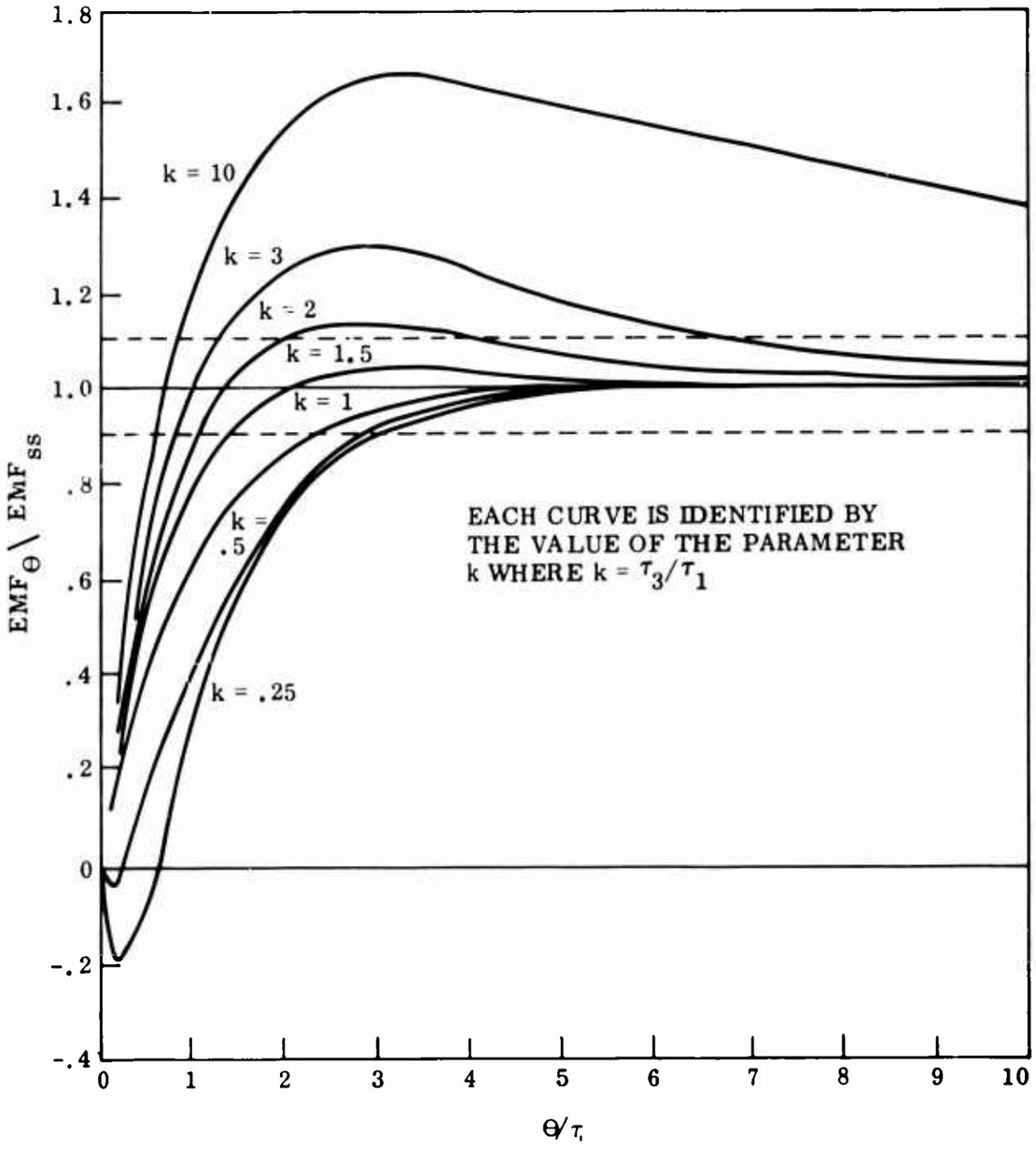

Figure 3. Calculated Response Curves for Multijunctions as a Function of Time θ Normalized by the Time Constant τ_1.

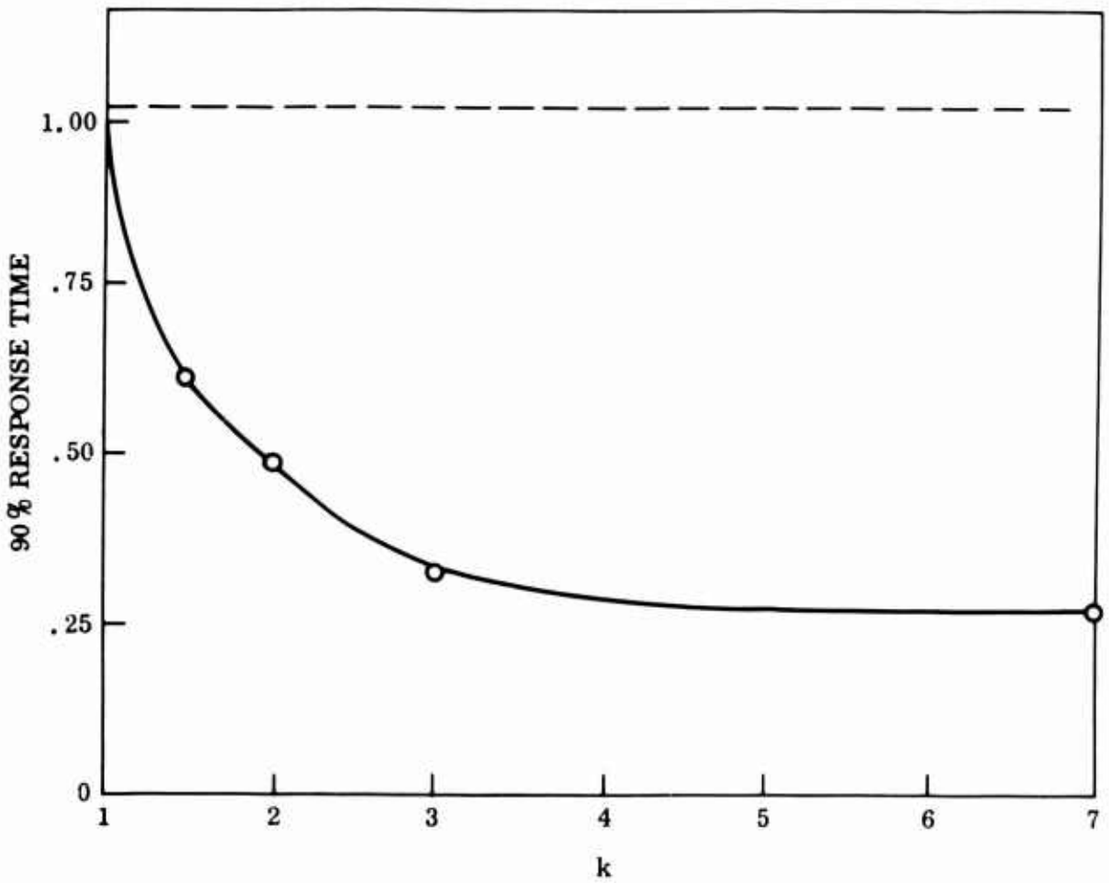

Figure 4. Multijunction Response Time as a Function of k, Where $k = \tau_3/\tau_1$.

3. Design a "direct reading" sensor which will indicate a sufficiently accurate approximation to the gas stagnation temperature over the expected range of environmental conditions.

The first approach will involve calibration of each sensor "in-situ" with the possibility of recalibration whenever a sensor is changed, and will also require detailed knowledge of the environment (using total and static pressure probes) for calculation of the correction factors involved. This approach is clearly useless where the sensor is to be incorporated in the engine control system.

The second approach is feasible, but the only device currently available which achieves this condition is the so-called sonic aspirated probe, which entails placing the sensor at the throat of a sonic nozzle.[3] The resulting indicated temperature is corrected to gas stagnation temperature by a simple multiplicative factor which is constant for all environmental conditions as long as the pressure ratio across the nozzle is greater than critical. Such a device may be acceptable as a sensor for

small gas turbines and will be investigated as necessary. It has the disadvantages of allowing for the correction factor in the read-out instrumentation and the possibility of dimensional changes in an engine environment affecting the correction factor in an unpredictable manner. The response time of this device is commonly less than 0.5 second and is also markedly insensitive to environmental changes. This insensitivity may make it difficult to reduce the response time by a significant amount.

The third approach is the one that will be pursued in this program; namely, the design of a direct-reading sensor which will indicate the gas stagnation temperature to within the allowable steady-state error and attain the fastest possible response to minimize transient errors.

Gas Blockage Due to Probe Immersion

The basic effect of introducing a probe into a duct is a local loss in total pressure across the probe due to its obstruction or blockage. This total head loss can readily be estimated in terms of the gas conditions upstream of the probe by applying the equations of continuity and momentum to the flow across the probe.

This result does not tell us the disturbing influence that the probe will have in an actual engine duct. Placing a probe in an engine duct will generally cause a change in the flow conditions upstream of the probe due to rematching of the engine components. The rematch will depend upon the engine and the location of the probe, and it is even possible for the probe to cause compressor surge leading to unstable engine operation. For example, a probe placed in a compressor intake cannot affect the upstream total pressure, so the pressure loss caused by it will result in reduced compressor mass flow; the identical probe placed downstream of a choked compressor cannot affect the mass flow, so the upstream total pressure must increase and the engine rematches at a higher pressure ratio. Thus, it is impossible to generalize on the effects of probe blockage in engine ducting and each case must be treated as an individual engine matching problem.

Nevertheless, the pressure loss coefficient estimation is necessary in its own right to determine the orders of magnitude involved and as a preliminary to more involved engine matching considerations.

Let C_D = drag coefficient of the obstruction

S = projected area of the obstruction

P = total pressure

p = static pressure

q = $P - p$ = dynamic pressure

A = duct area

α = isentropic index

	R	= total to static pressure ratio
Suffix	0	= upstream of obstruction
	2	= downstream of obstruction

Then, equating the drag caused by the obstruction to the change in momentum across the obstruction,

$$C_D \cdot q_0 \cdot S = p_0 A_0 \left(1+\alpha M_0^2\right) - p_2 A_2 \left(1+\alpha M_2^2\right) \tag{23}$$

and applying the equation of continuity across the obstruction,

$$p_0 A_0 M_0 \left(1 + \frac{\alpha - 1}{2} M_0^2\right)^{1/2} = p_2 A_2 M_2 \left(1 + \frac{\alpha - 1}{2} M_2^2\right)^{1/2} \tag{24}$$

Now, assuming that the duct has constant area upstream and downstream of the obstruction, then

$$A_0 = A_2 = A$$

and equation (23) may be written as

$$\frac{C_D S}{A} = \frac{R_0}{R_0 - 1} \left\{ \frac{\left(1+\alpha M_0^2\right)}{R_0} - \frac{P_2}{P_0} \frac{\left(1+\alpha M_2^2\right)}{R_2} \right\} \tag{25}$$

also, equation (24) may be written as

$$\frac{P_2}{P_0} = \frac{M_0}{M_2} \cdot \frac{R_2}{R_0} \frac{\left(1 + \frac{\alpha - 1}{2} M_0^2\right)^{1/2}}{\left(1 + \frac{\alpha - 1}{2} M_2^2\right)^{1/2}} \tag{26}$$

where

$$R_0 = \left(1 + \frac{\alpha - 1}{2} M_0^2\right)^{\alpha/\alpha - 1} \tag{27}$$

and

$$R_2 = \left(1 + \frac{\alpha - 1}{2} M_2^2\right)^{\alpha/\alpha - 1} \tag{28}$$

It is clear from equations (25) and (26), together with the two auxiliary equations (27) and (28), that the total pressure ratio P_2/P_0 (which is unity when there is no pressure loss) is a function of the drag parameter C_DS/A and the approach Mach number M_0 only because the downstream Mach number M_2 is a function only of P_2/P_0 and M_0. Unfortunately, the nature of the equations does not allow an explicit elimination of M_2 to give P_2/P_0 as a direct function of C_DS/A and M_0, so the equations must be solved by assuming values of M_0 and M_2 and calculating the resulting values of P_2/P_0 and C_DS/A. This has been done using an electronic digital computer, and the results are plotted in Figure 5 for a value of $\gamma = 1.33$.

In this figure the results are plotted as pressure loss coefficients

$$\frac{\Delta P}{P_0} = \frac{P_0 - P_2}{P_0} = 1 - \frac{P_2}{P_0} \tag{29}$$

and

$$\frac{\Delta P}{q_0} = \frac{P_0 - P_2}{P_0 - p_0} = \frac{R_0}{R_0 - 1}\left(1 - \frac{P_2}{P_0}\right) \tag{30}$$

The first form of the pressure loss coefficient is useful for engine performance and matching calculations. The second form of the coefficient gives the loss in terms of the approach dynamic head and is the usual form for incompressible ($M_0 = 0$) flow calculations.

If the engine is initially matched (at constant speed) on the vertical portion of the compressor characteristic, then the mass flow cannot change as a result of inserting the probe downstream of the compressor. The compressor delivery pressure must then increase to compensate for the pressure loss, and the turbine inlet temperature will increase to maintain a correct turbine match. If these small changes in pressure and temperature are neglected as second-order effects, then Figure 5 can be used directly to get the effect of inserting a probe in an engine upstream of a choked turbine and downstream of a choked compressor.

However, if the engine is originally matched on a horizontal portion of the compressor characteristic, then (again at constant speed) the pressure ratio cannot increase, so the mass flow must decrease. Again, if the necessary increase in turbine top temperature is neglected, this case can be analyzed by assuming that

$$P'_0 = P_0 \tag{31}$$

$$P'_0 = P_2 \tag{32}$$

where the primed quantities are the values obtained before inserting the probe.

Thus,

$$R'_0 = P'_0/p'_0 = P_0/p_2 \tag{33}$$

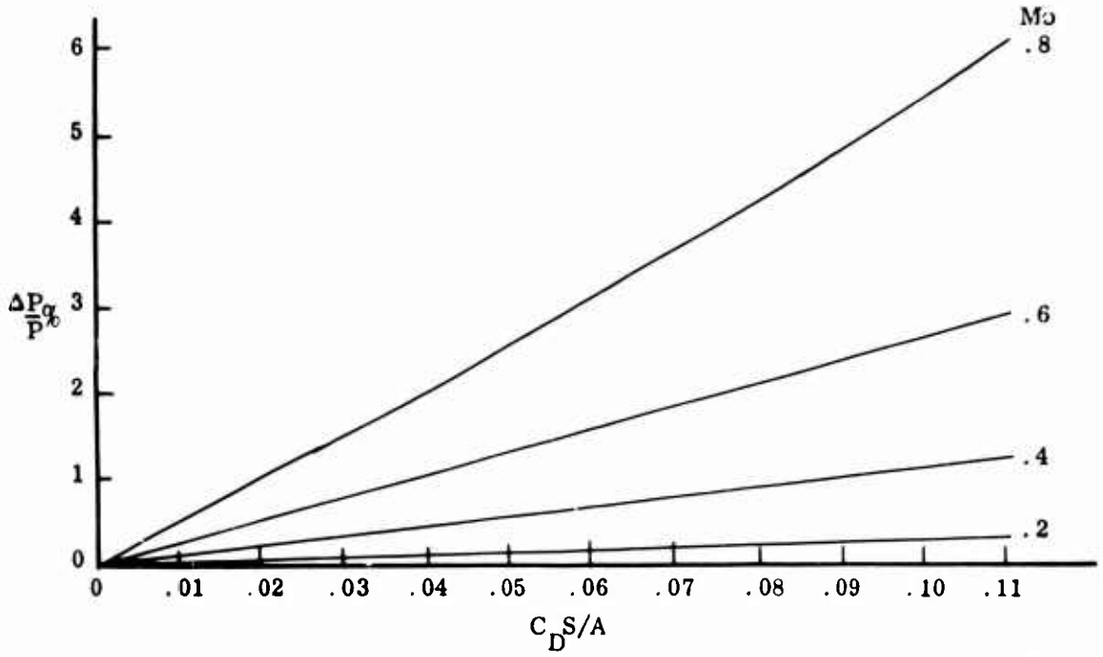

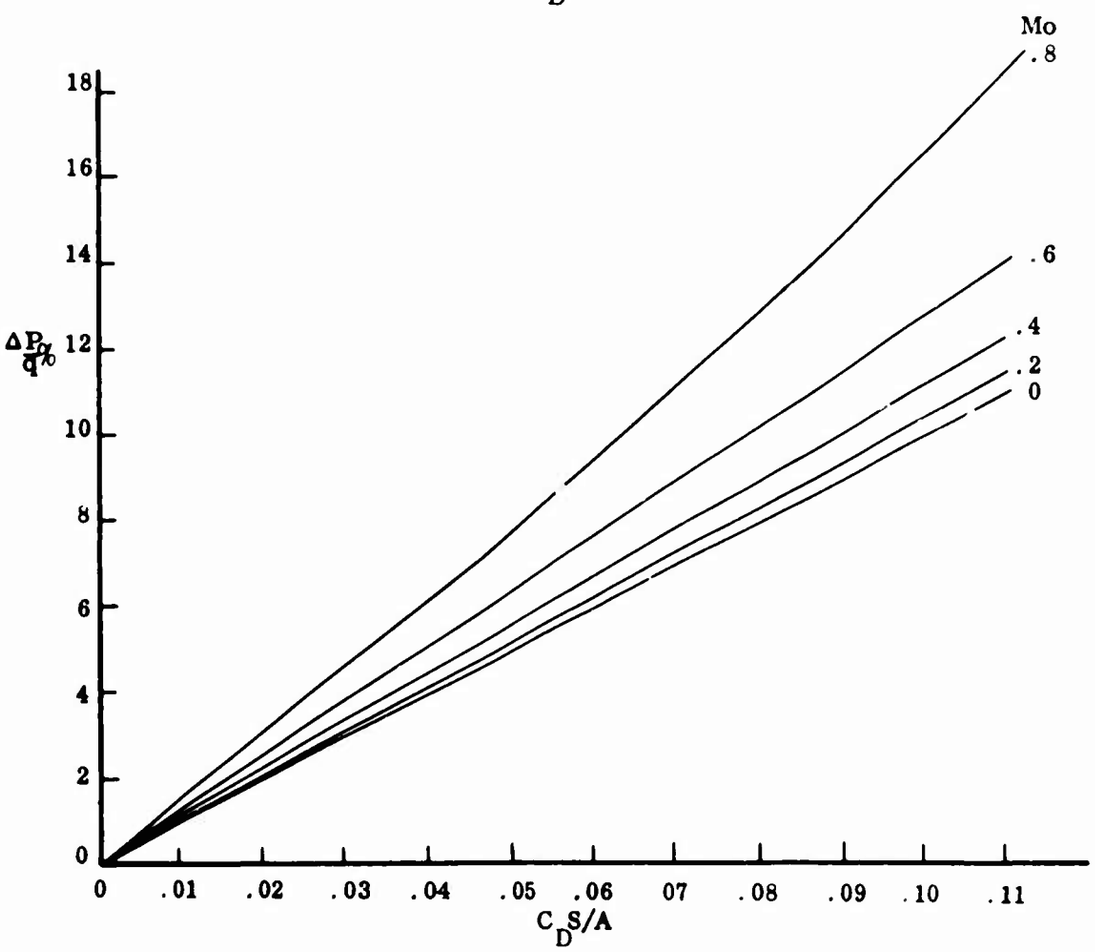

Figure 5. Estimated Pressure Loss Due to Duct Blockage.

and

$$M_0' = \left\{\left(P_0/p_2\right)\right\}^{\frac{\alpha - 1}{\alpha}} - 1^{1/2} \tag{34}$$

The fractional change in approach Mach number

$$\frac{\Delta M}{M_0'} = 1 - \frac{M_0}{M_0'}$$

can then be calculated from the total to total pressure ratio P_2/P_0, since

$$R_0' = \frac{P_0}{P_2} = \frac{P_0}{P_2} \cdot \frac{P_2}{p_2} = \frac{\left(1 + \frac{\alpha - 1}{2} M_2^2\right)^{\alpha/\alpha - 1}}{P_2/P_0} \tag{35}$$

It can also be shown that the fractional decrease in mass flow is given by

$$\frac{\Delta W}{W} = \frac{W' - W}{W'} = 1 \frac{M_0}{M_0'} \frac{1 + \frac{\alpha - 1}{2} M_0'^2}{1 + \frac{\alpha - 1}{2} M_0^2} \frac{\alpha + 1}{2(\alpha - 1)} \tag{36}$$

This analysis has also been carried out on a digital computer and the results are given in Figure 6.

For the incompressible case ($M_0 = M_0' = 0$), equation (23) reduces to

$$\frac{C_D S}{A} = \frac{P_0 - P_2}{q_0} \tag{37}$$

and equation (24) reduces to

$$V_0 = V_2 \tag{38}$$

where V is velocity.

Thus,

$$q_0 = q_2 = P_0 - p_0 = P_2 - p_2$$

and

$$P_0 - P_2 = p_0 - p_2 \tag{39}$$

with

$$\frac{C_D S}{A} = \frac{\Delta P}{q_0} \tag{40}$$

and

$$\frac{\Delta P}{P} = 0 \tag{41}$$

It can also be shown for the nonchoked compressor case that, for incompressible flow,

$$\frac{\Delta W}{W} = 1 \frac{1}{1 + \frac{C_D S}{A}} \tag{42}$$

$$= \frac{\Delta V}{V} = \left(\frac{\Delta M}{M}\right) \tag{43}$$

This latter equation implies that the fractional velocity change is the same as a (fictitious) fractional change in Mach number.

Summary

Figure 5 illustrates the pressure loss due to inserting a probe downstream of a choked compressor and upstream of a choked turbine. The pressure loss is equal to the increase in compressor delivery pressure.

Figure 6 illustrates the effect on mass flow and approach Mach number and the pressure loss caused by inserting a probe downstream of a compressor which is working at maximum pressure ratio and upstream of a choked turbine.

Both figures apply to a single shaft machine running at constant speed. Second order effects of temperature matching are neglected.

It is noted that with a nonchoked compressor, the additional penalty of reduced mass flow is partially compensated by a reduced pressure loss penalty, but in both cases the rematch will be closer to compressor surge.

Application to the High Temperature Probe Program

The above analysis started in an attempt to develop a general envelope of drag coefficients and blockage areas within which to design the temperature probes for a given allowable deterioration in engine performance. It is clear that any further development along these lines would need to be particularized with a specific engine in view. Nevertheless, the analysis has gone far enough to show the importance of environmental Mach number M_0, drag coefficient C_D, and blockage area ratio S/A

Upstream Total Pressure P_0 Remains Constant

Downstream Static Pressure Remains Constant

M_0' = Approach Mach Number Before Introduction of Obstruction

W' = Mass Flow Before Introduction of Obstruction
ΔW = Loss in Mass Flow Due to Obstruction
ΔP = Total Pressure Loss Across Obstruction
ΔM = Reduction in Approach Mach Number
$q = P_0 - p_0$ = Approach Dynamic Head
C_D = Drag Coefficient of Obstruction
S = Area of Obstruction
A = Area of Duct

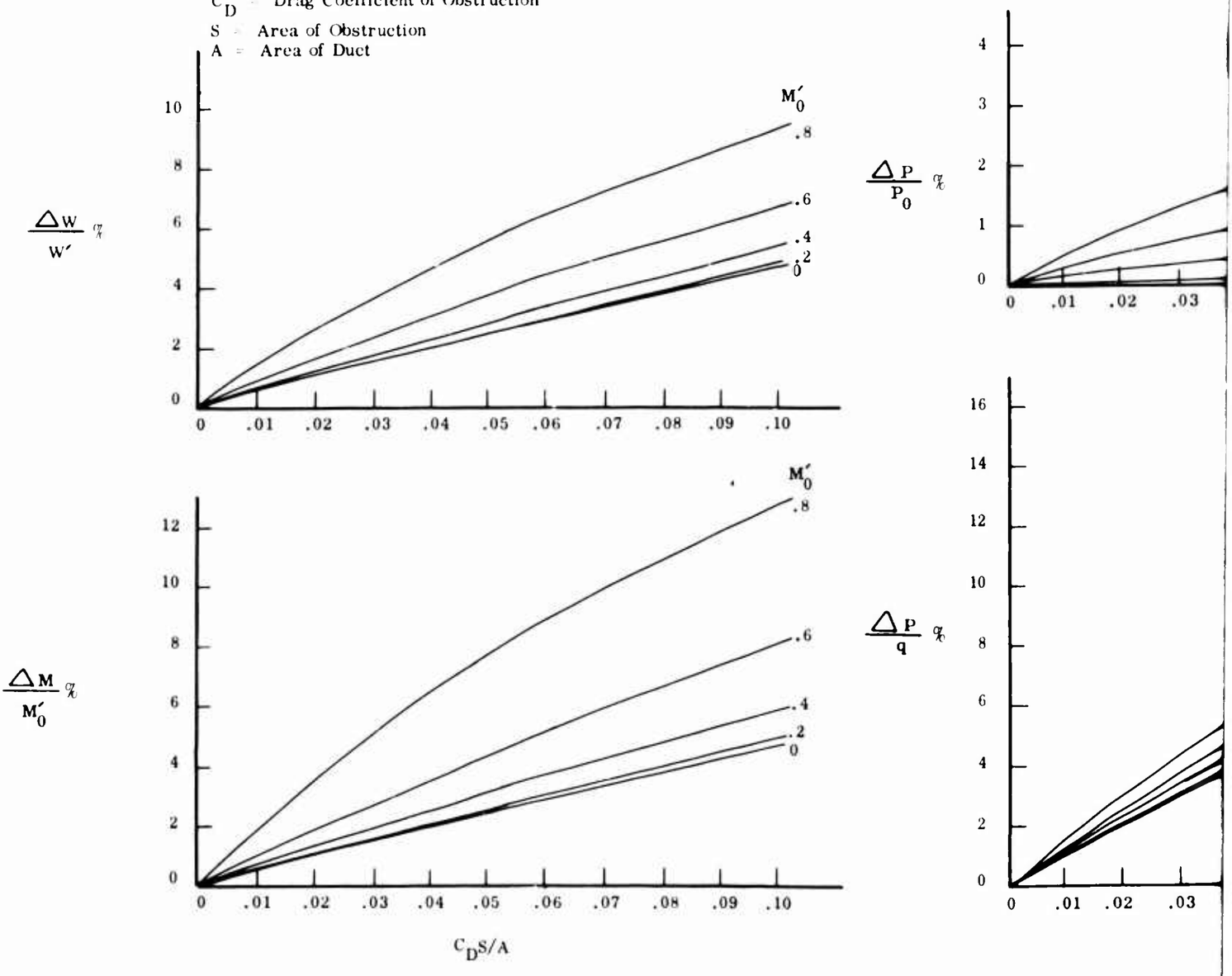

Figure 6. Estimated Effects of Duct Blockage.

Remains Constant

Remains Constant

r Before Introduction of Obstruction

oduction of Obstruction
ue to Obstruction
Across Obstruction
h Mach Number
namic Head

truction

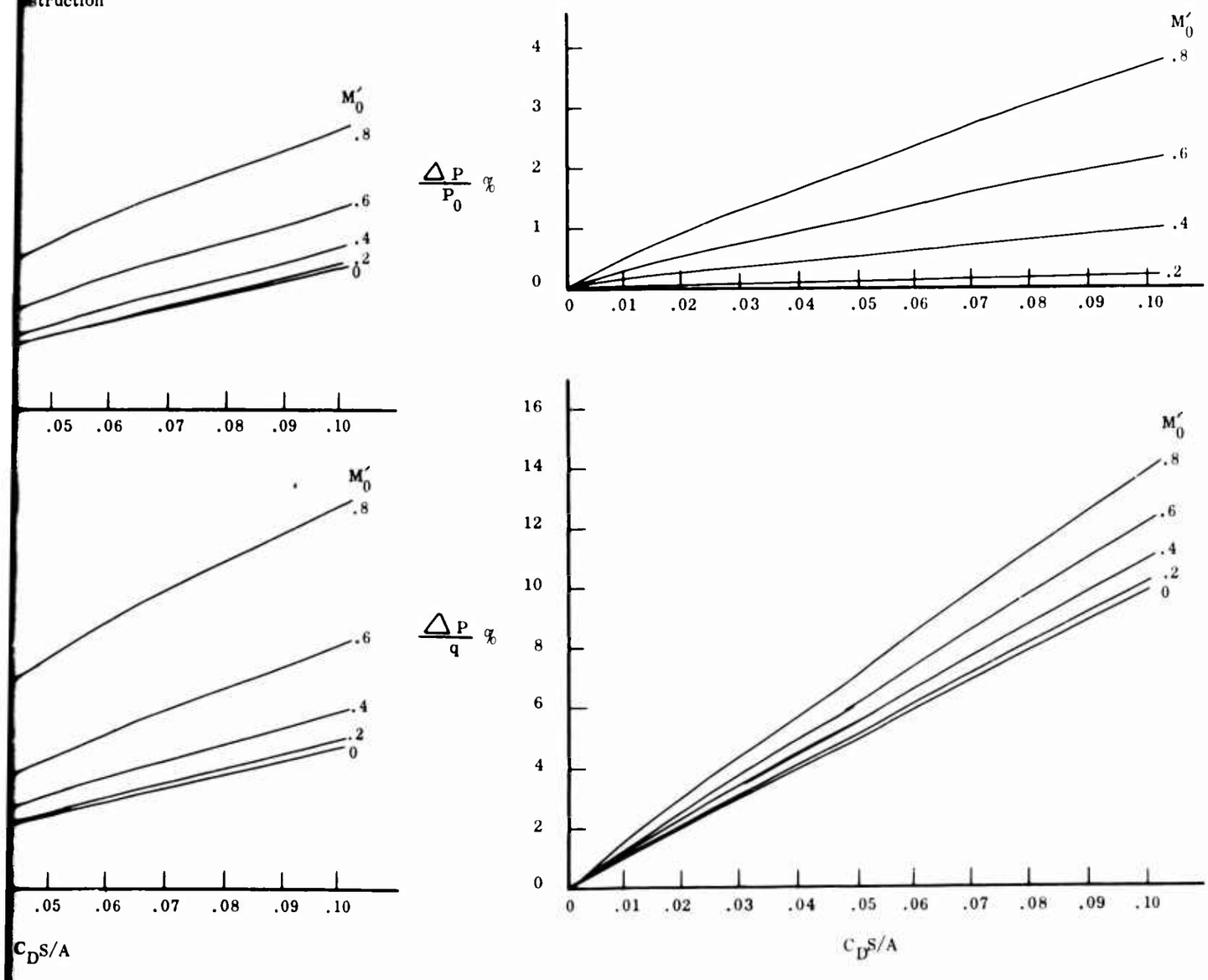

cts of Duct Blockage.

in the selection of probe geometry and location, and enables a rough quantitative approach to be made. Thus, it is clear that, to keep the pressure loss below 1% of the available total head, it is necessary to limit the environmental approach Mach number to 0.4 maximum and to keep the product of drag coefficient and blockage area ratio below 0.10. Even then, it is possible in an extreme case to lose up to 5% of the engine mass flow.

The annular dimensions of the small 2 pps engine are shown in Figure 7 scaled from the 4 pps engine but maintaining 0.5-inch blade height. If a row of cylindrical probes is positioned upstream of the nozzle row as shown, then assuming ten probes with a mean depth of penetration of 3/8 inch to cover the temperature profile, the blockage area for 1/8-inch-diameter probes is given by

$$S = 10 \times .375 \times .125 = .468 \text{ in.}^2$$

and the flow area is given by

$$A = \frac{\pi}{4} (3.5^2 - 2.5^2) = 4.72 \text{ in.}^2$$

The drag coefficient for a cylinder in crossflow $C_D = 1.2$[3], giving

$$C_D S/A = 1.2 \times .468/4.72$$

$$= .119$$

Furthermore, with

$$W = 2 \text{ pps}$$

$$T = 2960°F$$

$$P = 130 \text{ psia}$$

$$W\sqrt{T/AP} = 2\sqrt{2960/130} \times 4.72 = .1773$$

giving

$$M_0 = .20 \text{ (approx.)}$$

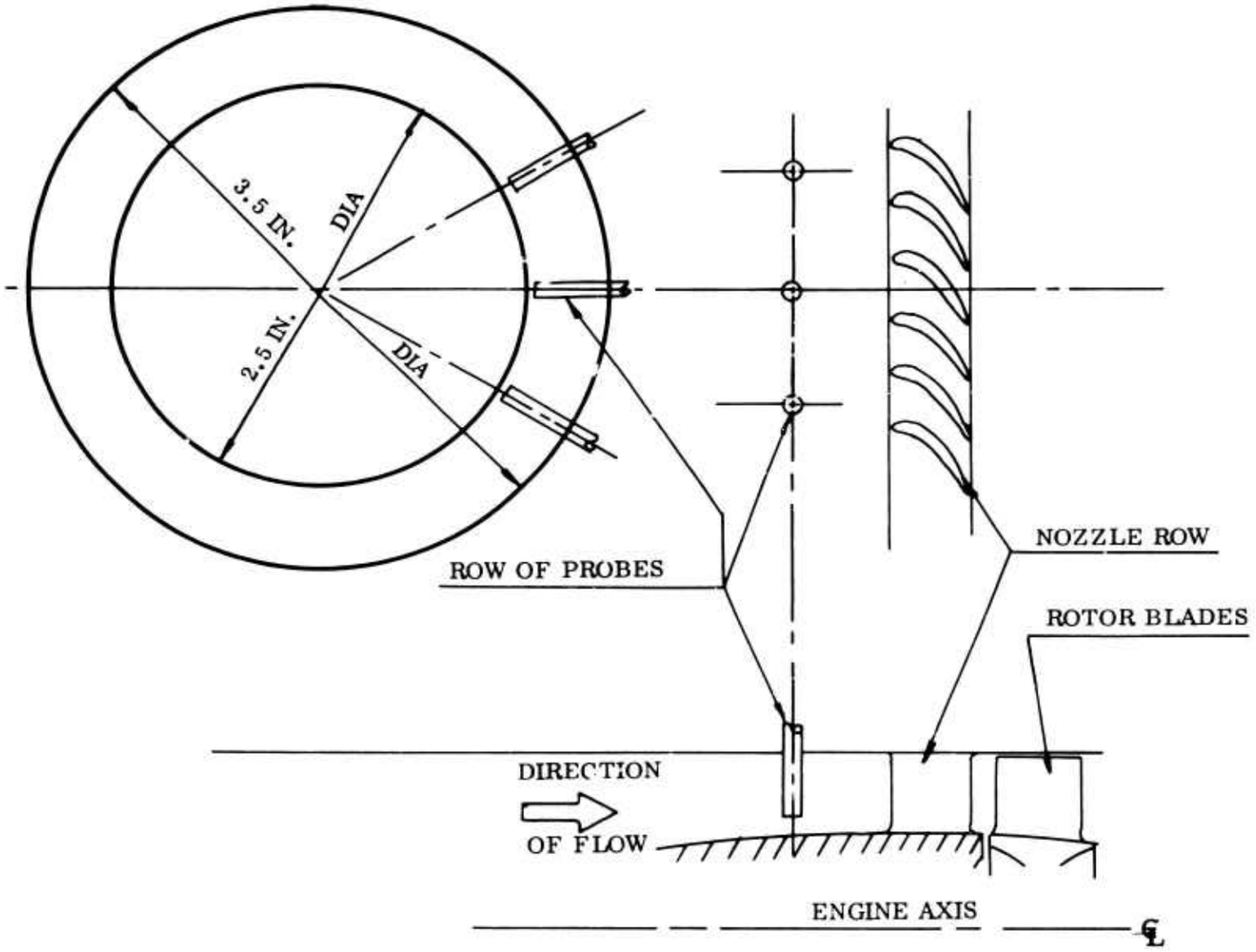

Figure 7. Schematic Diagram of a Two-Pound-Per-Second Engine.

From Figure 5 or Figure 6, the pressure loss with such a system would be about 0.3% of the available total head with a potential mass flow loss of about 5%. This pressure loss is possibly acceptable, but the mass flow loss is probably unacceptably high; and if the engine is such that this type of mass flow loss is possible, then $C_D S/A$ values of the order of .02 would be required.

It is apparent from the above that the use of an orthodox probe system could easily result in unacceptable blockage penalties in these small engines, and means must be sought to miniaturize the probes and choose locations which minimize the blockage area ratio. A good arrangement would be to locate the probes in the leading edges of the nozzles with the sensor heads protruding and the leads taken out through the body of the nozzle. This may, however, be an unacceptable mechanical arrangement from the disassembly point of view, and more orthodox methods may have to be resorted to with the $C_D S/A$ parameter reduced to acceptable values when these values are known.

EXPERIMENTAL PROGRAM

The experimental program was divided into the following three general areas:

1. Materials selection and thermocouple design.
2. Effect of environment on thermocouple performance.
3. Response.

The first area includes a discussion of the design and fabrication of the program thermocouples to conform with the guidelines laid down in the thermodynamic and analytical analysis. The program materials were chosen on the basis of compatibility tests and a survey of the literature. The study of the effect of the environment on the performance of the thermocouples was primarily concerned with accuracy and mechanical stability over the lifetime of the thermocouple. Both exposed and protected junctions were considered. Response is an important consideration in the incorporation of the transducer into the engine controls. Consequently, analysis of response rate and measurement of response times received a major portion of the experimental effort.

MATERIALS SELECTION AND THERMOCOUPLE DESIGN

Many material combinations produce a thermoelectric effect, but only a few produce an emf that is linearly proportionate to the temperature of the hot junction, thus making them useful as temperature measuring devices. Even fewer are capable of functioning at the elevated temperatures present at the turbine inlet. Thermocouples are limited to about 60° to 100°F below the melting temperature of the lowest melting phase. The temperature-millivolt potential curves for some commonly used thermoelectric elements are shown in Figure 8. To be considered for turbine application, a thermocouple must function over the entire range of temperature encountered in service. It can be seen that only the noble and refractory metals have the capability to function at 300°F (couples B, C, R, S, X and L). Platinum, rhodium, iridium, rhenium and tungsten in various combinations are the most often mentioned thermoelectric materials at high temperatures. Although many other combinations of these and other materials have been

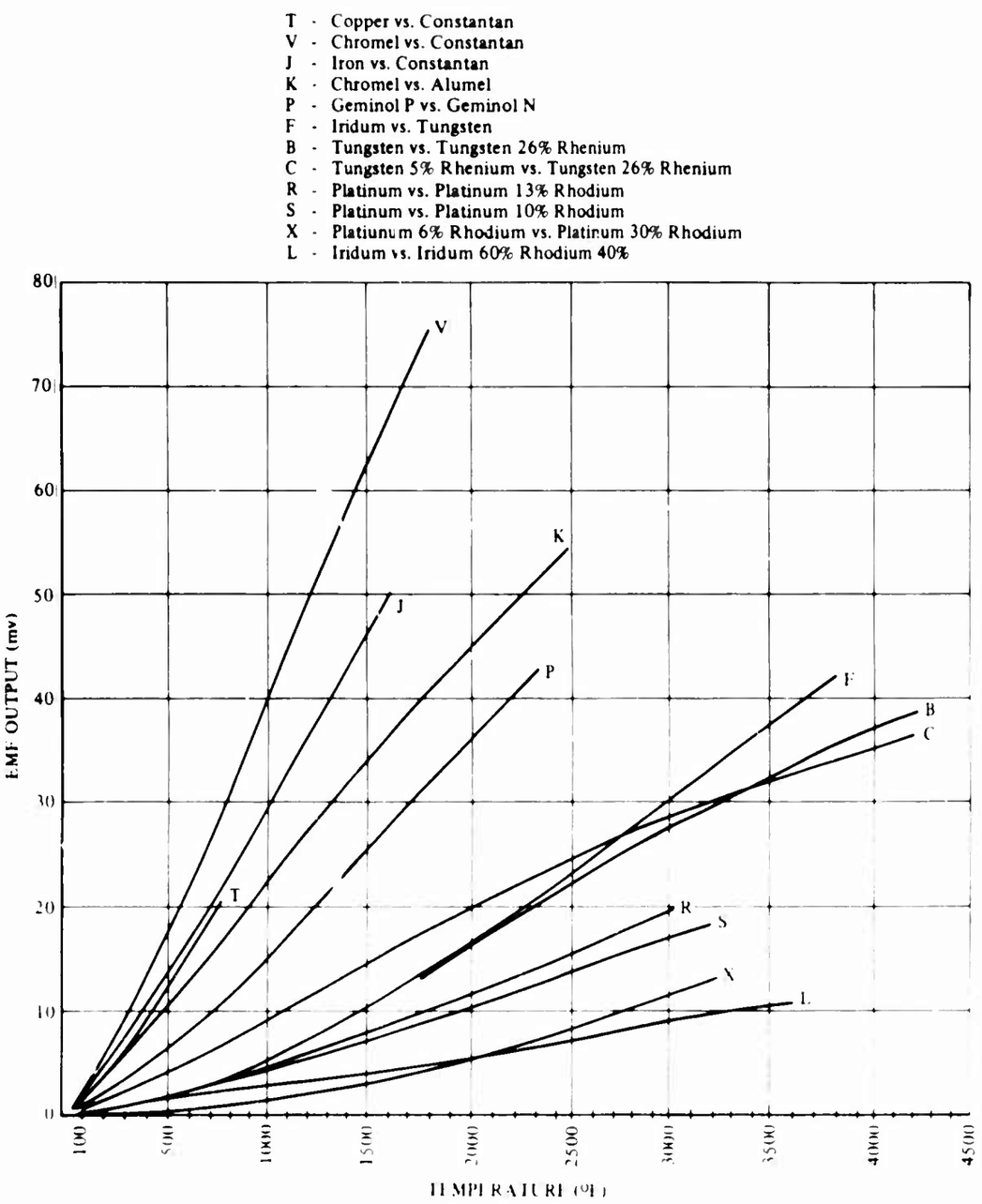

Figure 8. Temperature-Millivolt Curves for Some Commonly Used Thermoelectric Elements.

TABLE II. PROPOSED THERMOCOUPLE MATERIALS			
Type B	Tungsten	Versus	W26%Re
Type C	W5%Re	Versus	W26%Re
Type S	Platinum	Versus	Pt10%Re
Type X	Pt6%Rh	Versus	Pt30%Rh
Type L	Iridium	Versus	Ir40%Rh

investigated, the thermocouples listed in Table II were chosen for study based on the best information available in the literature.[4-8]

The thermocouples must also retain their electrical and mechanical properties during long-time exposures to the environment. This includes compatibility with insulating and sheathing materials, oxidation resistance, mechanical strength, and resistance to structural and chemical changes. The degree to which each thermocouple meets these requirements will depend upon the exact environment to which it is exposed.

Fabrication of Sensors

The most common thermocouple configuration is a single, fusion-welded wire junction. A second shape that increases the ratio of area to mass and thus increases the response rate is a foil junction made from the union of two thin foils. The multijunction concept can be used to increase the response of either type of junction. To increase life expectancy and reliability, a protective sheath may surround the junction. This approach sharply reduces the rate of heat exchange between the gas and the junction and thus reduces the response rate.

Wire junctions may be formed by fusion welding or by capacitance discharge welding. A fusion weld produces a bead at the junction with a diameter larger than that of the wires. When a junction of smaller mass is desired, the capacitance welder is used and no bead is formed. Foil junctions can also be fabricated in two different ways: diffusion bonding and fusion welding.

To fabricate a diffusion-bonded junction, the two foils are overlapped and heat and pressure are applied. Diffusion occurs very rapidly across the interface between the two foils until one continuous body is formed. The pressure is applied through two molybdenum alloy anvils by a hydraulic press. The anvils are heated electrically and the temperature is automatically controlled by an optical pyrometer. Tungsten foil is inserted to prevent sticking between the anvil and the platinum.

Figure 9A shows a cross section of a Pt6%Rh versus Pt30%Rh thermocouple bonded in this manner. The tungsten cover strips are still in place. Bonding pressures of 15,000 to 20,000 pounds per square inch were used at temperatures of 1600° to 1800°F. Bonding time was 10 to 20 seconds. Figure 9B shows the microstructure

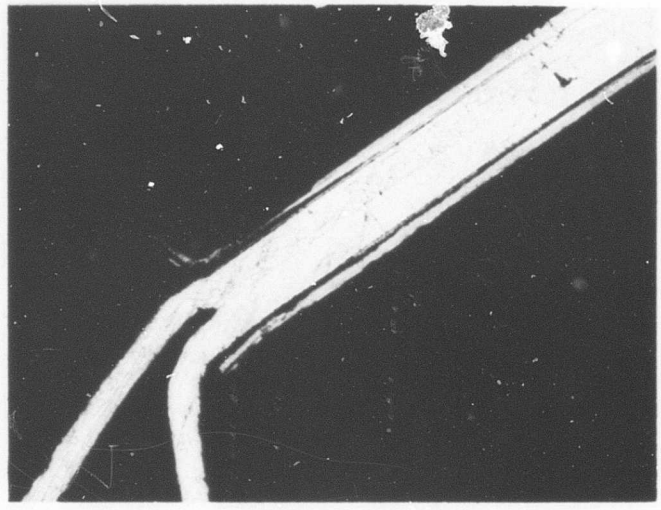

Magnification
100X
(Reduced 20%)

0.002-Inch Foils; Tungsten
Cover Strips Not Removed

A

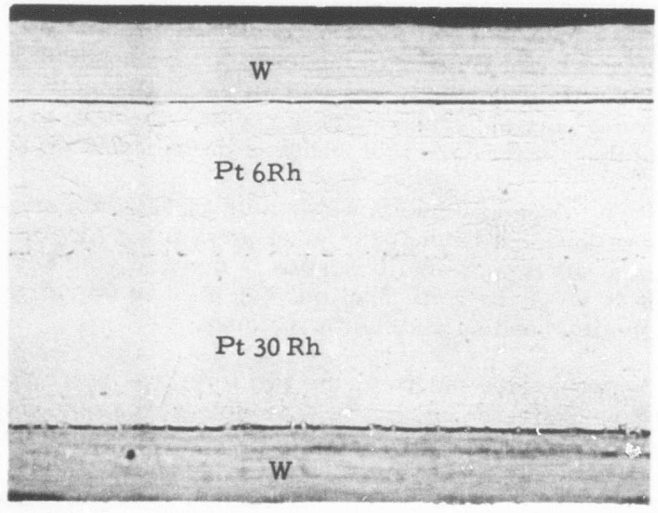

Magnification
600X
(Reduced 20%)

Microstructure

B

Figure 9. Microstructure of a Diffusion-Bonded Pt6%Rh-Pt30%Rh Foil Hot-Junction.

of the bonded junction. Electron microprobe analysis showed that compositional changes occurred over less than 0.001 inch on either side of the part line during bonding. Overlaps of 0.004 to 0.010 inch were used. Multiple junctions formed in this way were tack-welded in place to preserve the junction alignment and then were diffusion bonded. After bonding, the foils were formed into a tubular shape or left as a flat strip. Lead wires were then welded to the junction to form a thermocouple.

Fabrication of protected thermocouple probes posed a serious material-system problem. Compared with an exposed junction, a sheathed probe will have a slower response due to the barriers added to heat flow. Several advantages obtained by adding the protective sheath may offset the reduction in response rate for many applications. Thermoelectric materials may be used which are not resistant to oxidation but have higher signal strength than those that can be used exposed. Increased durability, reliability and lifetime are also important considerations. To maximize the response time of a protected junction, it must be made as a "grounded junction." That is, the thermocouple junction is in contact with the sheath, making it unnecessary for the heat to travel through the insulation to reach the thermoelement. Schematic diagrams of grounded and isolated junctions are shown in Figure 10. Material candidates for the sheath are quite limited due to the high temperatures involved. Tantalum and columbium, coated to resist oxidation, would be leading contenders. Tungsten-rhenium thermocouples offer high temperature capability and relatively high signal strength. Preliminary work was

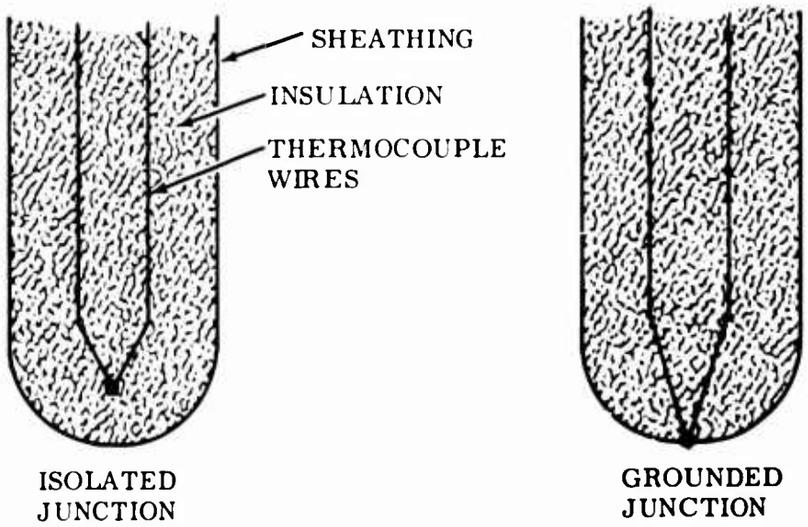

Figure 10. Grounded and Isolated Thermocouples.

conducted on fabrication of a grounded thermocouple probe consisting of a W5%Rh versus W26%Re thermocouple, Al_2O_3 powdered ceramic insulation and a tantalum sheath coated with Solar's "TNV-7"(9) coating. The principal problem arises in making the necessary welds at the junction-sheath interface without embrittling the W-Re wires. A satisfactory solution was not demonstrated but it is thought that further work can result in a workable probe.

COMPATIBILITY

The compatibility of the thermoelectric materials with the adjacent insulating oxides is an important consideration in choosing the entire materials system to be used. Material transport, solid-state diffusion, eutectic formation resulting in low melting phases, and recrystallization are some of the reactions which can occur at interfaces due to an unsatisfactory choice in materials systems. The term compatibility will be used with respect to properties covered by mechanical or physical metallurgy and not the thermoelectric stability of the alloy. Compatibility of a thermoelectric material and an oxide must be referred to a specified atmosphere. A system that is compatible in a reducing atmosphere might not be compatible in an oxidizing atmosphere or in a vacuum. All of the compatibility tests on this program were carried out in slowly moving air or in an inert atmosphere.

The oxidation of the platinum group thermocouple materials is excellent compared to the refractory metal thermocouple materials. However, at temperatures above 2200°F, all of the platinum group metals exhibit linear rates of weight loss through the formation of volatile oxides. The weight loss of the platinum group metals in air are shown in the Arrhenius plot in Figure 11, and are based on work by Krier and Jafee.[6] Noteworthy is the low rate of weight loss shown for platinum and rhodium compared to that of iridium. However, calculations by Krier and Jaffee on the degree of saturation of the airstream flowing around the specimens shows that the air was, for the most part, saturated with oxides of platinum and rhodium; the air was relatively unsaturated for the iridium test. Thus, a possibility exists for the oxidation rate of platinum and rhodium to be considerably higher than that shown. The influence of air velocity on the oxidation rate of the platinum group metals is important when consideration is given to the high velocities that are encountered in the turbine environment. Even in view of the foregoing, platinum and rhodium exhibit the best oxidation resistance in the temperature range of interest. The oxidation rate of iridium at 3500°F is not high enough to exclude it as a thermocouple material; and its higher temperature characteristics are attractive in consideration of possible overtemperature conditions in the engine. Tungsten and tungsten-rhenium alloys must be used with protective sheathing or coatings to protect them from rapid oxidation.

Selection of Oxides for Insulators

The use of oxides in this environment appears to be practical from a chemical stability point of view. The oxides are stable in a number of varied environments due to the low free energy of formation, as shown in Figure 12. The oxides, Al_2O_3, ThO_2, ZrO_2, BeO and MgO, are typically used for thermocouple insulation. The available data indicates that at the temperatures of interest, the oxides are more stable than their compounds of carbon or nitrogen which are present in

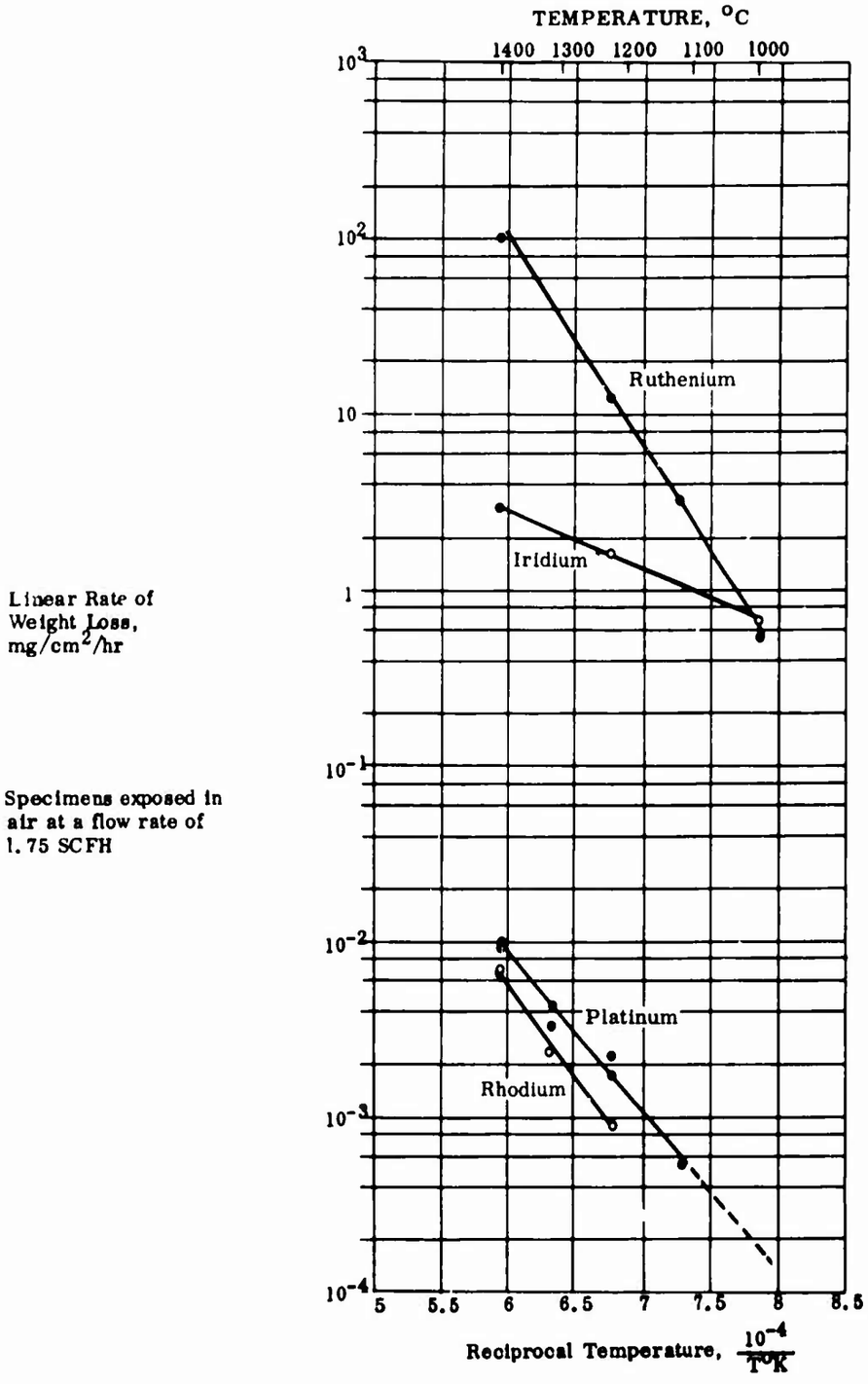

Figure 11. Variation of Rate of Weight Loss with Temperature in Air for Platinum-Group Metals.

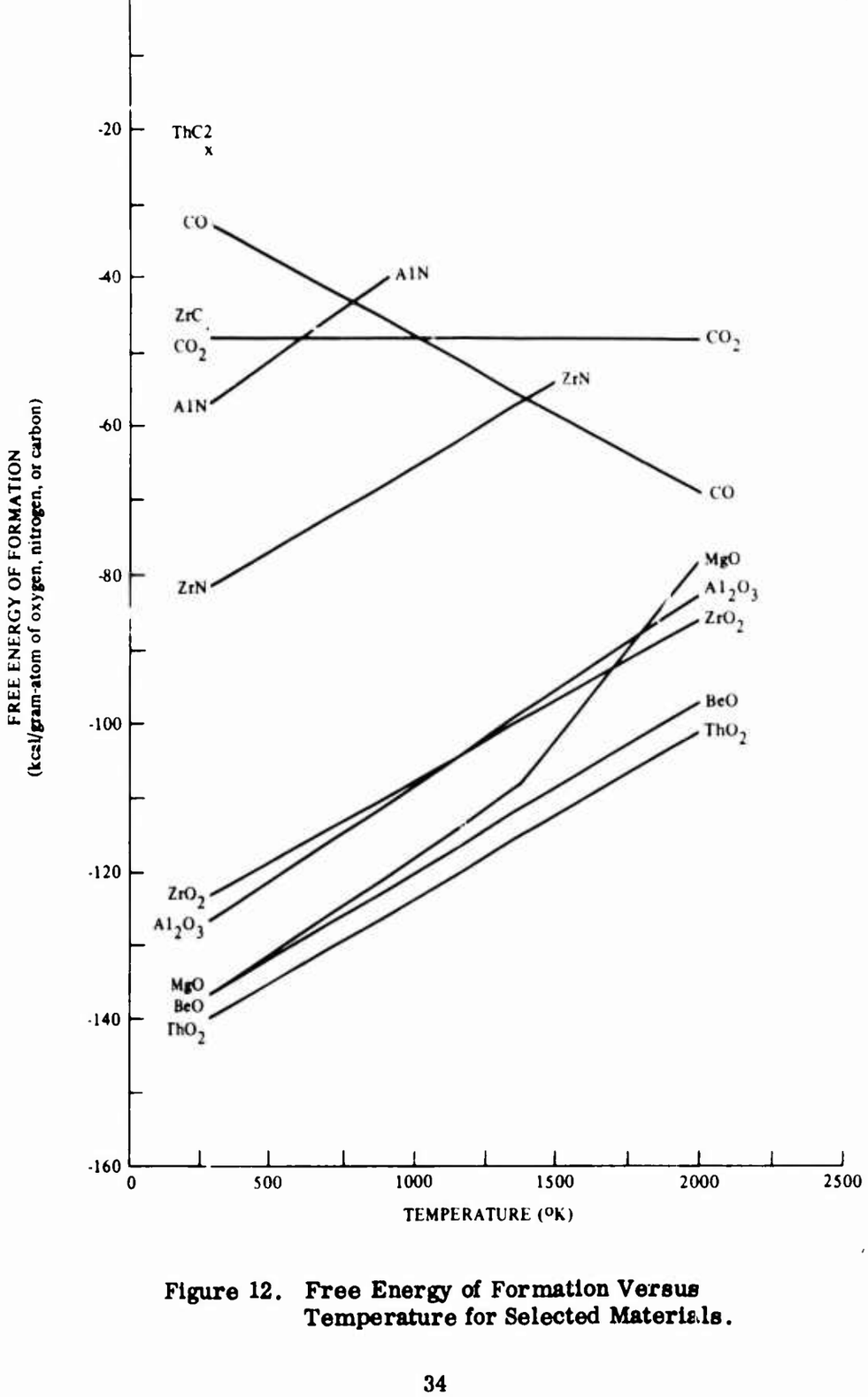

Figure 12. Free Energy of Formation Versus Temperature for Selected Materials.

TABLE III. PROPERTIES OF REFRACTORY OXIDES

Composition	Porosity (vol. %)	Max. Normal Use Temp. (°F)	Modulus of Rupture (psi) at 1832°F	Modulus of Elasticity 10^6 psi	Thermal Stress Resistance
99.9Al_2O_3 (sapphire)	0	3500	30,000-100,000	55	Very good
99.8Al_2O_3 (sintered)	3-7	3450	22,000	53	Good
99.8BeO	3-7	3450	10,000	45	Excellent
99.8MgO	3-7	3630	12,000	30.5	Fair-poor
99.5TiO_2	3-7	2910	6,000	—	Fair-poor
99.8Y_2O_3	2-5	3630	—	—	Fair-poor
99.[illegible]$ZrSiO_4$	5-15	3270	6,000	30	Good

large quantities in the turbine atmosphere. Physical properties of refractory oxides are listed in Table III, and electrical resistivity at several temperatures is shown in Table IV.[10]

Al_2O_3, ZrO_2, MgO, ThO_2, SiO_2, Yt_2O_3, and Nd_2O_3 were considered for use as insulating materials. The compatibility of the various thermoelements with the oxide insulating materials was determined by packing samples of carefully weighed and measured thermocouple materials in powdered metal oxides and exposing these in air or inert gas at 2000° to 2500°F for 100 hours. After exposure, the samples were removed from the oxides and reweighed and measured. Metallographic techniques were used to determine the occurrence of any metal-oxide reactions.

Experimental Method

Three thermoelectric materials systems were tested for compatibility with refractory oxides. These thermocouple alloys were platinum-rhodium, iridium-rhodium and tungsten-rhenium. The refractory oxides used for these tests were SiO_2, Al_2O_3, MgO, ZrO_2, and ThO_2. Samples of each alloy were cut from spools of standard 0.015-inch-diameter thermocouple wire. Each sample weighed approximately 200 milligrams. Three samples of each alloy were weighed and cold packed into the oxide powders (reagent grade) and placed in individual alumina boats. Several boats were then placed in a preheated tube furnace. The ends of the

TABLE IV. ELECTRICAL RESISTIVITY OF CERTAIN REFRACTORY OXIDES

Refractory Oxide	Electrical Resistivity (ohm-cm)	Temperature (°F)
Alumina	10^{13}	930
	10^{7}	1830
	10^{4}	2730
Beryllia	10^{9}	930
	10^{7}	1830
	10^{5}	2730
Magnesia	10^{12}	930
	10^{7}	1830
Thoria	10^{8}	930
	10^{4}	1830
	10^{2}	2730
Zirconia	10^{7}	93
	10^{5}	1830
	10^{2}	2730

furnace muffle were left open to allow slow circulation of air over the samples. After exposure at temperature for 100 hours, the boats were removed from the furnace and the samples cleaned, reweighed and observed microscopically. The average of the three samples was used to determine the percentage of weight loss during the test.

Platinum-Rhodium Alloys

Samples of platinum, platinum-10% rhodium, platinum-13% rhodium and platinum-30% rhodium were tested in the manner described on page 35. Exposure was at 2500°F for 100 hours. Table V shows the percent of the original weight lost during exposure. Each entry in the table is an average of at least three samples. Noteworthy is the absence of any weight gains in the material systems studied. This indicates that the principal reaction is with the oxygen in the air forming volatile oxides of platinum and rhodium. In all of the systems studied, no major incompatibility was found. It was noted that MgO sintered slightly to the surface

of the samples, indicating that there was a slight reaction between MgO and the platinum-rhodium alloys. The exact mechanism or extent was not determined due to the availability of other refractory oxides that appear to be compatible with platinum-rhodium.

All of the platinum and platinum-rhodium alloys examined after the 100-hour exposures at 2500°F exhibited considerable grain growth. Figure 13 shows a typical cross section of the wire (0.015-in. diameter). The effect of the grain growth on the stability and mechanical properties of wire was not investigated.

TABLE V. COMPATIBILITY OF PLATINUM-RHODIUM ALLOYS WITH REFRACTORY OXIDES IN AIR

Material	Oxide	Exposure Media	Average Wt Loss (pct)	Average Loss in Diameter (inch)
Pt	SiO_2	Air	2.40	0.0002
	Al_2O_3	Air	4.33	0.0004
	MgO	Air	-	-
	-	Air	4.66	0.0007
Pt10%Rh	SiO_2	Air	0.43	.0000
	Al_2O_3	Air	3.83	0.0001
	MgO	Air	0.40	-
	ZrO_2	Air	2.73	-
	ThO_2	Air	1.70	-
	-	Air	4.33	0.0004
Pt13%Rh	SiO_2	Air	6.20	0.0003
	Al_2O_3	Air	1.80	0.0002
	MgO	Air	-	-
Pt30%Rh	Al_2O_3	Air	1.71	-
	SiO_2	Air	1.25	-
	ThO_2	Air	1.99	-

Iridium-Rhodium Alloys

Pure iridium and iridium-40% rhodium were studied for their compatibility with the refractory oxides in the same manner as the platinum-rhodium alloys. The weight loss data is presented in Table VI, where the effects of the higher oxidation rate of Ir are clearly shown. All of the specimens had clean surfaces, indicating that the only reaction was a continual loss of metal due to the formation of volatile oxides. The data in Table VI indicates that pure iridium will not be an acceptable material for thermocouples due to its poor oxidation properties when compared to Ir40%Rh or the platinum and platinum-rhodium alloys.

TABLE VI. COMPATIBILITY OF IRIDIUM-RHODIUM ALLOYS WITH REFRACTORY OXIDES IN AIR

Exposed Material	Exposure Media (*)	Average Preexposure Weight (mg)	Average Weight Loss (mg)	Average Weight Loss (pct)
Ir	Al_2O_3	105.77	33.93	32.1
Ir	ThO_2	105.13	64.03	60.9
Ir	ZrO_2	106.60	35.50	33.3
Ir	SiO_2	107.63	82.10	76.3
Ir40%Rh	Al_2O_3	75.17	3.63	4.8
Ir40%Rh	ThO_2	75.2	3.13	4.2
Ir40%Rh	ZrO_2	74.47	6.67	8.9
Ir40%Rh	SiO_2	76.30	11.27	14.8

(*) All specimens exposed at 2500°F for 100 hours in slowly moving air.

Etchant:
80% H_2O
Saturated with
NaCl + 20% HCl
Electrolytic

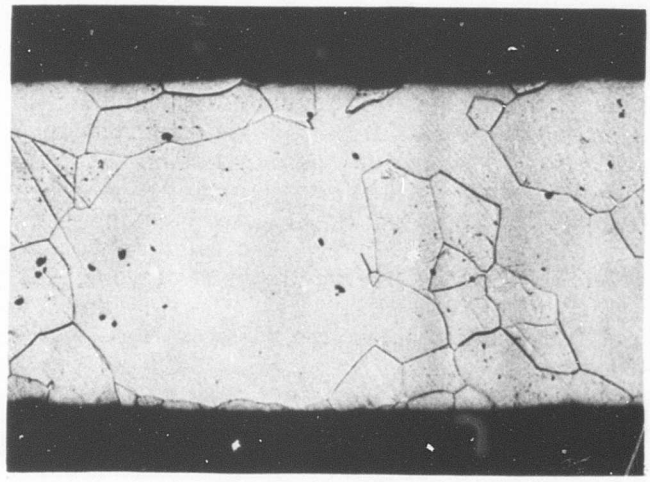

Magnification
125X
(Reduced 20%)

Pt 10% Rh Exposed in ZrO_2

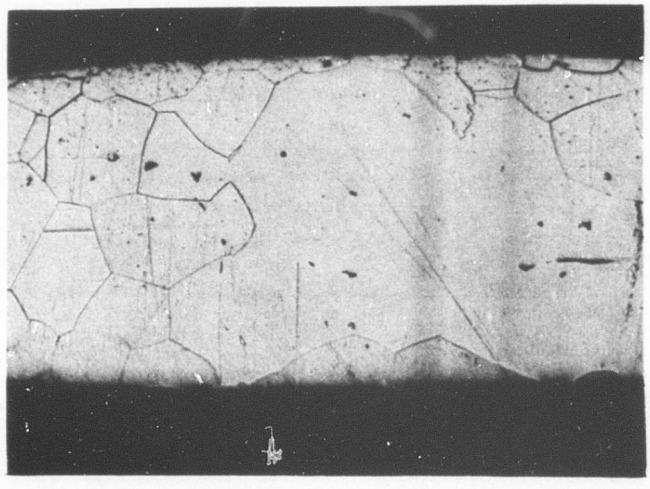

Magnification
125X

Pt 10% Rh Exposed in ThO_2

Figure 13. Microstructure of Platinum 10% Rhodium After 100 Hours at 2500°F.

Tungsten-Rhenium Alloys

Tungsten reacts very rapidly with oxygen and therefore cannot be considered for use as an exposed junction. Tungsten-rhenium thermocouple alloys have very good high temperature characteristics and a much higher signal strength than the platinum-rhodium alloys. The tungsten-rhenium couple can be used inside a protective sheathing, where it does not come into contact with oxygen. To test their compatibility with Al_2O_3 and ThO_2 and Nd_2O_2, two tungsten-rhenium alloys were exposed, in argon, for 98 hours at 2350°F. The samples were weighed before and after exposure. Table VII lists the average percent of weight loss from three samples, each weighing about 100 milligrams. The very small weight loss indicates that in an inert atmosphere, there are no compatibility problems with the two principal refractory oxides.

Complete thermocouples of Ir-Rh and Pt-Rh were exposed to air at 2500°F for times between 25 and 100 hours. The weight loss measured for each couple is shown in Table VIII. Compared at equal exposure times, the Pt-Rh couples were much more resistant to weight loss than the Ir-Rh couples. Also, the Pt6%Rh versus Pt30%Rh performed slightly better than Pt versus Pt10%Rh.

Summary

Platinum-rhodium alloys appear to be the best suited for use in an oxidizing atmosphere. Pt versus Pt10%Rh and Pt6%Rh versus Pt30%Rh are both adequate in this respect. Although Pt6%Rh versus Pt30%Rh has not received widespread use, it is inherently more resistant to preferential oxidation (due to the Rh content) and calibration drift caused by the possible diffusion of platinum or rhodium from one leg to the other. The Pt versus Pt10%Rh couple has been widely used in industry and is used as a standard thermometer to define the International

TABLE VII. WEIGHT LOSS OF W-Re ALLOYS IN ARGON

Material	Oxide	Atmosphere	Average Weight Loss (pct)
W5%Re	Al_2O_3	Argon	0.1
	ThO_2	Argon	0.36
	Nd_2O_3	Argon	1.2
W26%Re	Al_2O_3	Argon	0.1
	ThO_2	Argon	0.4
	Nd_2O_3	Argon	0.2

TABLE VIII. WEIGHT LOSS OF THERMOCOUPLES EXPOSED IN AIR AT 2500°F

Thermocouple	Time (Hr)	Preexposure Weight (Mg)	Weight Loss (pct)
Ir/Ir40%Rh	30	158.3	17.6
Ir/Ir40%Rh	48	136.4	24.3
Ir/Ir40%Rh	70	163.6	37.2
Ir/Ir40%Rh	96	143.2	46.7
Pt-6Rh/Pt30%Rh	25	144.2	0.28
Pt-6Rh/Pt30%Rh	70	121.5	0.91
Pt-6Rh/Pt30%Rh	100	128.7	1.55
Pt/Pt10%Rh	25	110.8	0.72
Pt/Pt10%Rh	70	109.1	1.65
Pt/Pt10%Rh	100	104.3	1.82

Temperature Scale between 1167°F and 1927°F. It should be pointed out that all exposed hot-junction thermocouples will drift during long-time exposures at temperatures in the range of 2500°F; allowances must be made for this, since little can be done to suppress the mechanism causing oxidation. The high oxidation rate of iridium eliminates this couple for consideration in an oxidizing atmosphere.

Tungsten-rhenium thermocouples have a much larger output than the platinum-rhodium alloys. They may be used in conjunction with protective sheathing to avoid oxidation.

None of the refractory oxides, with the exception of MgO, appear to be incompatible with the platinum-rhodium alloys. The principal reaction during exposure at 2500°F in air seems to be the formation of volatile oxides, causing slight weight losses over the 100-hour exposures. Two oxides were chosen for further study and use during the course of the program. Al_2O_3 and ThO_2 were chosen because of their apparent compatibility and availability. Al_2O_3, in particular, is available in several grades and in almost any shape or form desired.

ACCURACY AND RELIABILITY

The steady-state accuracy and reliability of thermocouples placed at the turbine inlet will initially be dependent upon the design of the entire probe. These considerations were discussed in the section on thermodynamic and analytical analysis and stem chiefly from the conduction and radiation losses from the hot junction. Through proper probe placement and design, these errors will be minimized and their magnitude known. Over the lifetime of the probe, other factors contribute to increased error levels and reduced reliability. These include calibration

drift due to contamination by the combustion products or impurities in the air or fuel, reaction with impurities in the ceramic insulators and reduced reliability caused by the mechanical action of the high velocity gases or thermal fatigue during startup or shutdown of the engine. The cause and extent of these effects must be understood and contained within acceptable limits. Progress toward this goal has been made, but further work will be necessary before definite design data is obtained.

Drift Tests

The net potential produced by a thermocouple originates in the region of thermal gradient. The "Seebeck" effect describes the potential produced by junctions of dissimilar metals held at different temperatures. The potential is dependent upon the composition of the wires and the temperature difference between the junctions. In addition, a wire of homogeneous composition placed in a temperature gradient will produce an electrical potential (the Thompson effect). The sum of these two effects is the total potential produced by the thermocouple. Any change which occurs in the composition of the thermoelements anywhere in the thermal gradient zone will change the thermocouple potential.

Thermoelectric instability (drift) can be caused by several factors. Gradual compositional changes caused by preferential volatilization of one of the constituents is one of the most widely held mechanisms. In the case of Pt-Rh couples, the rhodium tends to form a volatile oxide faster than platinum, causing a net platinum enrichment of the high alloy leg and the consequent reduction of the electromotive force. Other workers discount the importance of this effect and find that the principal source of thermoelectric instability is contamination, often from the ceramic insulators. Walker, Ewing and Miller[11] report that drift of Pt-Rh couples is very minor when they are heated in an inert atmosphere and supported by very pure alumina. Very small amounts of Si and Fe were found to have a large effect on drift in these couples.

Applied to TIT probes, an exposed junction would be subject to contamination by combustion products and impurities in the fuel as well as impurities in the insulation. A protected junction would be exposed only to the insulation and sheathing material.

Drift tests were performed on Ir versus Ir40%Rh and Pt6%Rh versus Pt30%Rh thermocouples. The thermocouples were exposed for 50 to 100 hours in slowly moving air or argon at 2400°F. The thermocouple emf was measured and compared to a referee thermocouple placed adjacent to the test thermocouples. The difference between the indicated temperature of the test probes and the referee thermocouple was taken as an indication of drift. The results of Ir versus Ir40%Rh are shown in Figure 14.

The drift results for the iridium thermocouples in air indicate that there is a time (at temperature) dependent mechanism that results in alternating positive and negative drift prior to failure. All of the Ir versus Ir40%Rh thermocouples tested in air failed due to excessive oxidation of iridium thermoelement. The times to failure varied from 24 hours to 104 hours. A photograph of the hot junction after 100 hours' exposure is shown in Figure 15A. The pure iridium thermoelements are badly oxidized, whereas the Ir40%Rh has hardly any oxidation loss. There

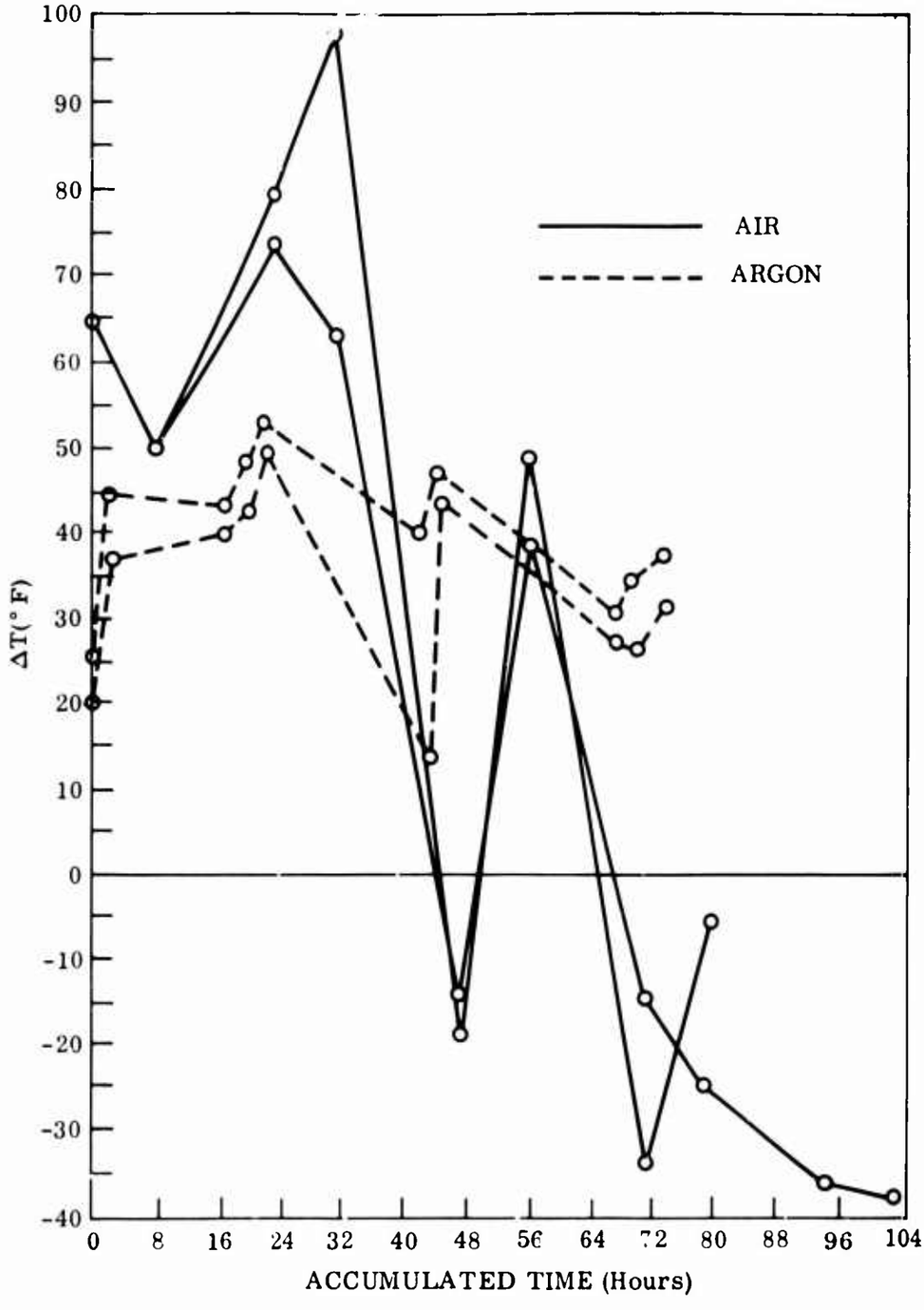

Figure 14. Drift Tests for Ir Versus Ir40%Rh Thermocouples.

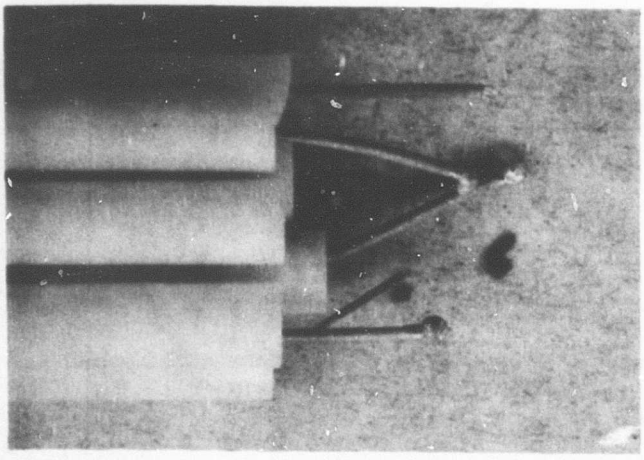

A

Ir vs Ir40%RH
104 Hours' Exposure
at 2400°F in Air

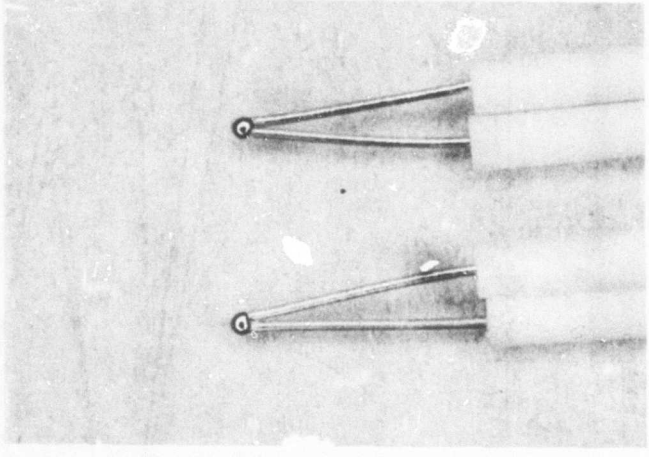

B

Ir vs Ir40%Rh
74 Hours' Exposure
at 2500°F in Argon

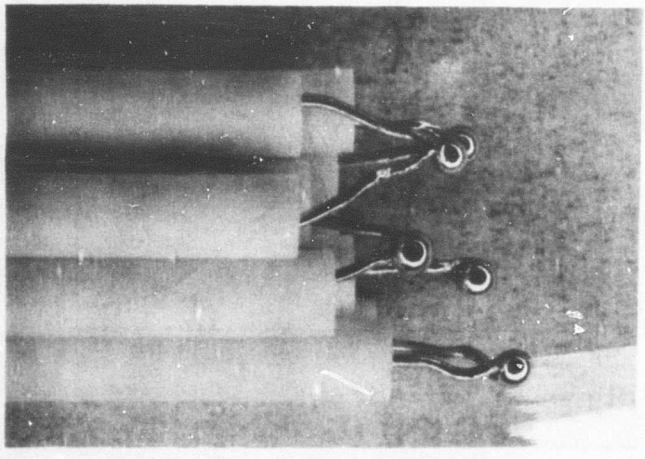

C

Pt6%Rh vs Pt30%Rh
104 Hours' Exposure
at 2400°F in Air

Figure 15. Drift Test Thermocouples After Exposure.

is no satisfactory means available by which the oxidation rate of iridium can be reduced other than by alloying the iridium with rhodium. This method, however, would reduce the already low thermoelectric emf of this type of thermocouple. It forms a volatile oxide at a lower temperature and at a much greater rate than Rh, indicating that preferential oxidation was the cause for the instability of the Ir-Rh couples when exposed in air. The tests in argon confirm this assumption, as much less drift was measured. The thermocouples illustrated in Figure 15B show no visible deterioration after 74 hours in argon at 2500°F.

The drift results for the Pt6%Rh versus Pt30%Rh thermocouples are shown in Figure 16. This thermocouple did not show such wide variations in emf output versus time, and all of the test probes were in very good condition after 104 hours (Figure 15C).

The calibration drift with time for the Pt-Rh couple was well within the ±15°F limits set by the program. The absolute difference between the referee and test couples was not considered as important as the change with time of the reading in this test. Ir-Rh thermocouples must be used in an inert atmosphere where preferential oxidation will not affect their mechanical and electrical properties.

Two Pt6%Rh versus Pt30%Rh thermocouples were exposed for 28 hours to the hot combustion products in a turbine atmosphere simulator. The atmosphere simulator burned JP-4 fuel. Sample temperatures varied between 1850°F and 2300°F, and gas velocity was approximately 700 feet per second. The thermocouples were calibrated at 2000° and 2400°F before and after exposure. One of the two thermocouples mechanically failed during the test and was repaired by spot welding to allow completion of the final calibration. During exposure, the unbroken couple had drifted +3 degrees at 2000°F and -5 degrees at 2400°F. The rewelded couple had drifted -5 degrees at 2000°F and -30 degrees at 2400°F.

The measured drift, with the one exception, was very small and was within the program limits. These tests indicate that for this length of time, exposed Pt6%Rh versus Pt30%Rh thermocouples would not be adversely affected by contamination by combustion products in a turbine atmosphere. Final conclusions on this subject must await a more complete investigation.

Volume interdiffusion in platinum-rhodium alloys was studied to investigate mass transport across diffusion-bonded junctions. Diffusion couples were made by bonding 0.020-inch by 0.250-inch square foils of Pt to Pt10%Rh to Pt30%Rh. Bonding pressure was 20,000 psi at 1600°F for 25 seconds. Interdiffusion during bonding was limited to less than 0.001 inch on either side of the part line. The couples were exposed to 2400°F for 25, 50 and 100 hours in a resistance furnace open to the atmosphere. The couples were then sectioned; the composition profiles for the Pt30%Rh versus Pt10%Rh are shown in Figure 17A, and those for Pt versus Pt10%Rh are shown in Figure 17B. Measurable changes in composition were limited to less than 0.007 inch on either side of the mean concentration for the Pt versus Pt10%Rh samples and to less than 0.004 inch for the Pt6%Rh versus Pt30%Rh. Volume diffusion should have little effect on calibration drift, since all composition changes occur with the junction itself and not in the thermal gradient zone.

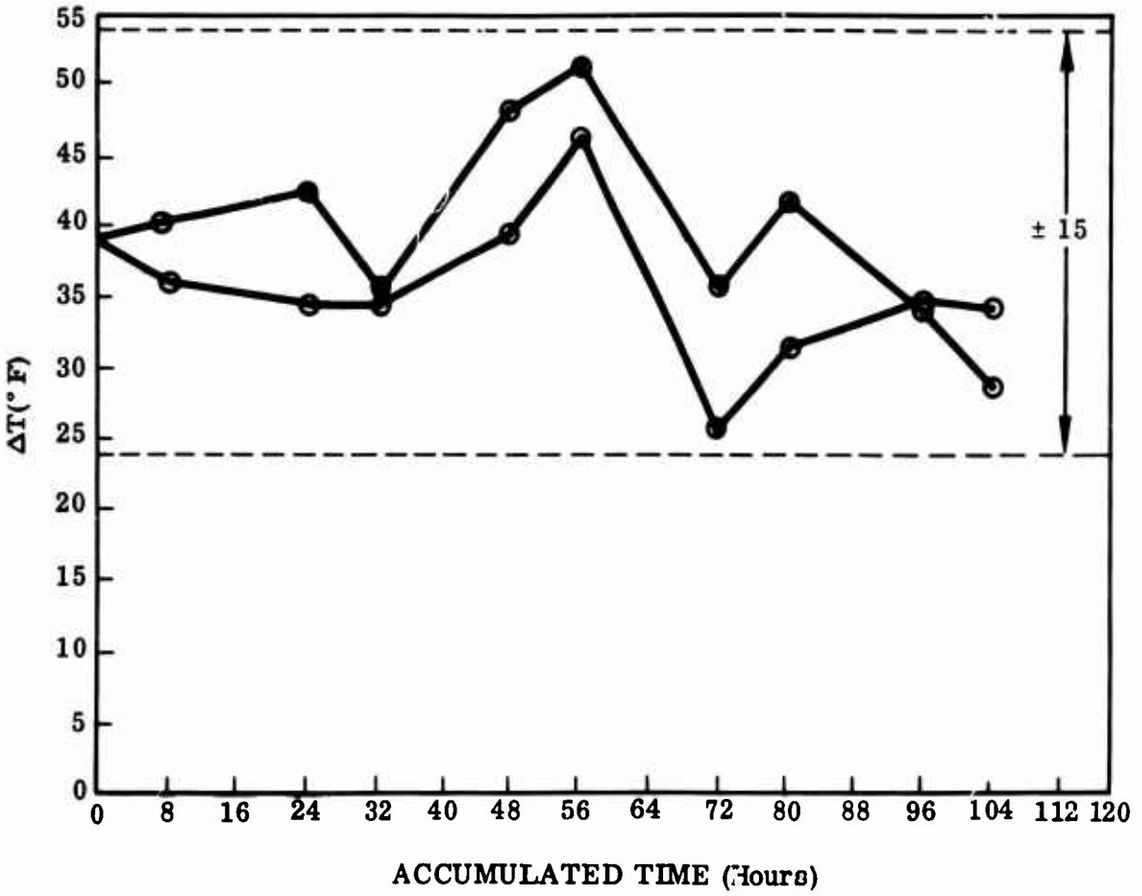

Figure 16. Drift Test Results for Pt6%Rh Versus Pt30%Rh Thermocouples.

Mechanical Stability

A sample of 0.010 inch-diameter Pt30%Rh thermocouple wire was exposed to high-velocity gases to measure erosion of exposed junctions. The sample was placed in the atmosphere simulator and maintained at an average temperature of 2000°F. The gas velocities were approximately 700 feet per second. No measurable reduction in the wire diameter was observed after exposure for 28 hours. Weight loss data was unreliable in this case due to deposits of carbon adhering to the surface. These results indicate that erosion of an exposed junction will not prove to be a major problem. Creep and thermal and mechanical fatigue, however, undoubtedly will pose serious design problems. Specific tests were not undertaken to investigate these effects.

RESPONSE

The response rate of a thermocouple subjected to a step change in temperature was described by equations 13 and 21. In this idealized case, errors due to conduction radiation and recovery losses were not considered. In addition, it was assumed that the temperature change occurred instantaneously. This, of course, can only

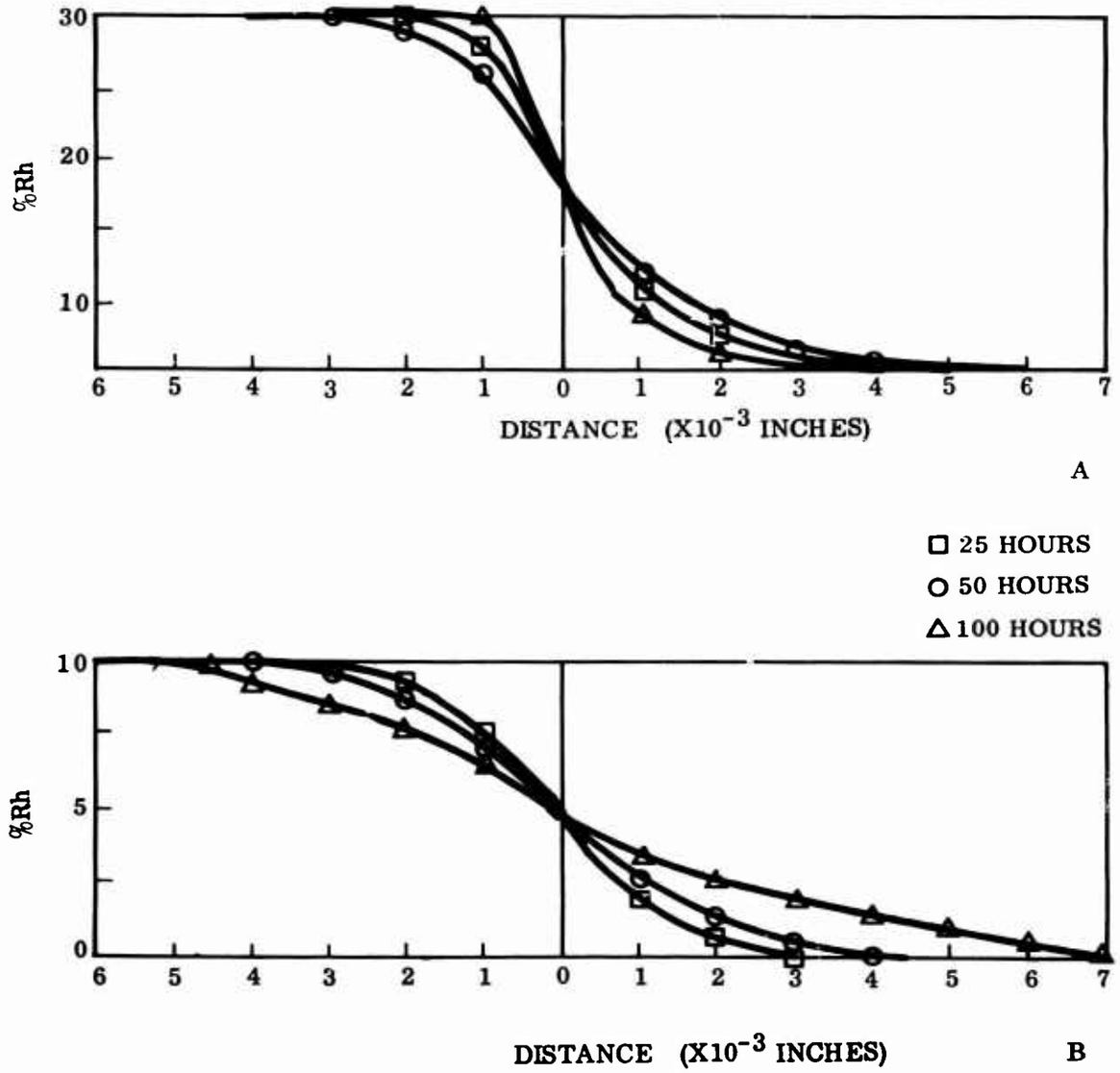

Figure 17. Composition Profiles for Pt-Rh Diffusion Couples Exposed at 2400°F.

be approximated. Good results are obtainable as long as the temperature change occurs at least one order of magnitude faster than the response time of the sensor. Response time measurements were carried out in two phases during this program. The first consisted of the comparative testing of different thermocouple sizes, materials and configurations under constant reproducible conditions. The second phase employed high-velocity moving gas atmosphere to simulate actual conditions in a turbine engine.

Experimental Methods

The response time of each thermocouple was determined by sudden immersion into a hot fluidized bed. The step change in temperature occurs in the time needed to translate the thermocouple from essentially ambient conditions into the fluidized bed. The test apparatus is shown in Figure 18. The use of a fluidized bed eliminates radiation and recovery errors and provides a consistent and accurate means of assessing the response characteristics of the test probes.

In operation, a bed of solids (200 mesh ZrO_2) is placed into a resistance heated tube and supported on a permeable plate. Air, or other suitable gases, is admitted to flow through the bed until fluidization occurs, at which point the particles behave in a fashion analogous to a boiling liquid. The test probe is attached to a linear actuator for rapid immersion into the fluid bed. The thermocouple hot junction is cooled by compressed air supplied through a diffuser ring at the starting location. When a stable starting temperature is achieved, the actuator is energized, plunging the probe into the fluid bed, where the probe rapidly reaches an equilibrium temperature. During the step change in temperature, the emf output of the probe is recorded as a function of time on a high-speed oscillograph. The time response of the actuating system (determined experimentally) was subtracted from the overall elapsed time for response time calculations.

Experimental Results and Discussion

The time constant, τ, was shown previously to be given by

$$\tau = \frac{W C_p}{A h_c} \qquad (14)$$

The time constant for single-junction couples of a given material may be lowered by

1. Lowering the mass
2. Increasing the area
3. Increasing the convective heat transfer coefficient

The fluidized bed provides a means of keeping the heat transfer coefficient constant.

A series of tests was conducted using 0.010-inch-diameter chromel-alumel wire to determine the effect of junction configuration on thermocouple response. Each thermocouple was mounted into an alumina protection tube with approximately

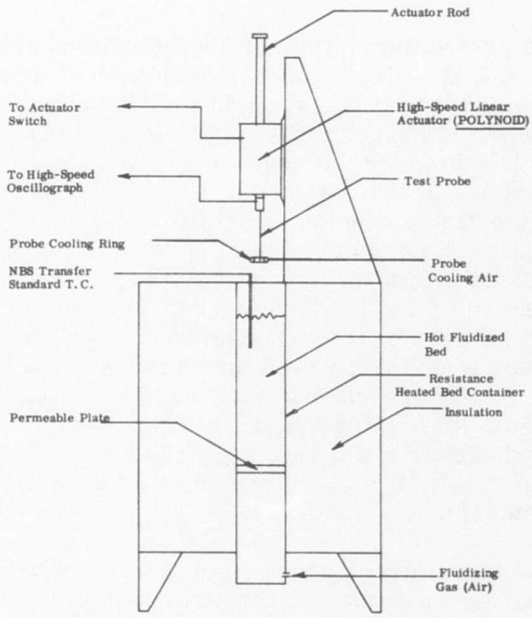

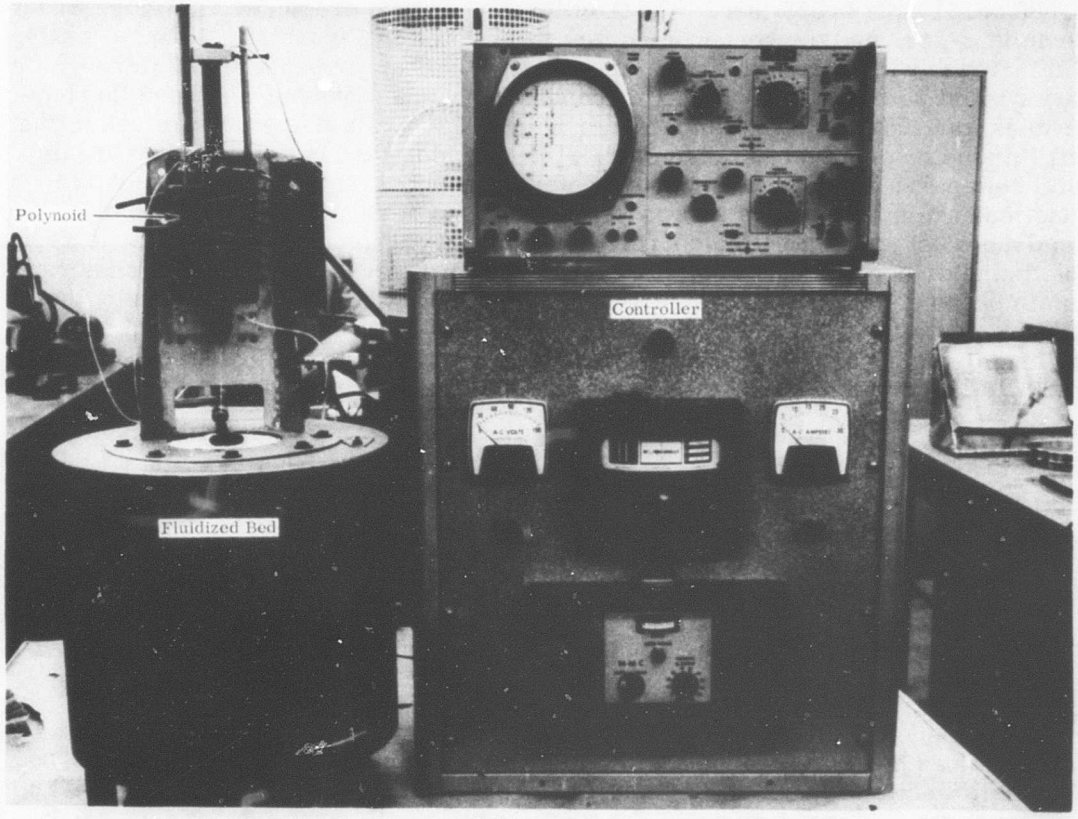

Figure 18. Fluidized Bed Testing Apparatus.

1 inch of exposed wire protruding. Typical configurations are shown in Figure 19. Junctions shown are: A & B - single junction with helical wound leads; C - multijunction with helical wound leads; D - straight multijunction; and E - straight single junction. The purpose of this experiment was to evaluate the effects of coiled hot leads (to increase the hot-immersion length and to reduce the conduction losses) on the characteristic response of the thermocouples, as well as to demonstrate the effect of the multiple junction concept. In addition, a single junction thermocouple made of flattened 0.010-inch chromel-alumel wire was also tested. The response curves for these tests are shown in Figure 20. The fraction of the steady-state temperature change indicated by the thermocouple is shown as a function of time. All the thermocouples were compared with couple E, the straight single junction. Adding to the immersion length decreased the response rate (curve A) by adding mass to the junction. Flattening the wires (curve F) increased the area while the mass remained constant, increasing the response. The multijunction couples (curves C & D) responded even more rapidly. The helical lead configuration also slowed the response of the multijunction and caused the overshoot to persist longer than for the straight multijunction.

The effect of mass, or more directly the effect of the diameter of fusion-welded wire hot junctions, was investigated by performing response tests in the fluidized bed on Pt6%Rh versus Pt30%Rh thermocouples. Wire of three diameters was used: 0.005, 0.010 and 0.015 inch. The oscilloscope curves are shown in Figure 21 for each diameter, and the response curves are plotted in Figure 22. Response rates did increase with decreasing wire diameter. The 90% response times were recorded at 305, 540 and 765 milliseconds. The time constant for these thermocouples was plotted against diameter in Figure 23. Two diameters are used: the wire diameter and the bead diameter. The time constant is seen to vary linearly with both parameters as would be expected from equation (13), even though the junctions are not cylinders as was assumed by the derivation of the equation. The bead diameter gives a better correlation of the data, since it extrapolates to zero as the diameter approaches zero. The most effective way to increase response rate is simply to decrease the mass as much as possible within the limits set by the requirements for mechanical strength. When this limit has been reached and the optimum single junction described, then the response may be further enhanced by adding a larger (stronger) junction to form a multijunction.

Multiple Junctions

The characteristic response of a multijunction thermocouple is compared to the response of a single junction of the same size in Figure 24. Oscilloscope traces are shown for both thermocouples on two different time scales. The multijunction was twice as fast as the single junction at 63% and 4 times faster at 90% of the step change. The multijunction also approached steady state more rapidly than the single junction, even though a large overshoot was recorded.

The response times of multijunction thermocouples measured using the fluidized bed are dependent upon the configuration of the thermocouple. The multijunction is vertically translated from a cold zone to the hot fluidized bed; thus, the leading portions of the thermocouple will reach the hot zone and be heated before the trailing portion. Since the response time of the thermocouple depends on the relative rate of heating in the three junctions, it will be

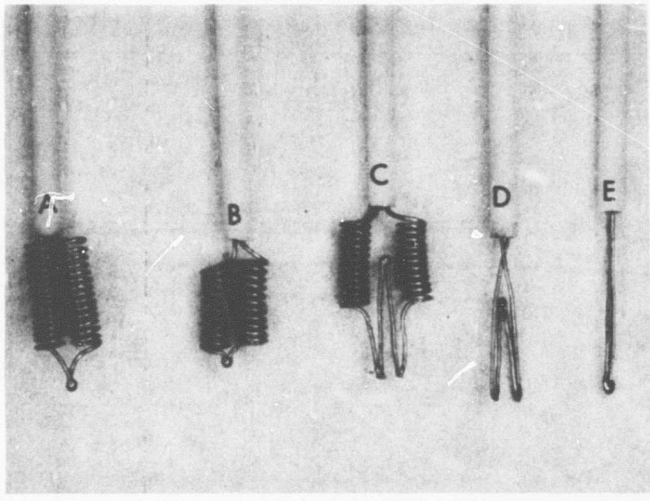

Figure 19. Typical Thermocouple Configurations Used for Response Testing.

influenced by their relative vertical position in the test apparatus with respect to the hot fluidized bed.

The enhancement of response time is dependent upon the more rapid heating of the additive junctions with respect to the bucking junction. Thus, if the additive junctions reach the hot zone first, the total response will be more rapid than if the backing junction is heated first. This was verified by tests made on chromel-alumel multijunction thermocouples of wire diameter equal to 0.010 and 0.005 inch. The configuration of each thermocouple tested is shown in Figure 25. The results are given in Table IX. Single-junction thermocouples were also tested for comparison. A considerable difference in the response time of configurations B and D was measured. All subsequent tests were made using thermocouples with configuration D.

For all wire of equal diameter, the multijunction thermocouples are considerably faster than a single-junction couple, the average 90% response being less than half that for the single junction. Comparing similar configurations made from different diameter wire shows that halving the diameter of the wire more than halved the 90% response time.

A series of three tests was made on a multijunction thermocouple to demonstrate the effect of relative junction size. Figure 26A shows the oscilloscope trace for a Pt6%Rh versus Pt30%Rh multijunction thermocouple with wire diameter of 0.010 inch. Figure 26B shows the response of the same thermocouple with the additive junctions trimmed to reduce their mass. The response curves are shown in Figure 27. The 90% response time was reduced from 660 to 350 milliseconds. No overshoot was observed in either case, indicating that the bucking junction had a time constant approximately equal to the additive junctions. Extra mass was then added to the bucking junction to slow its response, and the resulting multijunction response is shown in Figure 26C. The 90% response time was again reduced from 350 milliseconds to 242 milliseconds. This illustrates that the response time of a multijunction thermocouple is controlled by the mass of the additive junctions and by the ratio of their mass to that of the bucking junction.

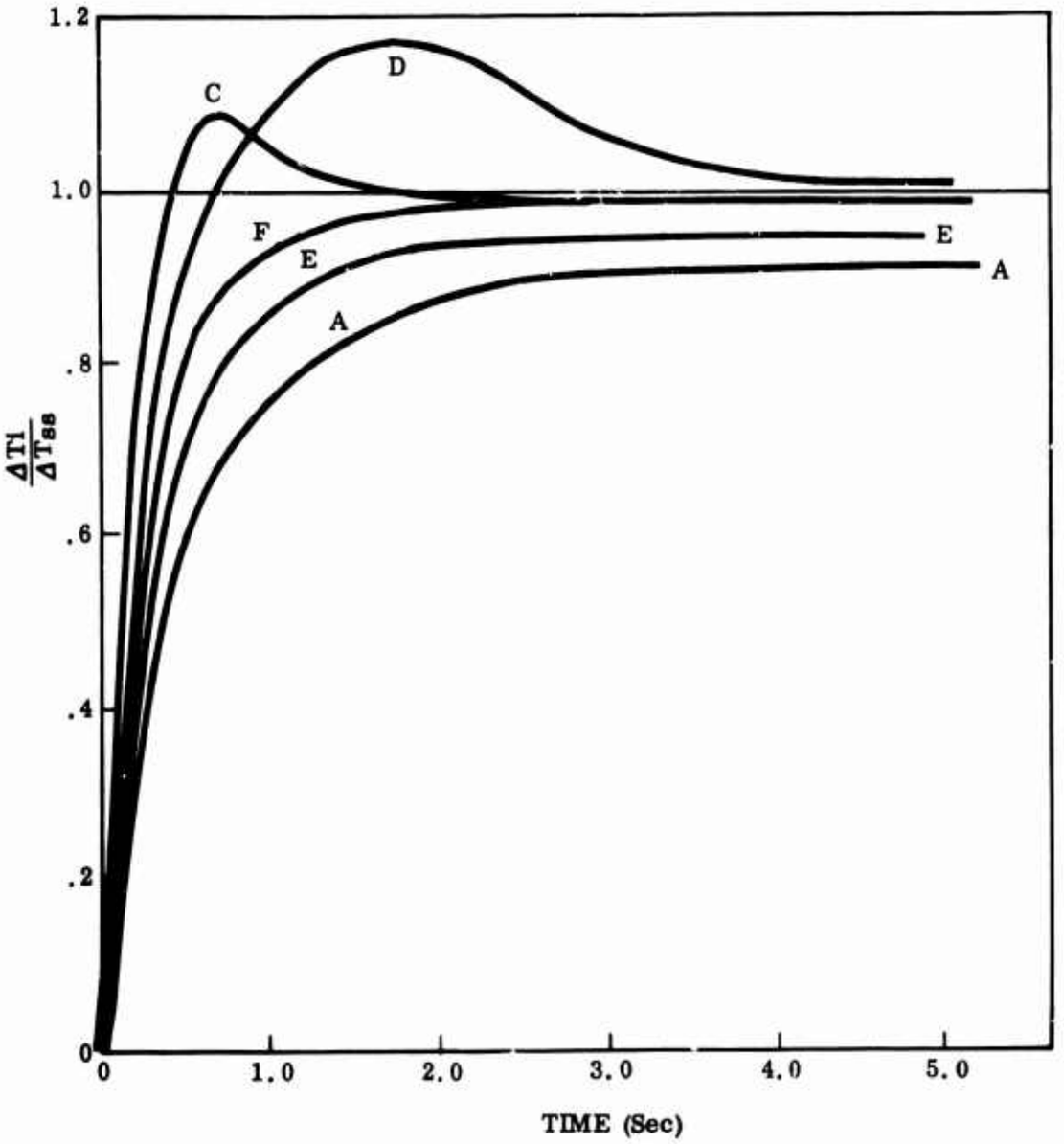

Figure 20. Response Curves for Various Hot Junction Configurations.

Foil Thermocouples

The time constant for a given material is influenced by the ratio of surface area to mass. Increasing this ratio increases the response rate of the thermocouple. The area to mass ratio may be increased with respect to wire couples by using thin foils in the form of flat or tubular junctions.

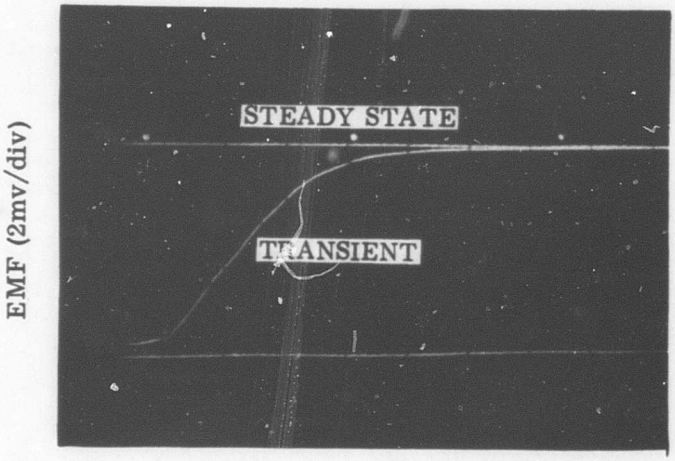

EMF (2mv/div)

Diameter = 0.005 inch

Time (100ms/div)

Diameter = 0.010 inch

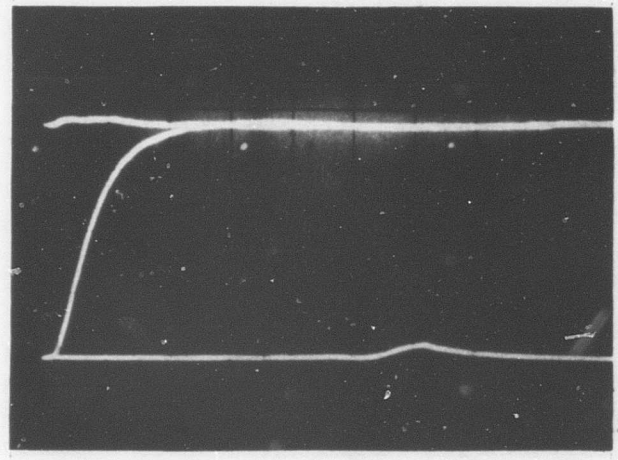

EMF (2mv/div)

Time (500ms/div)

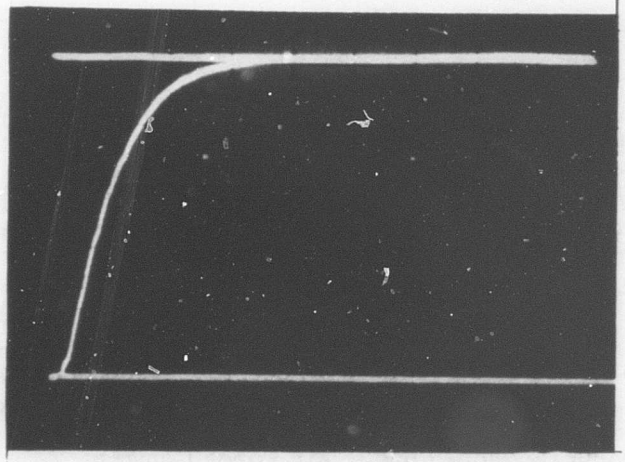

EMF (2mv/div)

Diameter = 0.015 inch

Time (500ms/div)

Figure 21. Oscilloscope Traces Showing the Response of Wire Thermocouples of 3 Diameters.

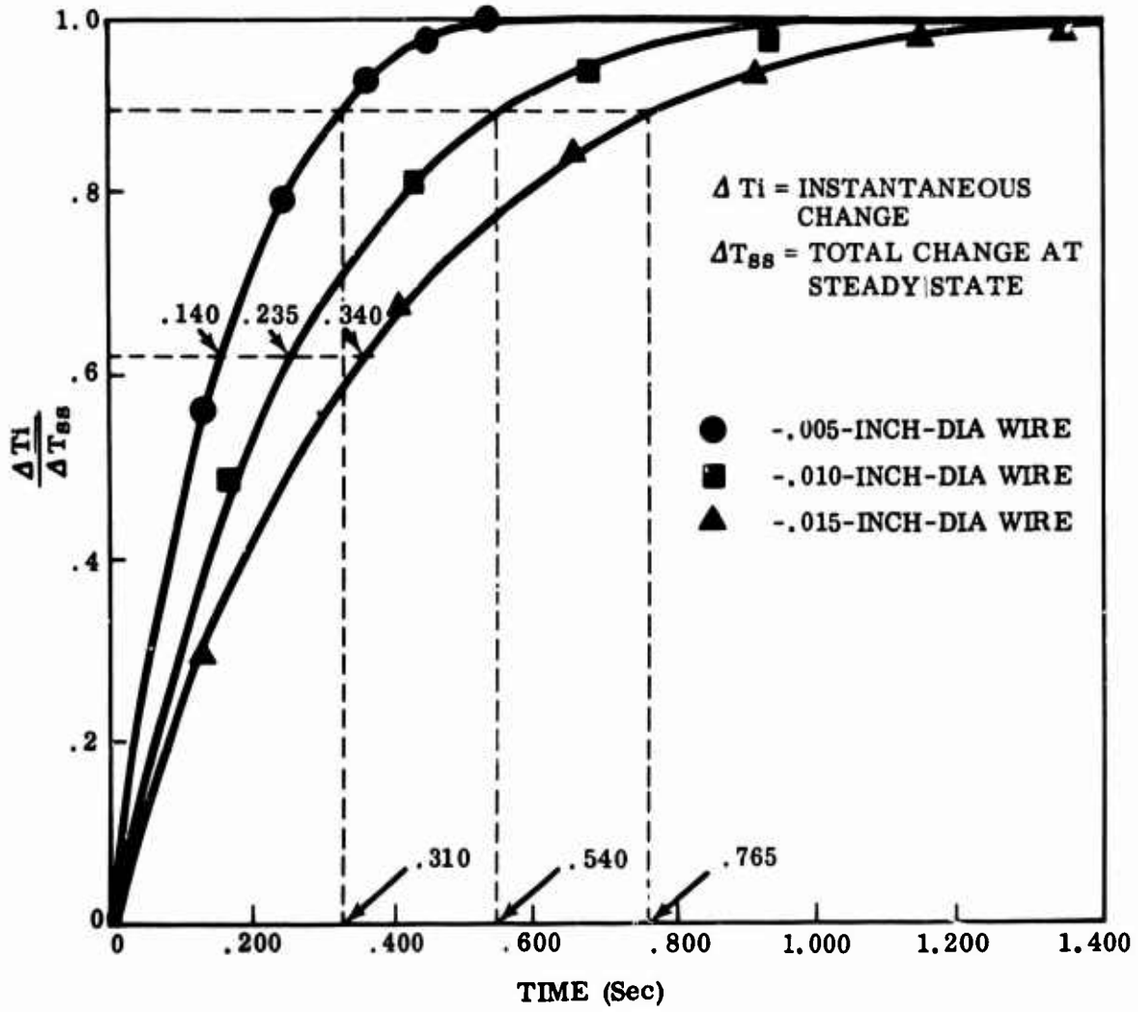

Figure 22. Response Curves for Wire Single-Junctions of 3 Different Diameters.

Tubular thermocouple junctions were fabricated using diffusion-bonding techniques to join 0.002-inch Pt6%Rh and Pt30%Rh foils. The foils were overlapped and then bonded in the Solar Diffusion Bonder.* A bonding pressure of 20,000 psi at 1500°F was applied for a period of 10 to 20 seconds. The mass of the junction was controlled by the extent of the overlap. The bonded foils were then rolled into a tubular shape 0.75 inch long by 0.025 inch in diameter. An example of a tubular junction including lead wires welded to either end is shown in Figure 28. Two preliminary thermocouples were made with 0.004-inch overlapping junctions. The longitudinal seam that was formed when the foil was rolled to form a tube was welded in the first couple and left open in

*The Solar Diffusion Bonder is being Developed under Air Force Contract AF 33(615)2304.

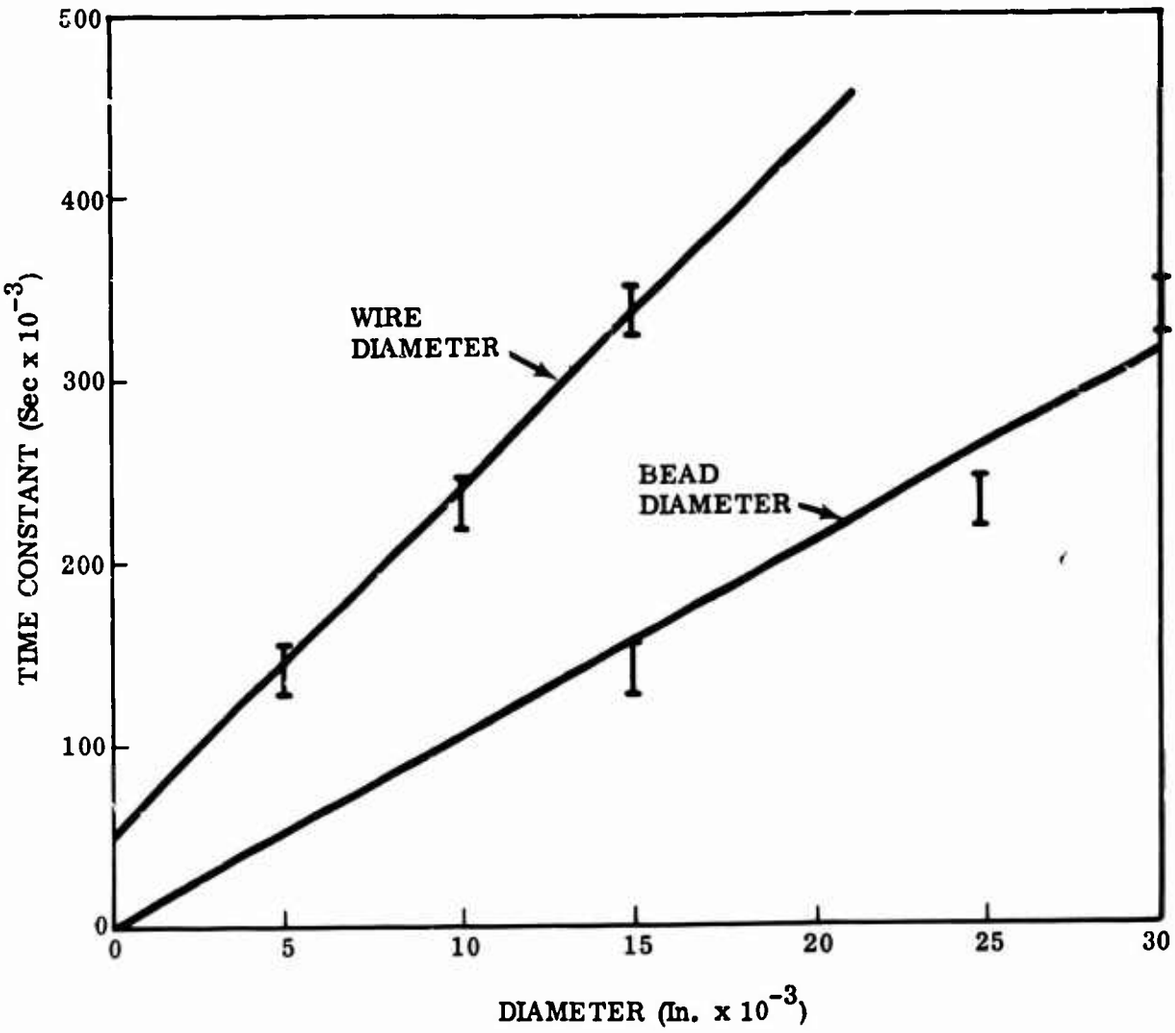

Figure 23. The Time Constant τ Plotted Against Wire and Bead Diameters for Three Single-Junction Thermocouples.

the second. The welded seam junction exhibited a 90% response time of 1500 milliseconds and a time constant equal to 900 milliseconds. The response time was greatly enhanced by not welding the seam. A 90% response time of 850 milliseconds and a time constant of 300 milliseconds were recorded.

A tubular multijunction was constructed by tack-welding the three overlapping junctions in place and then diffusion bonding. The additive junctions were overlapped 0.005 inch and the bucking junctions 0.025 inch. The overall dimensions of the multijunction were 0.025 inch in diameter by 3/4 inch long to conform to the single junction tubular thermocouples previously tested. The three junctions were separated by 1/8 inch. The lengthwise seam was overlapped but not welded. An oscilloscope trace for the response test of this multijunction thermocouple is shown in Figure 29. The output emf is shown as

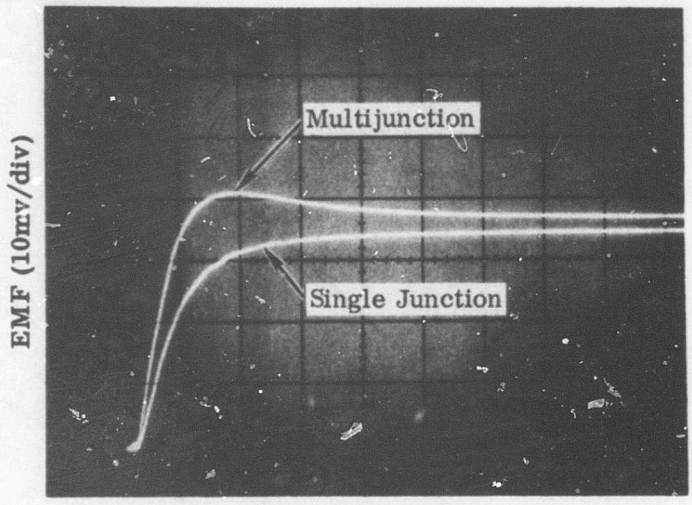

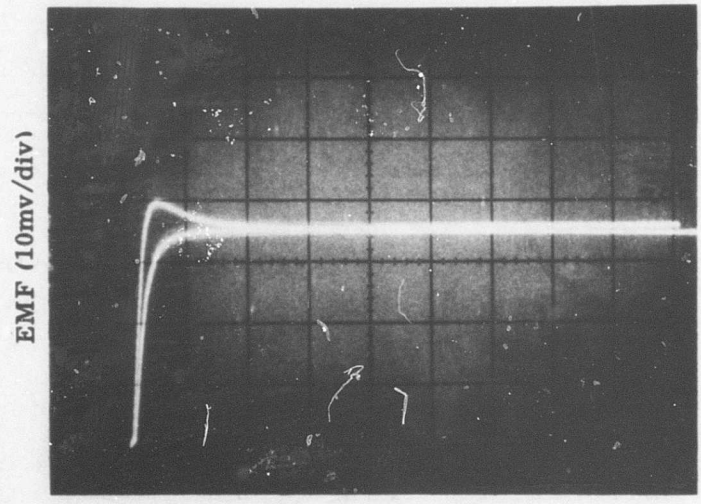

Figure 24. Oscilloscope Traces Comparing the Response of Single-Junction and Multijunction Thermocouples.

TABLE IX. EFFECT OF CONFIGURATION ON MULTIJUNCTION RESPONSE IN THE FLUIDIZED BED

Configuration	90% Response Time	
	0.010 Diameter (ms)	0.005 Diameter (ms)
A (Single Junction)	1350	600
B	700	250
C	640	225
D	350	-

Measured Response Times for Chromel-Alumel Multiple Junction Thermocouples.

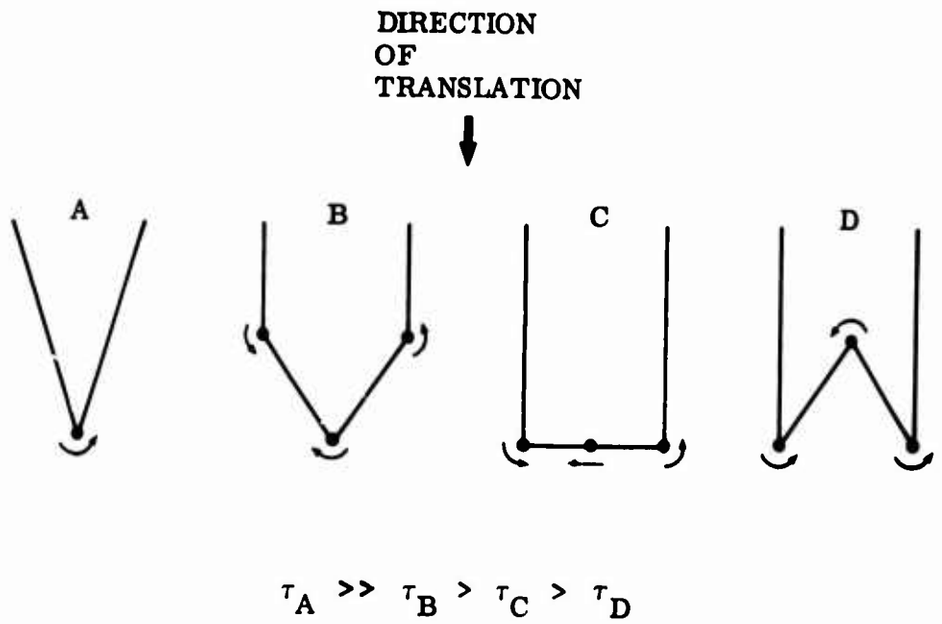

Figure 25. Geometrical Configurations of Multijunctions Tested in the Fluidized Bed.

a function of time. These data are plotted in Figure 30 as the fraction of the total step change in temperature that is registered by the hot junction as a function of time. The response time for 90% of the step change was 430 milliseconds and for 63% of the step change was 130 milliseconds. This response time is considerably better than the single-junction tubular thermocouples tested earlier. No overshoot was observed, indicating that the response may be further enhanced by adding more mass to the bucking junction.

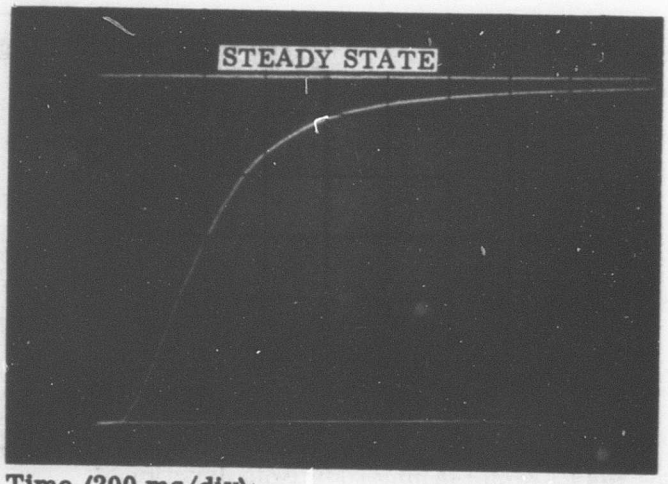

A
Multijunction with
Untrimmed Additive
Junctions ($n < 1$)

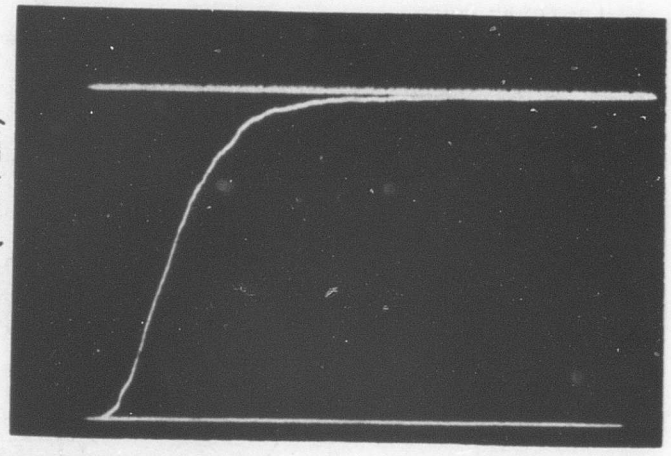

B
Multijunction with
Additive Junctions
Trimmed ($k \approx 1$)

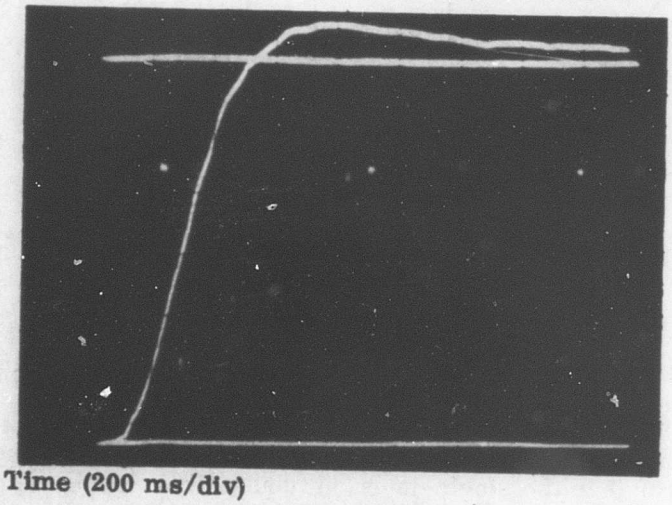

C
Multijunction with
Mass Added to
Bucking Junction
($k > 1$)

Figure 26. Oscilloscope Traces Showing the Response of Multijunction Thermocouples with Different Junction Masses.

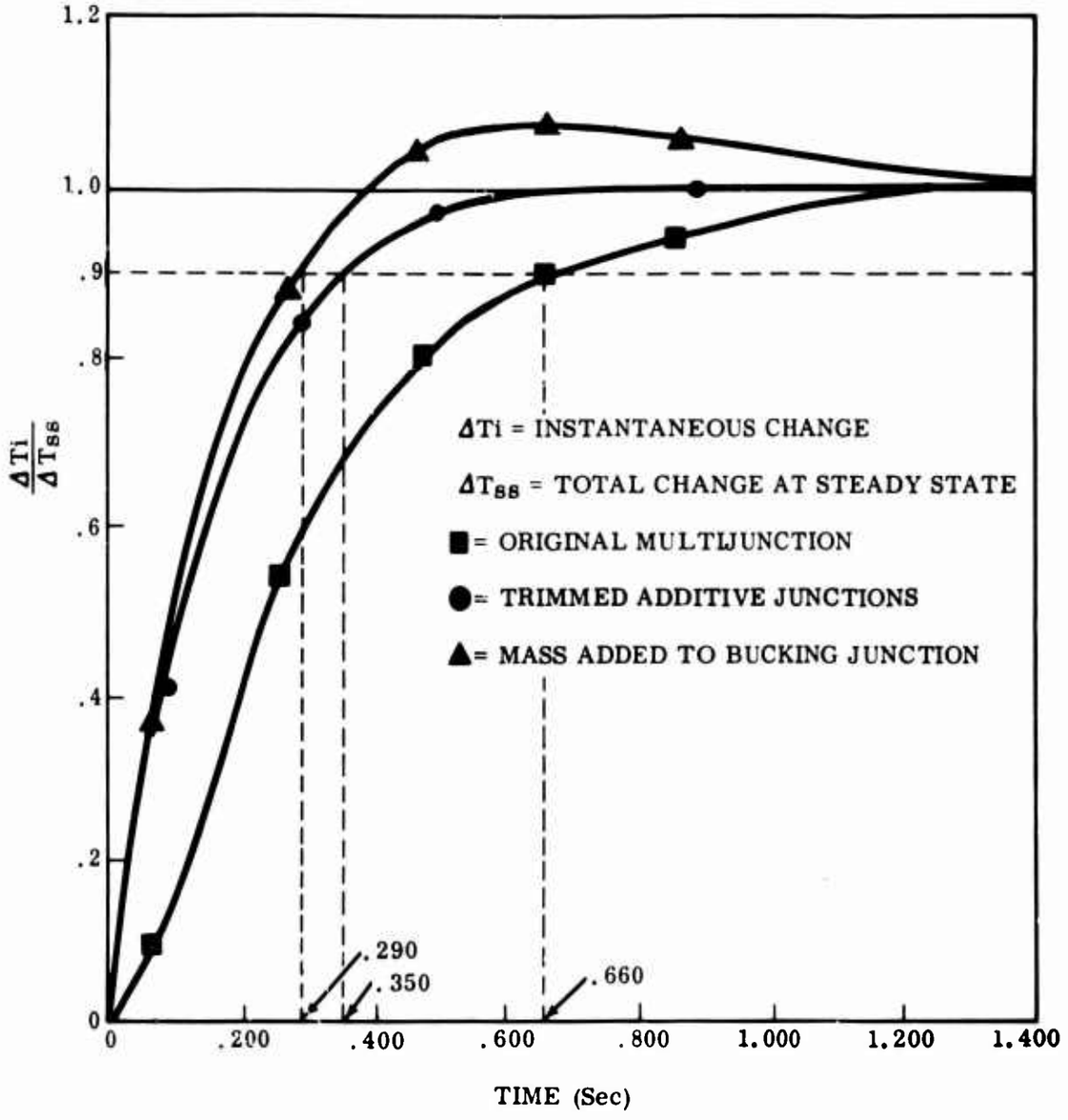

Figure 27. Response Curves for Wire Multijunctions of Different Junction Masses.

A flat foil thermocouple was fabricated by fusion welding 0.002-inch Pt6%Rh and Pt30%Rh foils. The thermocouple was in the form of a strip 1/8 inch wide by 3/4 inch long. Lead wires were spot-welded to the foil 1/4 inch from the junction. An oscilloscope trace is shown for the response test in Figure 31, and the fraction change in temperature as a function of time is illustrated in Figure 32. It can be seen that 90% of the step change is recorded in 430 milliseconds. The time constant was measured to be 155 milliseconds.

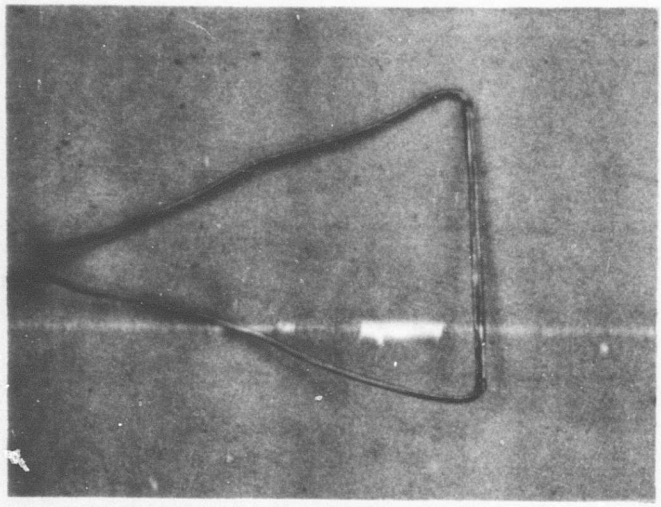

Figure 28. Seam-Welded Tubular Hot Junction.

Figure 29. Oscilloscope Trace Showing the Response of a Tubular Multijunction.

Miniature Sheathed Thermocouple Probes

A miniature sheathed thermocouple probe with an overall diameter of 0.010 inch was tested for its response time. The Pt versus Pt10%Rh thermocouple wires (0.001 in. diameter) were welded to the platinum sheath at the junction to provide maximum heat transfer. Figure 33 plots the fraction of the steady-state step change recorded by the thermocouple as a function of time. The time constant was measured as 140 milliseconds, and the 90% response time was measured as 310 milliseconds.

Response Tests in Moving Gas

Thermocouple response was measured in a moving gas atmosphere. A single wire junction, a multijunction and a fusion-welded foil junction were tested at gas velocities ranging from 100 to 215 feet per second. Response rates were found to increase as the gas velocity increased and were higher than those measured using the fluidized bed. All the thermocouples were Pt6%Rh versus Pt30%Rh.

A diagram and a photograph of the test apparatus are shown in Figure 34. Acetylene and oxygen were ignited at the burner, and compressed air was added to increase the gas velocity. The hot gases were directed into an open ceramic tube which served as a test chamber. The test thermocouples were plunged into the moving gas through ports in the side of the chamber by the polynoid used previously with the fluidized bed. The gas velocity was measured by a pitot tube and manometer. The thermocouple response was recorded by an oscilloscope and camera.

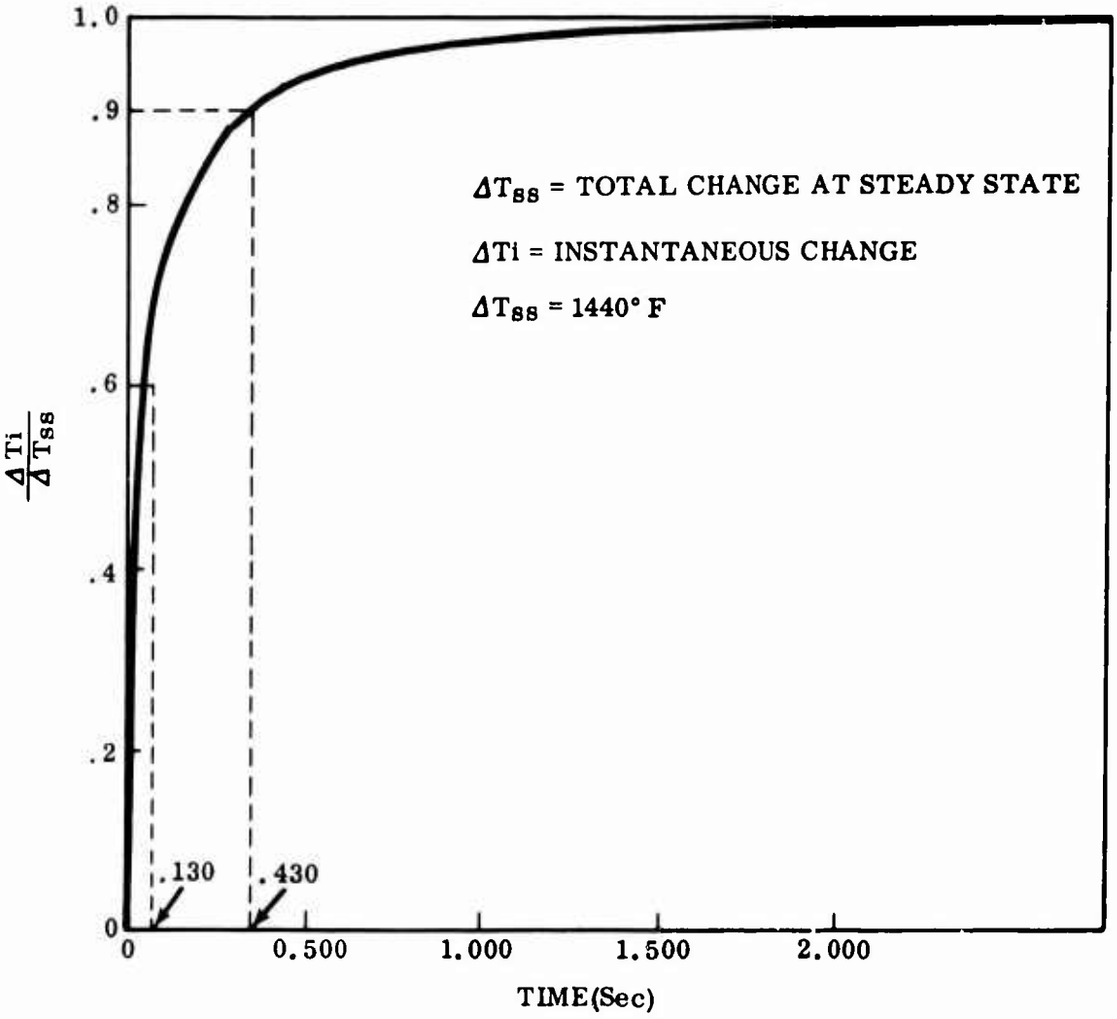

Figure 30. Response Curve for a Tubular Multijunction.

Oscilloscope traces of the response of a single-junction, spot-welded thermocouple (0.010-inch-diameter wire) are shown in Figure 35. The measured gas velocities were 105 feet per second for the first test and 210 feet per second for the second. The fraction of the total step change recorded by the thermocouple is plotted against time, for both tests, in Figure 36. The response rate increases for higher gas velocities. Ninety percent of the step change was recorded in 390 milliseconds in gas moving at 105 feet per second and in 320 milliseconds in gas moving at 210 feet per second.

A wire multijunction was tested at three gas velocities and compared with previous tests in the fluidized bed. Oscilloscope traces for gas velocities of 100, 145 and 190 feet per second are shown in Figure 37. These data are shown in Figure 38 as the fraction of the total step change recorded as a function of time. As before, a faster response was measured at higher gas

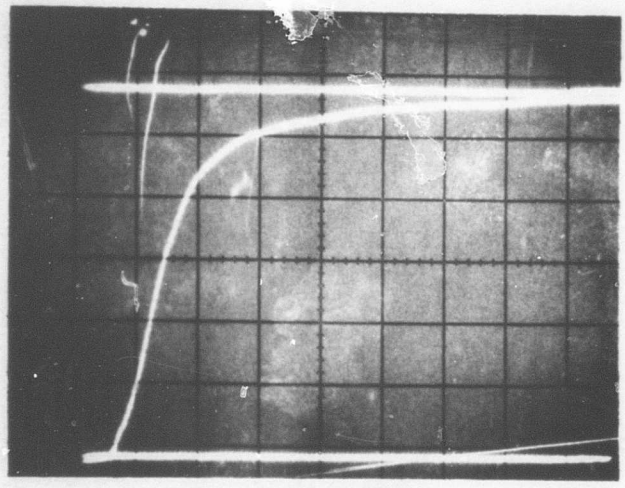

Figure 31. An Oscilloscope Trace Showing the Response of a Fusion-Welded Foil Thermocouple.

velocities. The overshoot characteristic of multijunctions was also observed. The maximum overshoot occurs at shorter times as the gas velocity increases. Return to the steady-state temperature is also more rapid, causing the response curves for different velocities to cross. The duration and importance of the overshoot will be minimized as the gas velocity increases.

Table X gives the time constant τ (63% response time) and the 90% response time for each gas velocity as well as for tests in the fluidized bed.

The fusion-welded foil thermocouple was also tested. The oscilloscope traces are shown in Figure 39, and a fraction of the steady-state temperature recorded after a step change is plotted as a function of time in Figure 40. Table XI gives the time constant and 90% response times in the moving gas and in the fluidized bed.

The time constant for a given thermocouple varies inversely with the square root of the gas velocity. Faster time constants than those recorded would be measured due to the increase in the coefficient of convective heat transfer as the velocity approaches the program specifications of 400 to 700 ft./sec.

TABLE X. RESPONSE OF A MULTIJUNCTION THERMOCOUPLE IN MOVING GAS

Environment	Time Constant τ (ms)	90-Percent Response Time (ms)
Moving Gas		
100 feet per second	115	225
145 feet per second	85	180
190 feet per second	70	150
Fluidized Bed	140	290

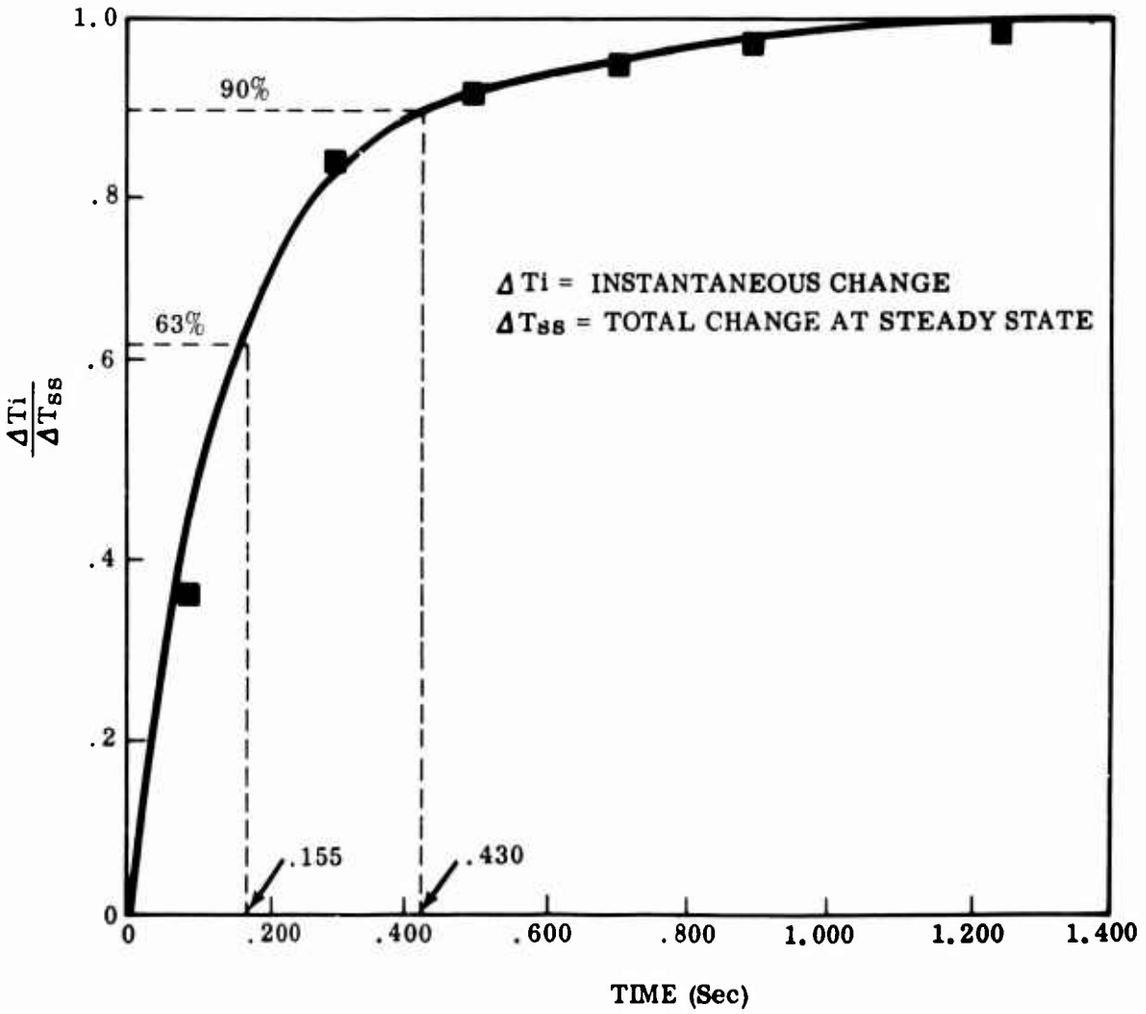

Figure 32. Response Curve for a Fusion-Welded Foil Thermocouple.

TABLE XI. RESPONSE OF A FOIL THERMOCOUPLE IN MOVING GAS

Environment	Time Constant τ (ms)	90-Percent Response Time (ms)
Moving Gas		
100 feet per second	130	385
215 feet per second	110	230
Fluidized Bed	155	430

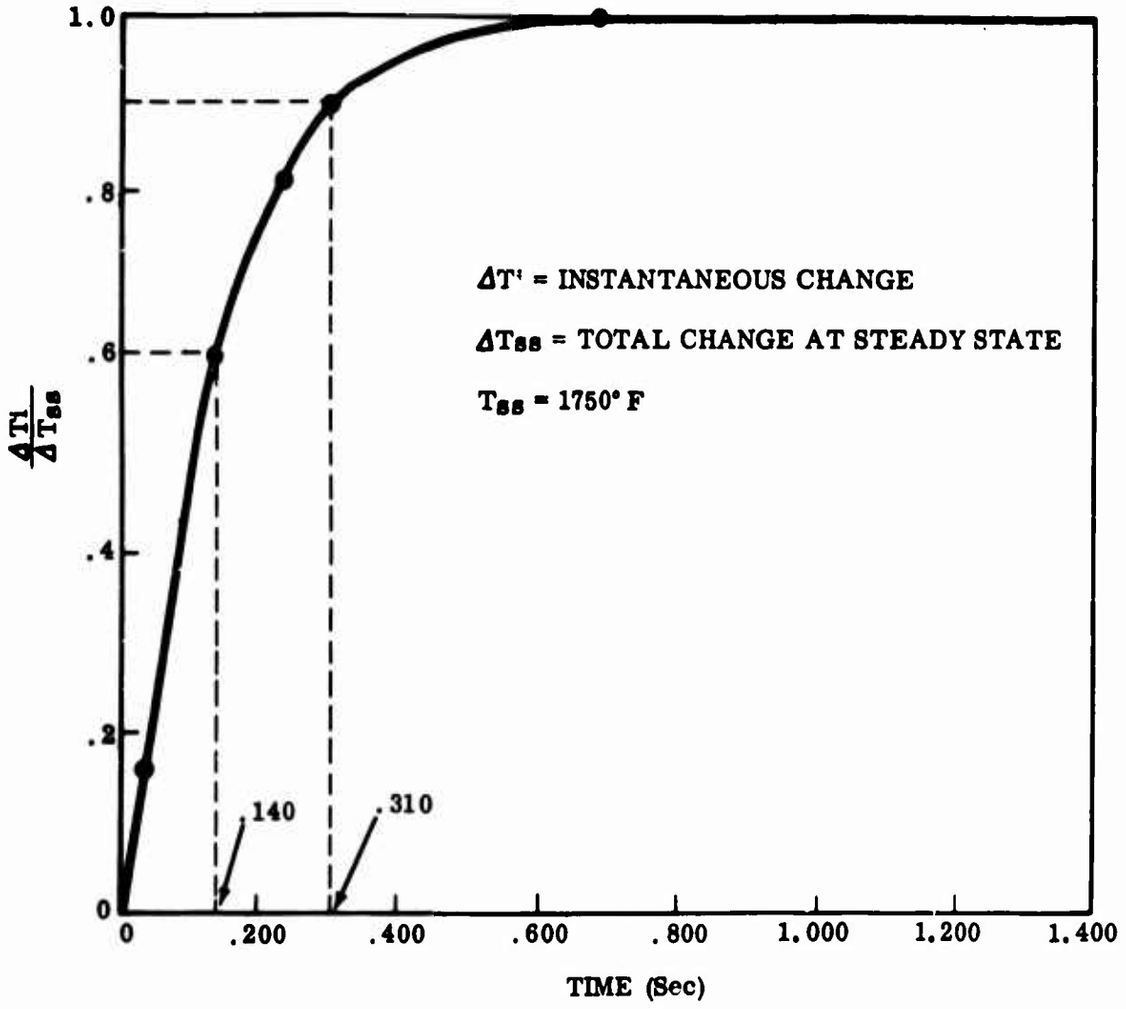

Figure 33. Response Curve for a Grounded Thermocouple Junction.

SUMMARY - TASK I

Platinum-rhodium thermocouples were chosen as the only alloy system that is capable of operating as an exposed junction in an oxidizing atmosphere at temperatures between 2000° and 2500°F. Reliability and drift tests indicated that calibration changes can be contained within acceptable limits but that further work is necessary to give quantitative design data.

Exposed junctions proved to be capable of fast response but were not able to meet the program goal of 10 milliseconds. In moving gas (velocity 200 feet per second), a single wire junction (diameter 0.012 inch) reached 90% of a step change in temperature in 320 milliseconds. A foil single junction (with a larger mass) was able to reach 90% in 230 milliseconds, and a wire multijunction of the same dimensions

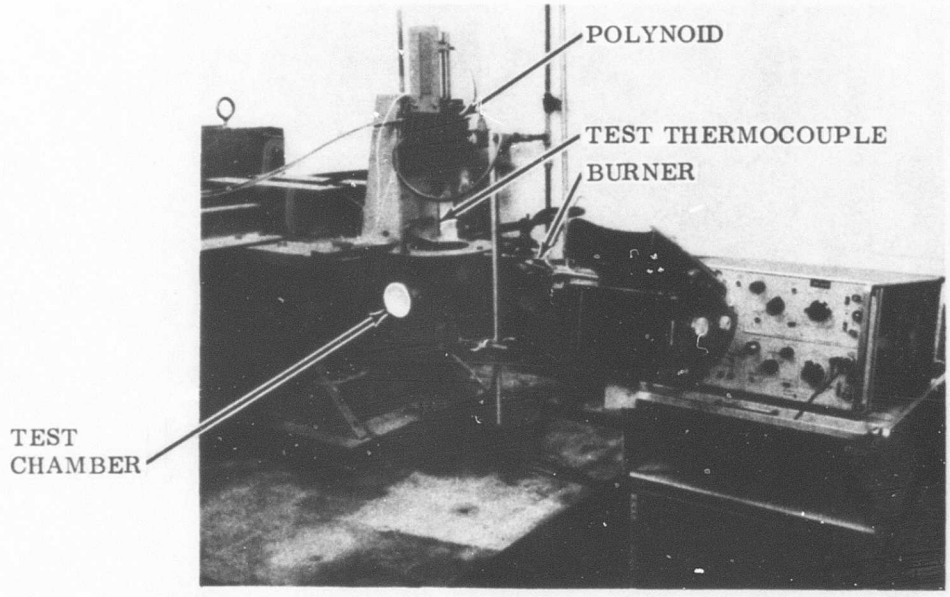

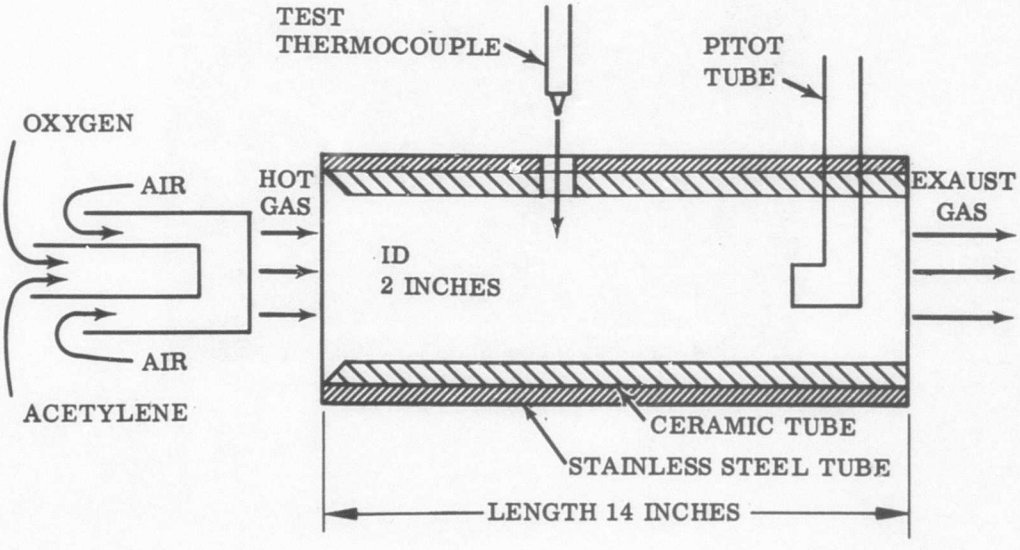

Figure 34. Apparatus Used for Thermocouple Response Testing in a Moving Gas Atmosphere.

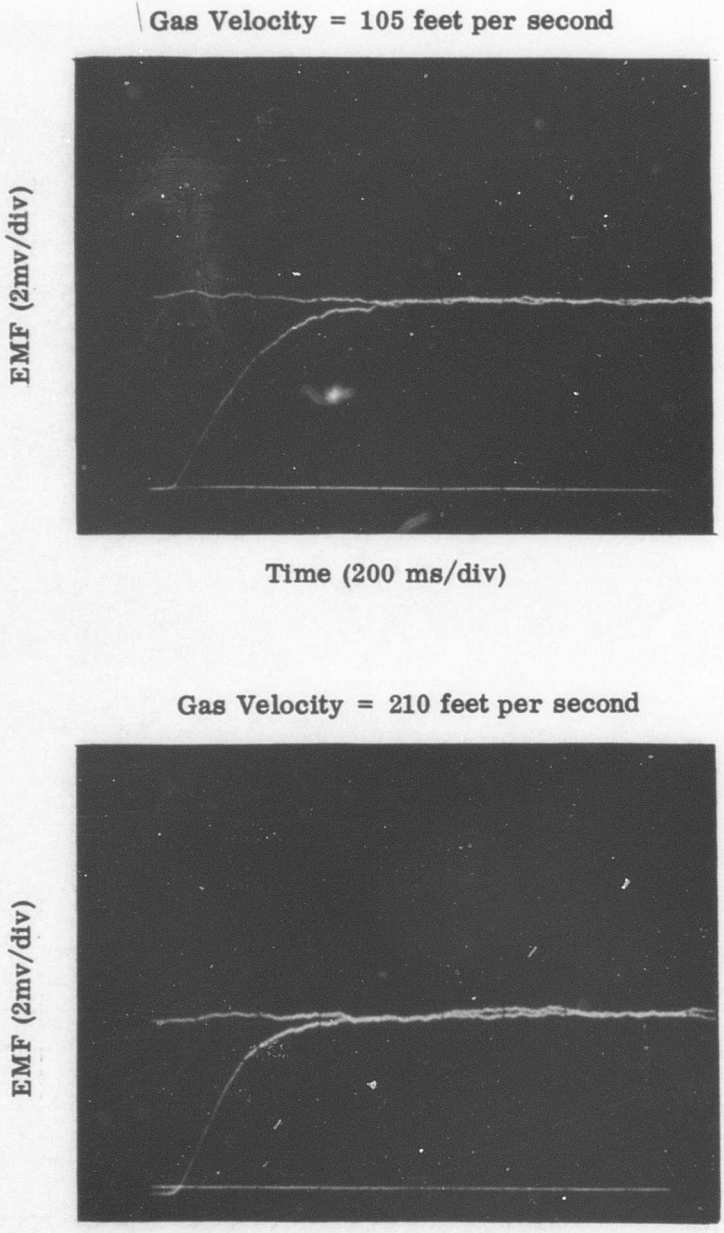

Figure 35. Oscilloscope Traces Showing the Response of a Single-Junction Thermocouple at Two Gas Velocities.

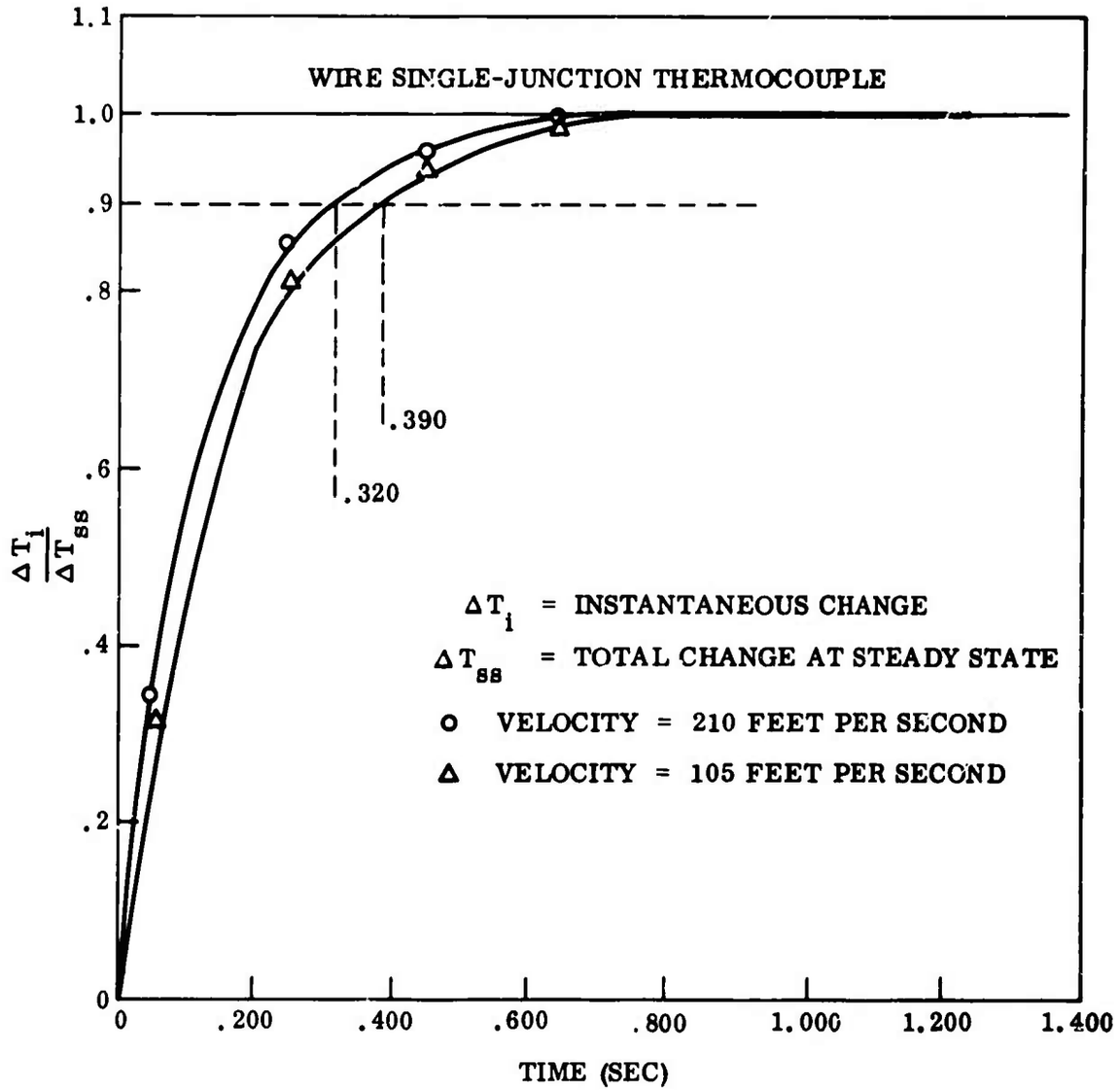

Figure 36. Response Curves for a Wire Single-Junction Thermocouple at Two Gas Velocities.

as the single junction recorded 90% of the step change in 150 milliseconds. Some improvement would be measured at higher gas velocities.

The strength of Pt-Rh alloys is very low at turbine inlet temperatures and will present some critical design problems.

The miniature Pt-Rh grounded thermocouple responded (310 milliseconds to 90% of the step change) quite rapidly for a protected couple. Reliability over a long period of time was not tested.

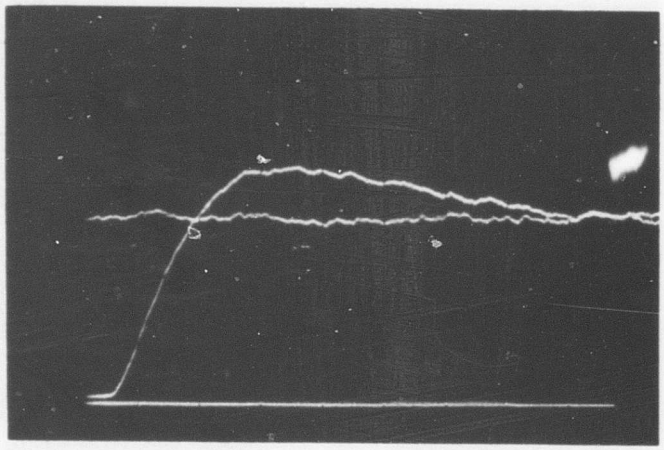

EMF (2 mv/div)

Gas Velocity = 100 feet per second

Time (200 ms/div)

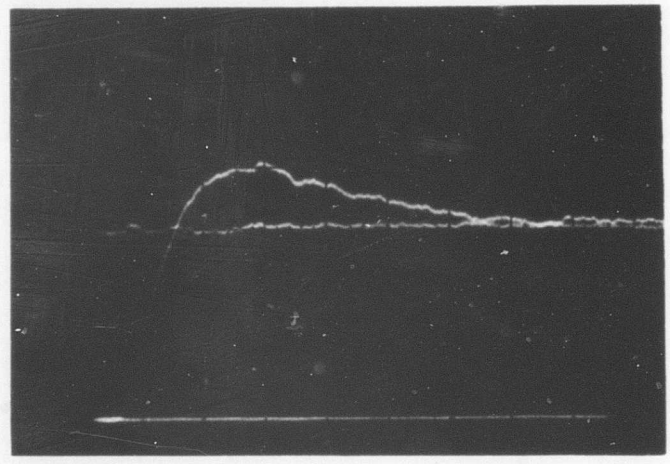

Gas Velocity = 145 feet per second

EMF (2 mv/div)

Time (200 ms/div)

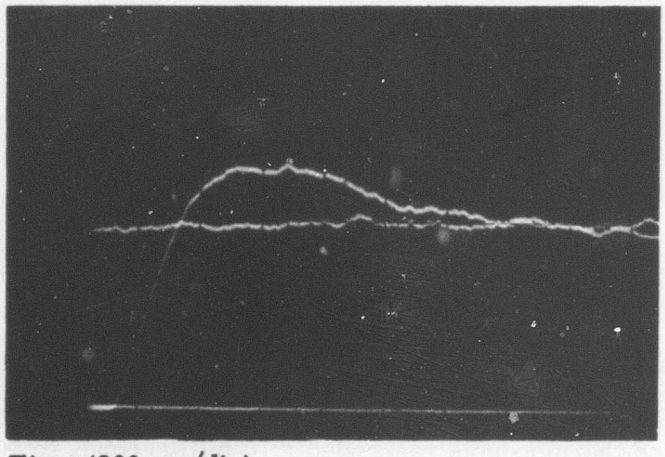

EMF (2 mv/div)

Gas Velocity = 195 feet per second

Time (200 ms/div)

Figure 37. Oscilloscope Traces Showing the Response of a Wire Multijunction at Three Gas Velocities.

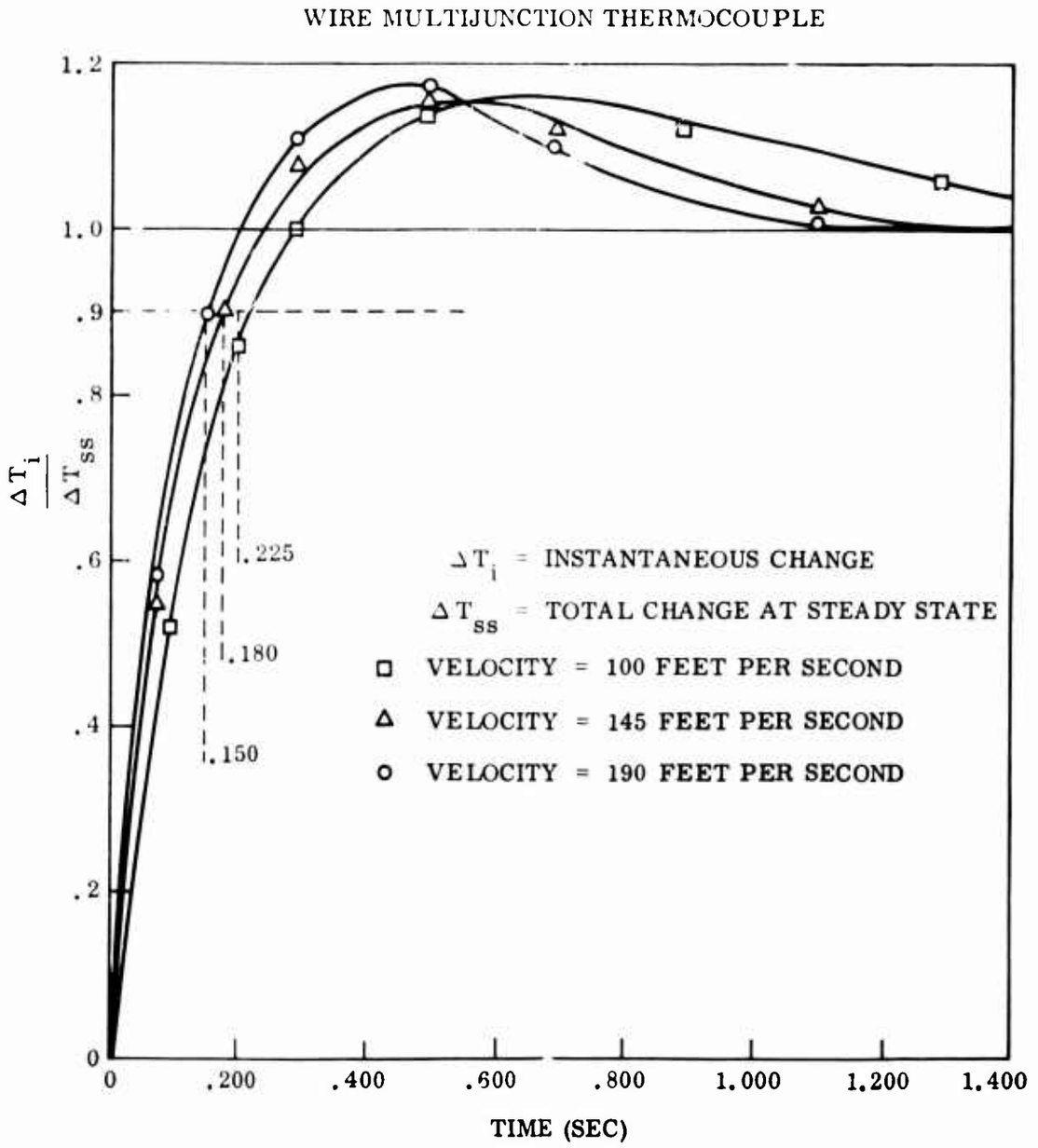

Figure 38. **Response Curves for a Wire Multijunction Tested at Three Gas Velocities.**

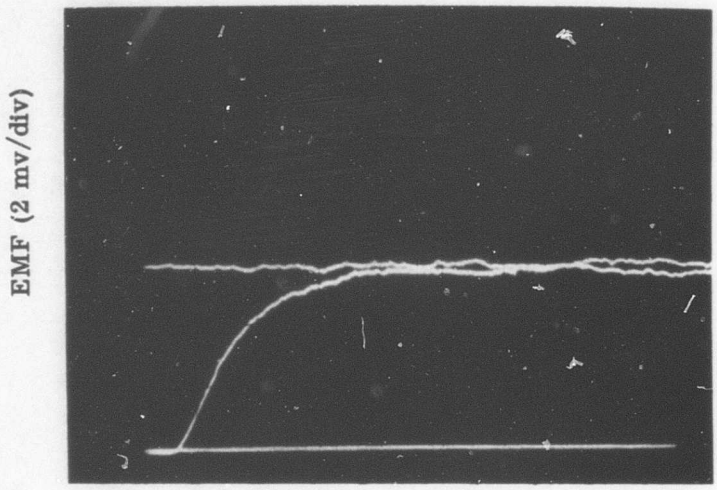

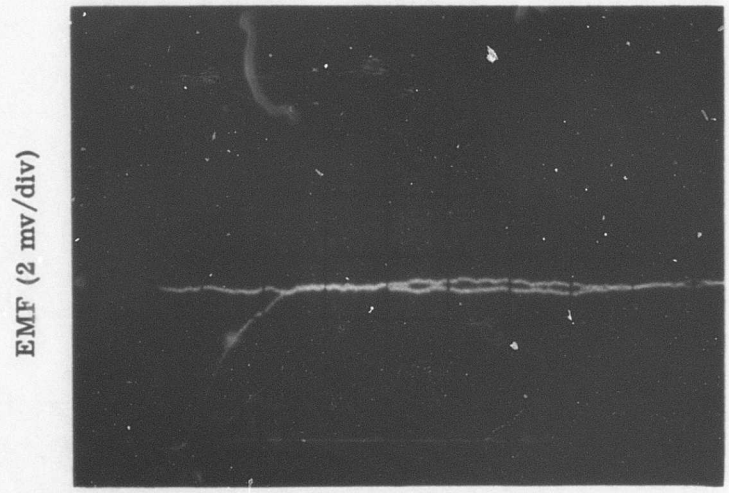

Figure 39. Oscilloscope Traces Showing the Response of a Fusion-Welded Foil Thermocouple at Two Gas Velocities.

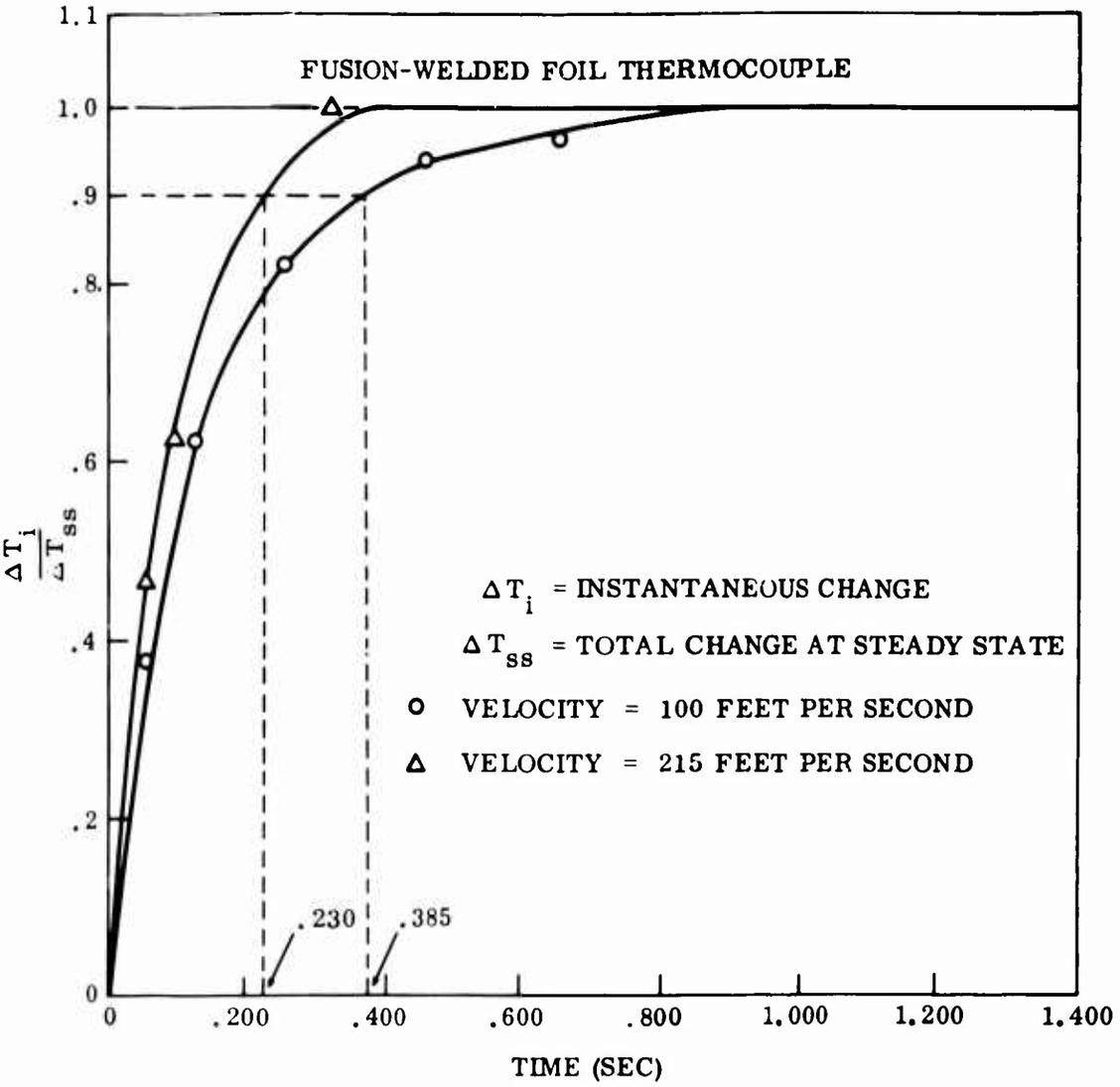

Figure 40. Response Curves for a Fusion-Welded Foil Thermocouple at Two Gas Velocities.

Alumina insulation (Al_2O_3) performed equal to or better than all the other refractory oxides tested during the program. At temperatures up to 3000°F, there does not seem to be any reason to use more exotic and expensive oxides. Al_2O_3 is inexpensive and is more readily available than any other refractory oxide.

TASK II - RESISTIVE DEVICES

Resistive devices are inherently capable of measuring temperatures with greater accuracy than the thermocouple, and are considered precise and reliable in the temperature range of -297° to 1200°F. However, to attain such precision, considerable care must be exercised in construction and use. The same material compatibility problems that exist with thermocouples are encountered with resistance thermometers; thus, combined compatibility studies will yield data that will be applicable to both sensing devices. With the exception of hot wire anemometers, resistive devices have not received widespread use as turbine sensors because at temperatures above 1304°F, normal resistive devices have been less reliable than the platinum versus Pt10%Rh thermocouple.[12] Resistive thermometers require a protective sheath for reliable operation in the turbine environment for the following reasons:

- To prevent continued loss of noble metal resistor cross section due to the formation of volatile oxides, resulting in calibration "drift".
- To reduce the possibility of introducing strains in the resistance element which causes unpredictable changes in resistivity.
- To prevent contact of water vapor with the resistance element.

The latter reason is based on work at the National Bureau of Standards (NBS), where water vapor was found to have a serious resistive shunting effect on platinum resistors at temperatures approaching 2000°F.[13]

Very accurate resistive thermometers often are of a "bird-cage" construction, where the resistance element is exposed to a controlled environment and maintains minimum contact with ceramic oxides or other insulators.[13] At very high temperatures, even good insulators may begin to cause substantial errors in temperature measurement.

Experimental Program

The results obtained in the compatibility studies in the thermoelectric task apply equally as well to resistive devices. Al_2O_3 is the best choice for insulating platinum resistance elements in the temperature range in question.

A miniature resistance probe was obtained and is shown in Figure 41. The resistive element is a 0.005-inch-diameter platinum wire embedded in 99.6% pure Al_2O_3 and sheathed in a 0.006-inch-thick Pt10%Rh tube with a diameter of 0.048 inch at the sensing element. The lead wire broke during the original calibration, and the device was returned to the manufacturer for repairs. After being repaired, the probe was calibrated using the bridge circuit shown in Figure 42. The emf measured across the bridge was adjusted to read 50 millivolts at a

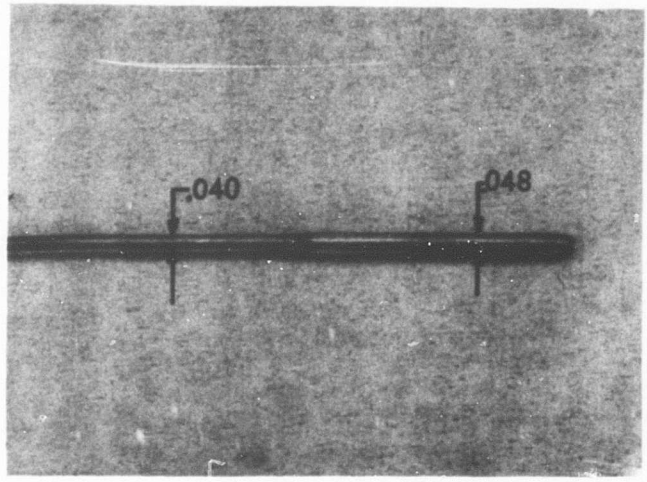

Sensing Bulb

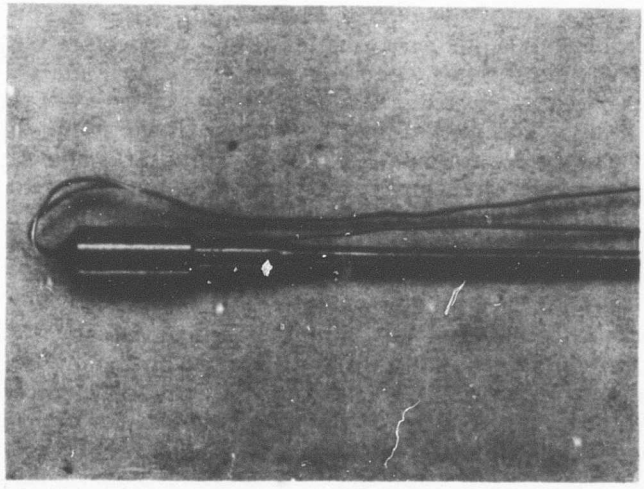

Connection Terminal

Figure 41. Miniature Resistance Probe.

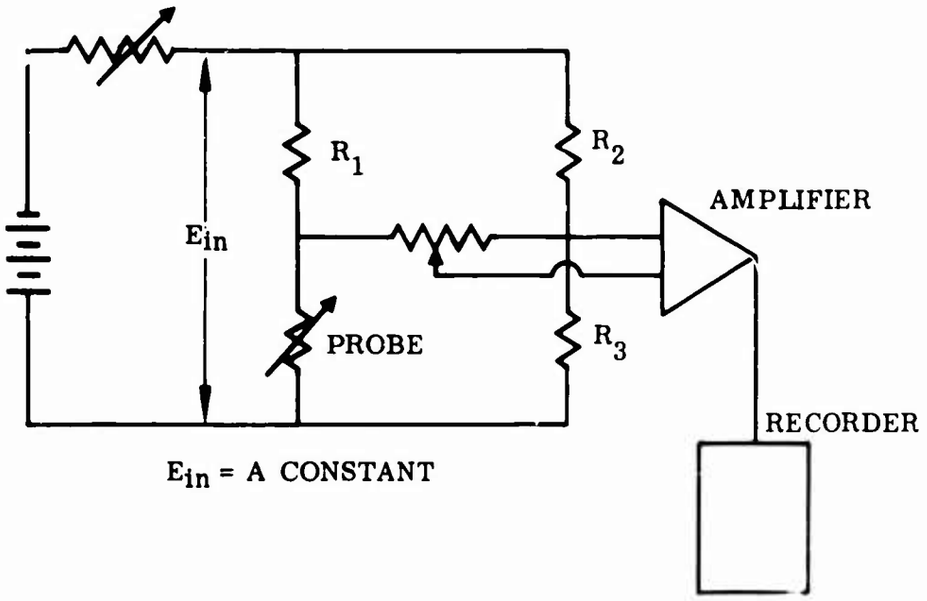

Figure 42. Measuring Circuit for the Miniature Resistance Thermometer.

probe temperature of 200°F and was then read to a probe temperature of 2000°F. The resulting emf versus temperature curve is shown in Figure 43. The potential difference measured across the bridge was not linear over the range measured. The resistance of the probe did change in a linear manner, as is shown in Figure 44. The resistance was measured by a digital voltmeter over the same range in temperature. In this temperature range, there does not appear to be any shunting effect caused by decreasing resistivity of the alumina insulation.

The response rate measured in the fluidized bed was quite slow. Oscilloscope traces for a 430° and 185°F step change are shown in Figure 45. The probe reached 90 percent of its steady-state temperature in 6.5 and 2.3 seconds, respectively. Time constants (63%) were measured as 2.1 and 1.0 seconds for the two tests. As can be seen in the oscilloscope traces, much longer times were needed to reach steady state due to the large amount of heat conducted away by the platinum sheathing.

SUMMARY

Resistance probes present many of the same advantages and problems as thermoelectric devices. The resistive element must be compatible with a ceramic insulator and must remain unaffected by long exposures to the environment. Experimental results obtained for the compatibility and reliability of thermoelectric

materials may be equally well applied to resistive devices. The resistance of the element is a function of the wire cross section as well as the resistivity of the material. The element must be protected by a metal sheathing and embedded in a refractory oxide to avoid changes in the cross section due to erosion by the turbine gas. This configuration offers no advantage over a protected thermocouple junction. In fact, a grounded junction would respond much faster than a resistance element embedded in an oxide.

Thermocouples appear to be more adaptable to turbine inlet temperature sensing either as protected or exposed junction probes.

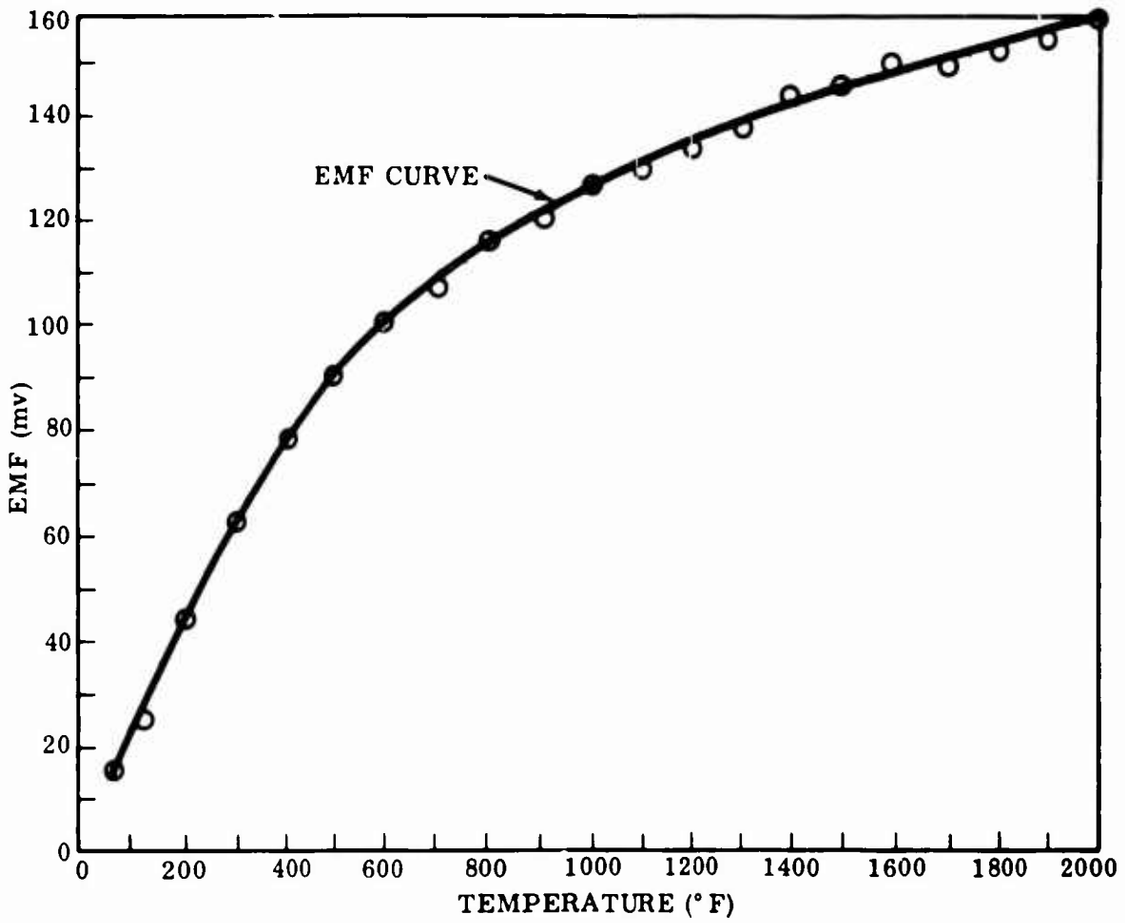

Figure 43. EMF Versus Temperature for the Resistance Probe.

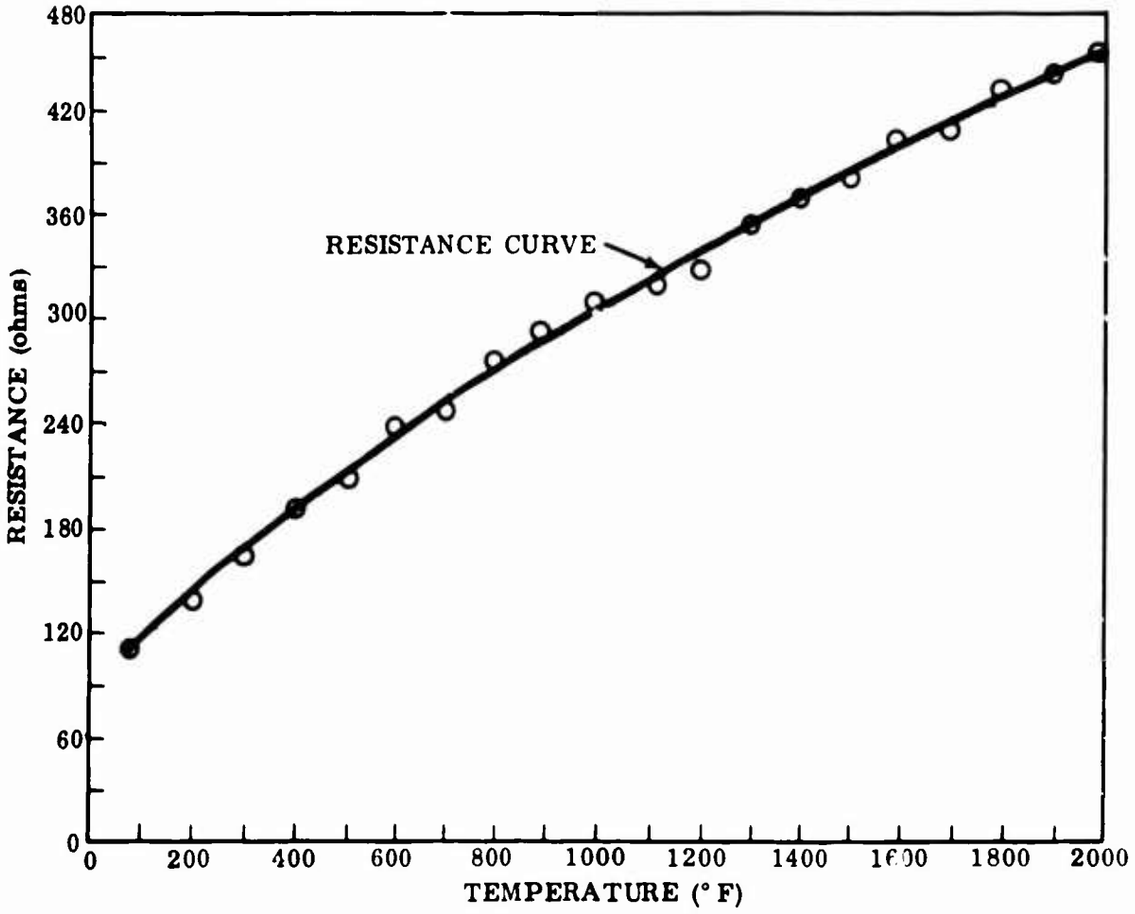

Figure 44. Resistance Versus Temperature for the Resistance Probe.

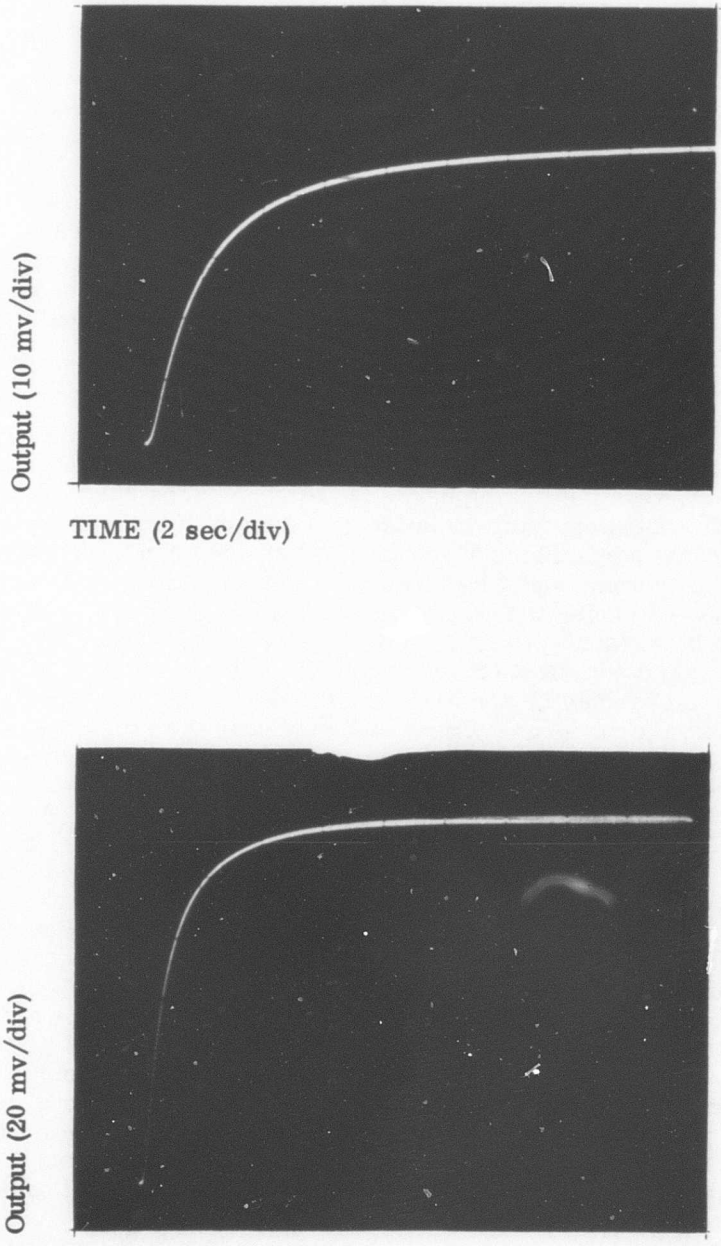

Figure 45. Oscilloscope Traces Showing the Response of the Resistance Probe

TASK III - RADIATION SENSORS

Radiation sensors offer several advantages over thermoelectric devices for use as turbine inlet temperature sensors. These include improved hardware protection, elimination of gas blockage, fast response and good temperature averaging. The principal problems presented by radiation sensors are concerned with maintaining the device in the ambient conditions imposed by a turbine engine and keeping the optical path between target and sensor clear.

Two basic systems may be used. One would measure the temperature of a small target placed in the moving gas. The other would use the guide vanes or turbine blades as the target, thus measuring hardware temperatures directly. The principal advantage of immersing a target in the gas stream is that with a target of low mass, the critical parameters of engine performance can be more quickly sensed than if the detection cannot be made until the temperature of the gas acts on hardware targets of larger mass. However, the same errors existing with a thermocouple will be encountered, i.e., steady-state errors (recovery, conduction, and radiation) and transient errors (response rate). A target immersed in the moving gas would probably not respond faster than a thermocouple and would not measure an average of the gas temperature but only the temperature at the target location. This system does not seem to offer significant advantages over the use of thermocouples. The emphasis will be placed, instead, on radiation sensors using turbine hardware as a radiation source.

One of the principal advantages of radiation pyrometry is that no extraneous sensors have to be physically placed in the region where the temperature determination is desired. The blockage caused by placing sensors in the gas stream can cause significant power losses in small gas turbine engines. Also, each sensor measures temperature only at one place, requiring a large number to be read to give an adequate average gas temperature. Using the rotating turbine blades as targets eliminates both of these problems. Nothing is immersed in the moving gas and the average temperature is measured by one sensor. The overall response rate is automatically lowered, due to the large thermal mass. The sensor must measure the temperature of each blade as it passes the field of view, requiring that the response rate of the sensor be very fast to indicate the true temperature of the blade.

A viewing time of approximately 40 microseconds would be available in an engine turning at 40,000 revolutions per minute. For the sensor to measure the temperature of each blade as it passed by, it would have to reach 100% of the temperature in this time period. With slower response, the sensor would produce a wave form output with a diminished amplitude approaching a straight line (at the median between the blade and the background temperature).

THERMAL RADIATION

A body, by virtue of its temperature, emits electromagnetic radiation of all wavelengths. The energy (or intensity) of the radiation is a function of wavelength. The intensity of the radiation emitted from a blackbody increases at all wavelengths as the temperature of the body increases. Also, there is one wavelength (at a given temperature) which emits a maximum amount of energy, and this maximum moves toward shorter wavelengths as the temperature is increased. The term spectral radiation refers to radiation emitted over a specified range of wavelengths as contrasted to the total radiation emitted at all wavelengths. Radiation pyrometers are sensitive to different spectral ranges, depending upon the particular detector used.

At a given temperature, different materials and different configurations of the same material will radiate different amounts of total radiation as well as show different spectral response. A blackbody is defined as an ideal emitter which radiates at the maximum possible rate for all temperatures and wavelengths. A blackbody also absorbs all of the radiation incident upon it. No material or body completely fulfills the definition, but nonreflective materials, such as carbon black, come very close to being a perfect blackbody radiator, while smooth reflective materials like platinum and silver do not. Any material may be made to approach the ideal by forming it into a hollow cavity with a small opening. The multiple reflection occurring inside the cavity causes the existing radiation to closely approach the theoretical values for blackbody radiation.

The emissivity of a material or body characterizes the intensity of the emitted radiation. Emissivity is a function of both wavelength and temperature.

The emittance, ϵ, which is defined as the ratio of the radiant energy emitted by the body to that emitted by a blackbody at the same temperature, may be defined for a given spectrum or for the total radiation. Thus, the emittance of a perfect blackbody is 1, and all real materials have an emittance value of less than 1. A properly constructed blackbody cavity will approach an emissivity of 1 very closely.

Radiancy, R, is defined as the rate of radiant energy emission from a unit area of a material. The radiancy distribution over all wavelengths as a function of temperature is given by Planck's distribution law:

$$R_\lambda = \frac{C_1 \lambda^{-5}}{e^{\frac{C_2}{\lambda T}} - 1} \tag{44}$$

where R = radiancy (watts per cm^2)

λ = wavelength (cm)

T = absolute temperature (°K)

C_1 = constant = 5.673×10^{-12} watt/cm^2 (°K)

C_2 = constant = 1.4388 cm (°K)

Thus, for any given wavelength or range of wavelengths, the intensity of radiation will increase with temperature. This is the property most often measured by radiation pyrometers.

Signal Detection

Two basic systems are used by radiation pyrometers to measure temperature. The simplest, a thermopile, measures a rise in temperature attributed to the wave energy absorption by some medium. The response of such a system is quite slow, since the absorber, by virtue of its mass, takes a finite time to reach an equilibrium temperature for a given target temperature. This type of pyrometer was not considered in this program. The pyrometers that were evaluated were based on the interaction of the incident electromagnetic radiation with the electronic structure of the detector material. This interaction was divided into photovoltaic (photoconductive) and photoemissive effects.

A photoconductive material is one whose electrical conductance changes as a function of the intensity and wavelength of the electromagnetic radiation incident upon its surface. Photons incident upon the material cause electrons and holes to move into the conduction band, allowing an increase in current due to an externally applied voltage. At a given incident wavelength, the increase in conductance is proportional to the intensity of the radiation. The minimum energy (maximum wavelength) needed to raise the electrons into the conduction band is much lower for doped semiconductors than for other materials. All radiation pyrometers employ semiconductors as detectors.

The photovoltaic effect is closely related to photoconductivity. If the radiation is incident upon a p-n junction, electrons are raised into the conduction band in the n-type material and holes enter the conduction band in the p-type material, causing an electric field to be created at the junction. If an external circuit is completed between the two regions of the semiconductor, a current will flow proportional to the intensity of the incident radiation without an externally applied voltage.

The photoemissive effect describes the interaction of electromagnetic radiation with the outer shell electrons of the detector material. When the photon interacts with an electron, it transfers all of its energy to the electron. If the photon loses sufficient energy, the electron will be disassociated from the atom and be emitted into the surrounding atmosphere. The emitted electrons are collected and their number is proportional to the intensity of the incident radiation.

The selection of the material which the photons strike is dependent upon the energy level of the photons. At high temperature levels (2000°-3000°F), the Planck distribution law shows that most of the emitted radiation will be in the visible or short infrared region. Thus, the principal requirement for the selection of the detector material is that the work function to pull an electron from the atom an infinite distance is less than the energy of the incident photons. The alkali metals (sodium, cesium, rubidium, etc.) are very effective in this range and are usually utilized in the commercial phototubes. Due to the low intensity of the signal emitted from the

phototubes, amplification methods by emission of secondary electrons are usually employed.

Signal Transmission

Interaction of the signal with the turbine gas, windows, lens, or other objects is a prime source of error in radiation pyrometry. Luminous gas and extraneous reflections may increase the signal while each medium through which the radiation passes reduces its intensity. The absorption is a function of the wavelength of the radiation and the condition and properties of the medium. The wavelengths of interest depend on the spectral range viewed by the detector. The transmissibility of all lens and window material under normal room temperature conditions is well known. The principal criterion for turbine application is that each element reduces the intensity by a constant, known amount. The transmissibility must not be changed by temperature changes or contamination by combustion products.

In order to choose a reliable and accurate sensor system, the absorption bands of constituent gases of the environment must be considered. The principal combustion product, CO_2, has absorption bands at 2.8 and 4.2 microns. Oxygen and nitrogen do not have significant absorption in the range of interest. To avoid interaction with the gas, the detector should be chosen to have a spectral response that avoids the above wavelengths.

PROGRAM GOALS

The program goals for Task III were to select the type of radiation pyrometer that is best suited for application in a turbine environment and to optimize its performance under the imposed conditions. Commercial pyrometers of various types were tested and analyzed for their potential. Commercial pyrometers are generally designed for the maximum possible versatility, making many models more bulky and complicated than is necessary for specific applications. Therefore, the potential utility of the detector system and not the particular model will be evaluated.

A radiation sensor used to measure turbine inlet temperature must respond very rapidly to temperature changes. For a stationary target, the program goal of 10 milliseconds is adequate. Application with a rotating target will require a response time three orders of magnitude faster due to the short period of time that a particular blade is in the field of view.

Accuracy of the detector must be within the program specifications of plus or minus 15°F over the entire temperature range. The output signal should be linear to make readout as simple as possible. The accuracy must be immune to changes in the environment, such as changes in gas composition, fuel to air ratio, or target emissivity.

Package size, weight, stability and reliability of the sensor under the ambient conditions imposed by a turbine engine are all important. The package size and weight have no specified maximum but should be as small as possible. Stability of the sensors refers to resistance to output changes or damage caused by mechanical vibrations or ambient temperature changes. The proposed sensor, mounted on the outer casing of the turbine engine, would certainly be exposed to high-frequency vibrations generated by the turbine plus any shocks or accelerations experienced by the engine as a whole. The maximum ambient temperature in which the sensor can

function properly should be as high as possible. After the engine is shut down, however, any cooling air would also stop and the subsequent temperature homogenization or "soak back" over the entire engine could raise the temperature to higher levels than are present while the engine is running. The sensor would have to withstand this higher temperature without damage but would not be required to function. Temperature changes below the maximum should not change the sensor output for a constant target temperature. If the detector is sensitive to its ambient temperature, then the output must be compensated to maintain accurate readings. The reliability generally increases with increasing simplicity. A sensor with a minimum of parts, particularly moving parts, will in most cases be more reliable.

EXPERIMENTAL PROGRAM

Procedure

Basic evaluation of the radiation pyrometers was carried out using a close approximation to a blackbody radiation source. A graphite bar (emissivity of 0.74) was machined into a hollow cylindrical cavity. With a length to diameter ratio of 20, the emissivity was calculated to be 0.98. The cavity was inserted into the tubular muffle of a standard platinum wound resistance furnace. The temperature of the cavity was measured by inserting an NBS transfer standard thermocouple.

For accuracy measurements, the output of the radiation pyrometer was read by its own metering equipment or by a potentiometer. For response tests, an oscilloscope was used to record transient output. A step change in temperature was simulated by cutting the beam of radiation at a point between the target and the sensor. Two devices were used: a camera shutter and a notched disc. The first is shown in Figure 46 with the shutter in place. The shutter was coupled with the oscilloscope so that both would be triggered simultaneously. A rotating target was simulated by rotating a notched disc (chopper) in the beam in place of the shutter (Figure 47). The beam would come into view or disappear from view in as little as 35 microseconds, depending on the speed of the driving motor. Two discs were used, one drilled with 0.5-inch holes spaced 1 inch apart and the other with 0.375-inch-wide notches milled in the circumference. Both of these discs allowed the incident signal to oscillate from the blackbody temperature to essentially room temperature (zero output voltage).

Lead-Sulfide Detector

The Ircon Model 300 radiation pyrometer utilizes a lead-sulfide detector to measure the intensity of the radiation incident to its surface. The device is sensitive to radiation between the wavelengths of 2.0 and 2.6 microns. It is a multiscale instrument capable of measuring temperatures between 550° and 7000°F with a full-scale output of 10 millivolts for any selected scale. After being focused by the objective lens, the incident radiation is passed through a rotating chopper which optically modulates the signal. The voltage from the detector is then amplified and demodulated by a circuit driven by a signal from a silicon photo cell. The final output of the detector circuit is proportional to the intensity of the radiation emitted by the target.

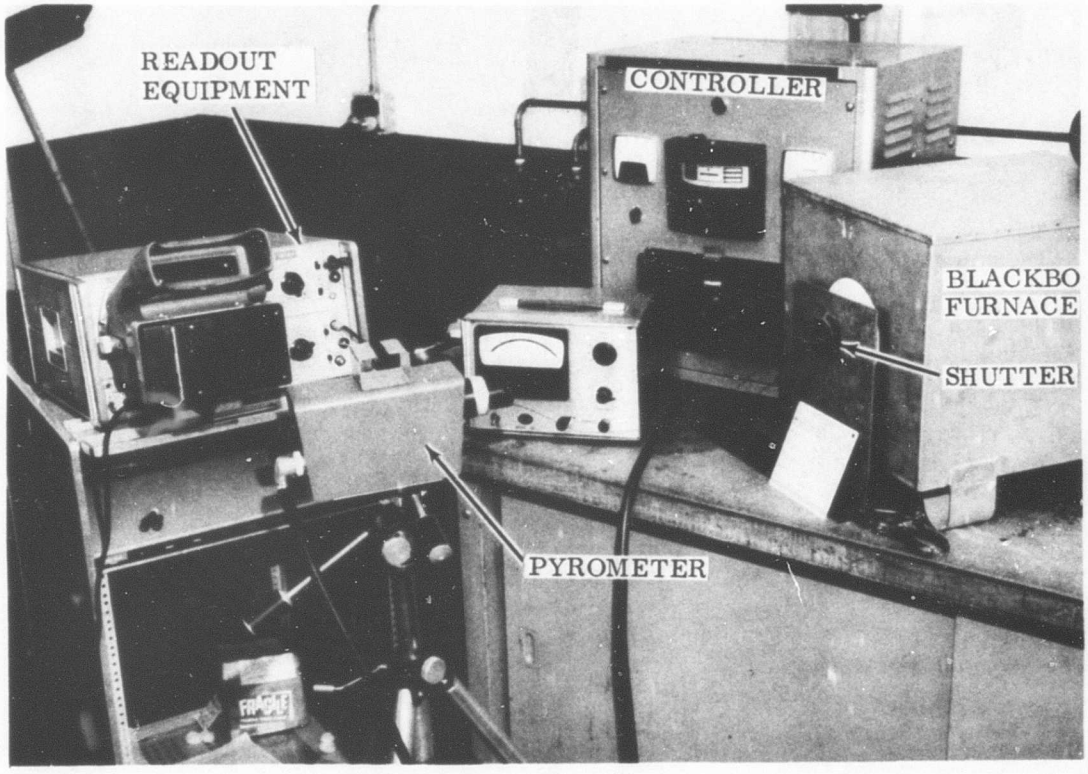

Figure 46. Test Setup To Measure Response Time of Radiation Pyrometers.

Accuracy

The accuracy of this instrument was judged by comparing the temperature indicated by the sensor with the temperature of the blackbody target. The indicated temperature was found to be lower than the correct reading. A 40°F (4%) error was measured at 1000°F and a 290°F error (12%) was measured at 2500°F. It was decided that the particular instrument being tested was off calibration but that this was not a characteristic of lead-sulfide radiation pyrometers in general.

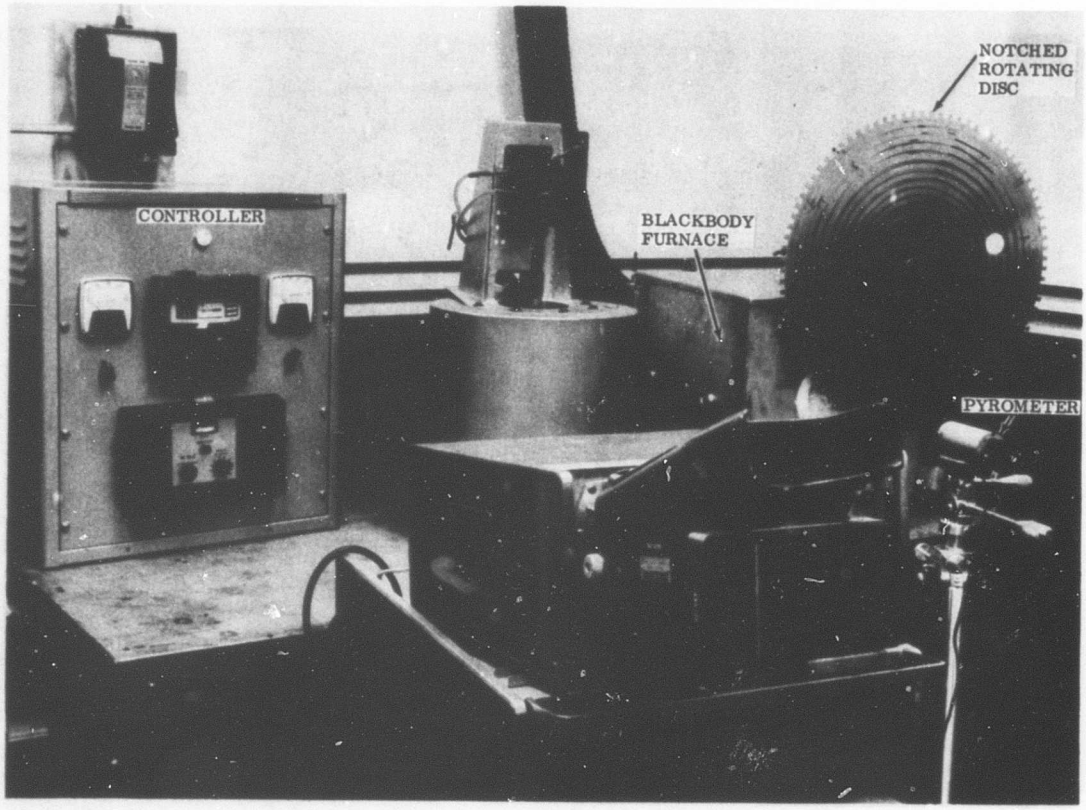

Figure 47. Rotating Disk Used for Response Testing of Radiation Sensors.

Response Time

Response time was measured using the camera shutter previously described. Response times for step changes from room temperature (which is far below the range of the instrument) to 2500°F were measured, as well as from 1000°F back to room temperature. The change of voltage with time during decay was symmetrical with the voltage change during a temperature rise. Noise seen in the oscilloscope occurred at a frequency of 420 cycles per second. This 7th harmonic of the 60-cycle current is characteristic of the optical chopper and did not result in the introduction of error.

The indicated temperature is proportional to the fourth root of the output voltage of the sensor. A small change in voltage indicates a large change in temperature over the lower portion of the scale. As the full-scale voltage is approached, the sensitivity increases and the same voltage change indicates a much smaller temperature change. The indicated temperature rises much faster than the output voltage, and the time necessary for the indicated temperature to reach 63% of its steady-state value was less than that for the voltage. The indicated temperature is plotted as a function of time in Figure 48 for a 2500°F step change. As would be expected, the decay in indicated

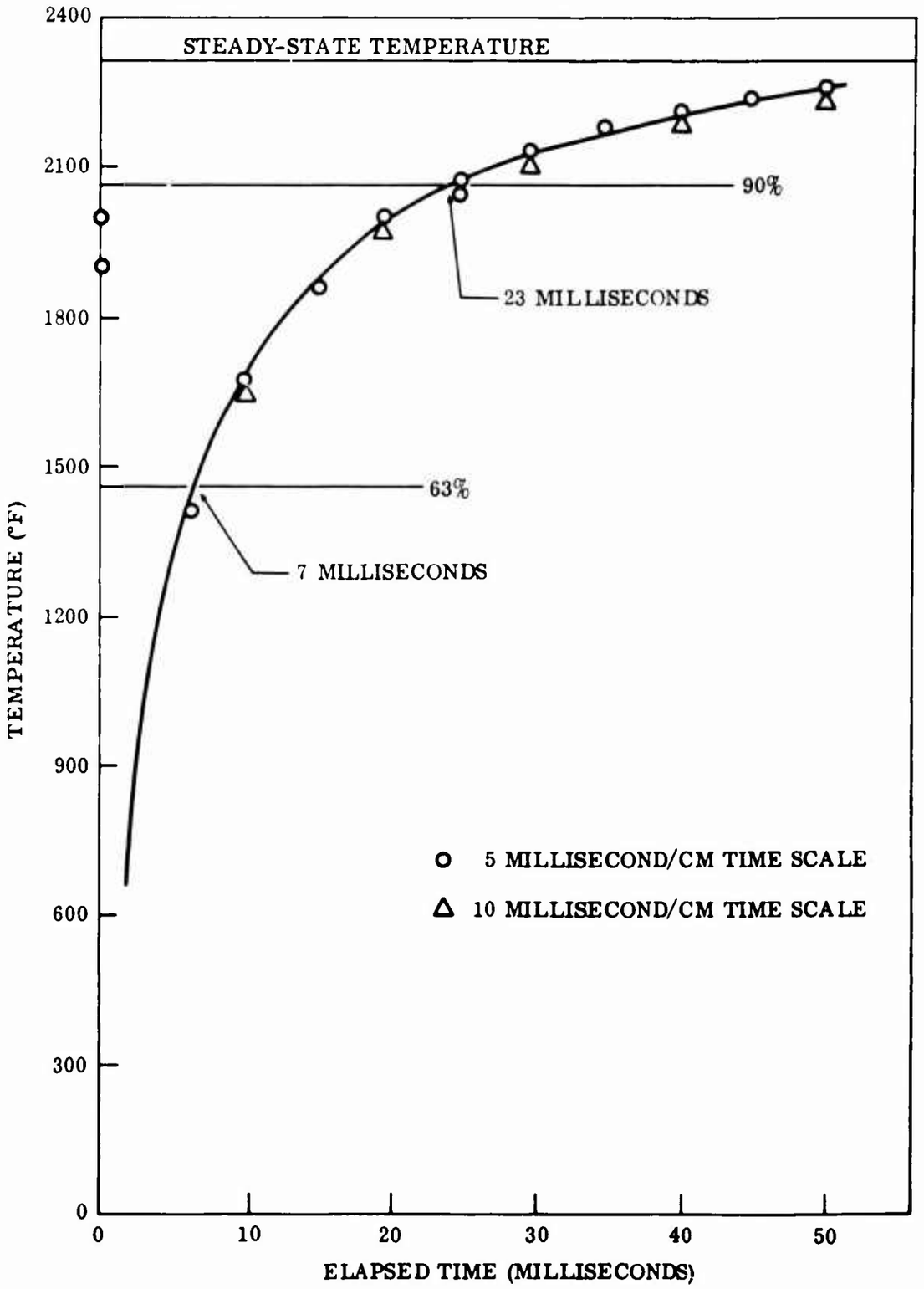

Figure 48. Response Curves for the Lead-Sulfide Pyrometer.

temperature is slower than the voltage drop. Seven milliseconds was necessary to return to 90% of the steady-state temperature, and 22 milliseconds was necessary to reach 63%.

Effect of Oscillating Temperature Target

The rotating chopper was used to cause the signal to oscillate between a voltage corresponding to a 2500°F target and room temperature. Figure 49 shows the results of two chopper speeds. The slower, producing 30 cycles per second, results in a wave form of 1 millivolt amplitude, and the faster (81 cycles per second) produces a 0.56 millivolt wave where the mean value approaches one-half the value of the target temperature voltage at steady state. The data for several chopper speeds is shown in Table XII. As the frequency goes up, the maximum value and the amplitude decrease. The mean value remains relatively constant. At frequencies typical of turbine blades, the amplitude would be zero (a straight line). Temperatures calculated by multiplying the mean by two are relatively accurate, as is shown in Table XII.

Photomultiplier Tube Pyrometer

The Pyro 650 photomultiplier tube pyrometer, made by Instrument Development Laboratories, is a brightness pyrometer which measures the intensity of the radiant energy emitted by the hot target. Radiation of only one wavelength, 0.653 micron is measured and compared with the constant radiation from a reference source lamp located within the pyrometer. This is accomplished by means of a 60-cycle-per-second rotary shutter.

The response time was measured and found to be relatively slow. Response data are plotted in Figure 50, where it can be seen that 180 milliseconds was needed to reach 63% of the steady-state voltage and 370 milliseconds needed to reach 90%.

TABLE XII. EFFECT OF OPTICAL CHOPPER ON OUTPUT OF LEAD-SULFIDE DETECTOR

Chopper Speed (cps)	Wave Form (MV)			Temperature Indicated by Mean x 2	
	Max.	Min.	Mean x 2	(°F)	% Error
0	4.0	--	--	2260	--
5	3.6	0.55	4.15	2280	+0.89
12	3.3	0.65	3.95	2250	-0.45
30	2.5	1.60	4.10	2275	+0.02
81	2.2	1.95	4.05	2270	+0.45

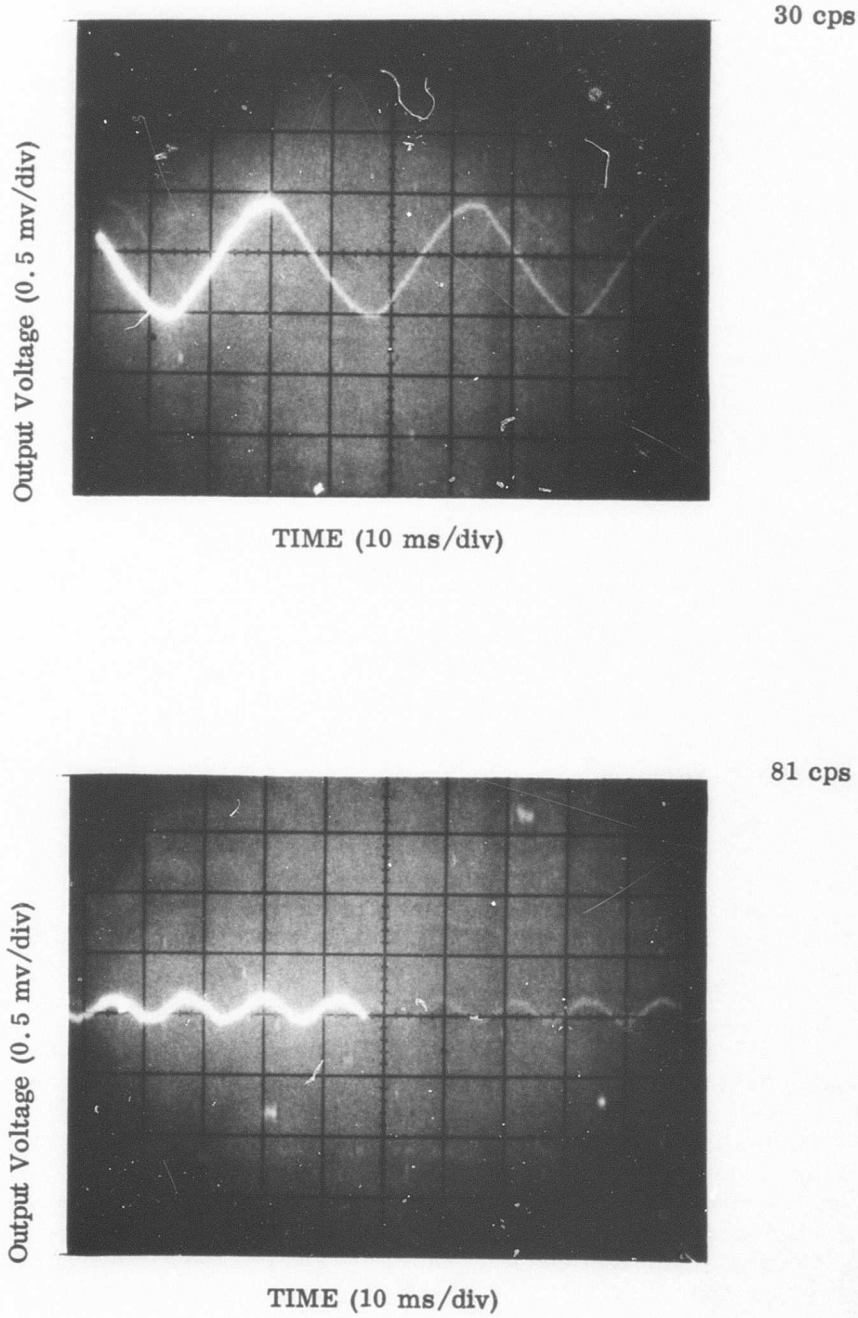

Figure 49. Output of Lead-Sulfide Detector due to Oscillating Target Temperature.

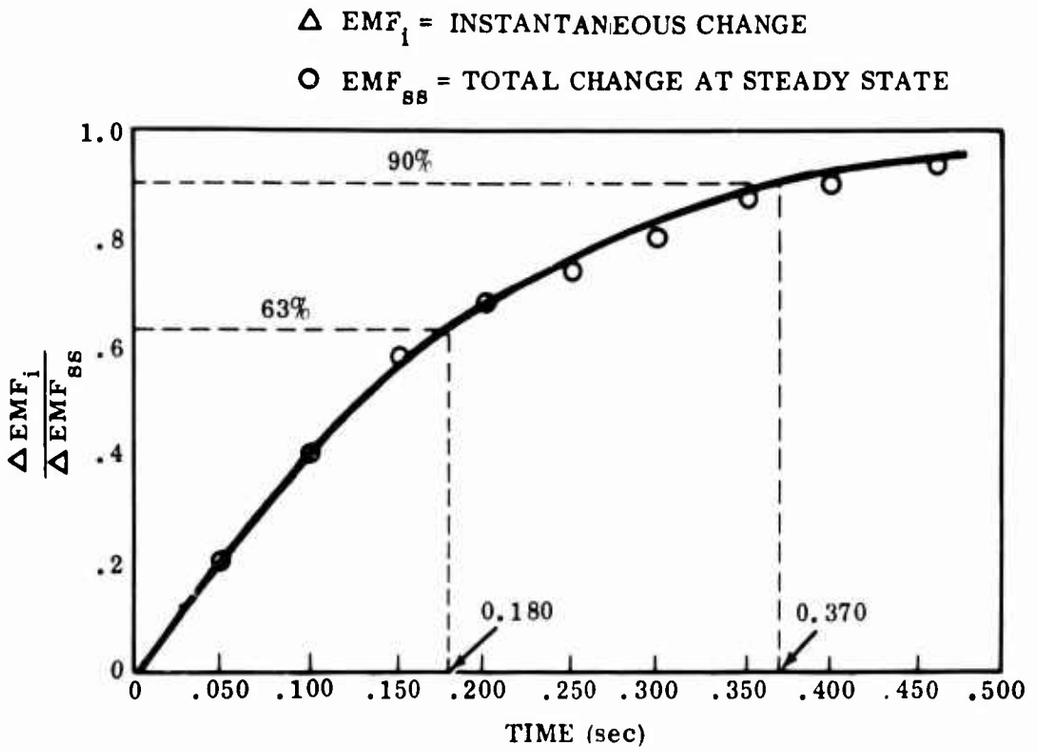

Figure 50. Response Curves for the Photomultiplier Tube Pyrometer.

The slow reponse was caused by a slowdown in the chopper assembly and circuitry to prevent damage to the photomultiplifer tube by sudden changes of incident radiation levels. The accuracy of this instrument was not determined experimentally.

Photoelectromagnetic Radiation Pyrometer

The instrument evaluated for this program was a laboratory demonstration instrument obtained on a rent-free basis from the manufacturer, Honeywell, Inc. The photoelectromagnetic radiation sensor (PEM) measures temperatures from 400° to 2900°F using seven suppressed ranges. The spectral response is adjusted to an infrared waveband of 4.5 to 5.1 microns or 5.0 to 7.0 microns by the use of optical filters. The device consists of an optical chopper (frequency 1140 cps) which interrupts both the incoming radiation and the radiation from an internal lamp used as a synchronization signal.

The motor-driven chopper causes an A-C signal to be generated by both the detector (PEM) cell and the internal lamp's photo cell, which then becomes the input to a synchronous amplifier. The detector cell output is amplified and sent to the output meter.

The speed of response for the PEM cell was obtained using the blackbody cavity and shutter arrangement. Tests were done for two different blackbody temperatures. These data are plotted in Figure 51 showing the fraction of the steady-state voltage reached as a function of time. Ninety percent of the steady-state signal was reached in approximately 6 milliseconds for both targets. Different ranges were used for the tests, indicating that the response times will be quite constant regardless of temperature.

Two-Color-Ratio Pyrometer

A two-color-ratio pyrometer (Milletron Therm-O-Scope) was evaluated for response time and accuracy. The operating range of the sensor is from 1800° to 3000°F; however, wider ranges are available. An important feature of this type of pyrometer is that no correction is needed for emissivity changes.

In operation, the incoming radiation from the target is focused by a rather complex lens system on a beam-splitting mirror which allows eyepiece viewing of the

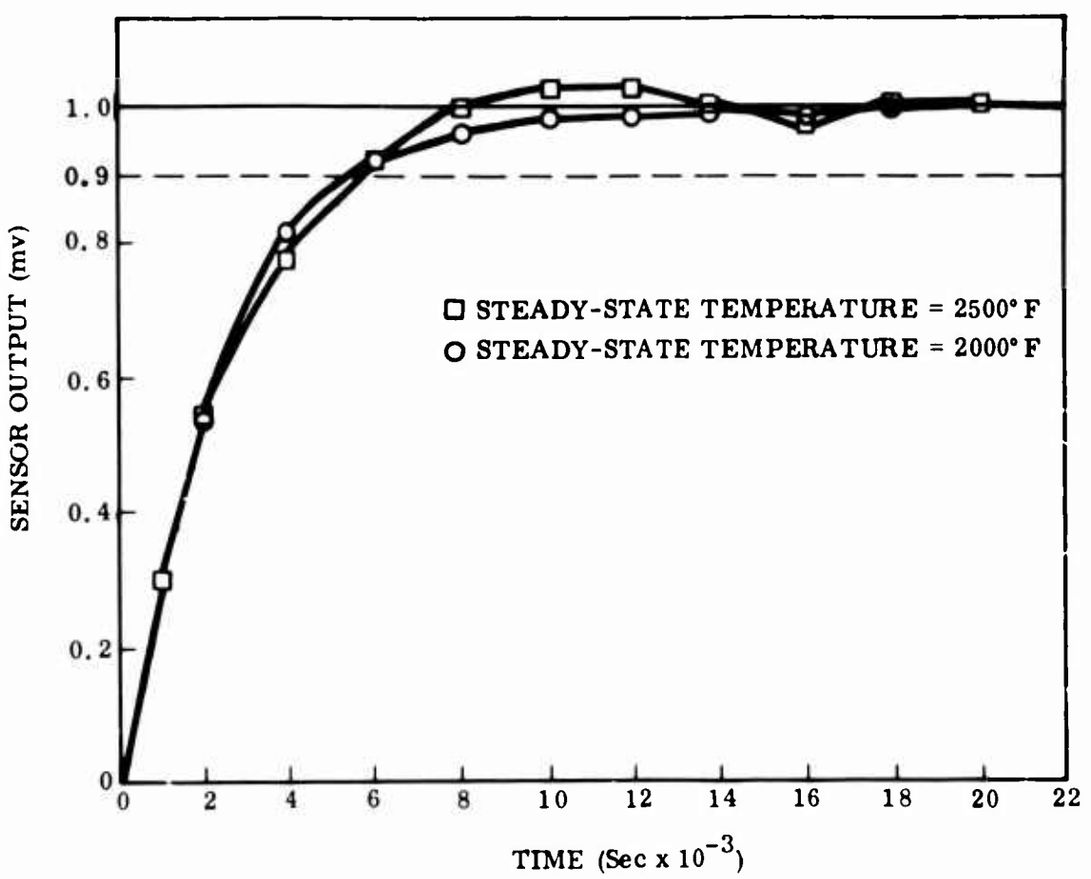

Figure 51. Response Curves for the PEM Radiation Pyrometer.

target. The majority of the radiation passes through a variable iris (motor-driven slit of variable width), through red (0.65 micron) and green (0.55 micron) filters, and into photomultiplier tubes. A complex electronic system is used to compare the strength of the two photomultiplier tubes which is proportional to the target temperature.

Response

The blackbody target was maintained at 2500°F, and the apparent step change in temperature was affected by opening and closing of the shutter placed between the target and the sensor. The results are shown as the fraction of the total step change in temperature plotted against time in Figure 52. The overshoot was probably due to time lag in the closing of the variable iris by the servo system. Until the iris was properly adjusted, too much radiation would enter the system, causing the overshoot. A 90 percent response time of 2.6 milliseconds was measured.

The decay rate was much slower, requiring 90 milliseconds for the indicated temperature to return to room temperature (shutter closed).

The accuracy of the two-color-ratio pyrometer was judged to be adequate for the intended application. The instrument read to within 2.5 percent of the measured blackbody temperature over a wide range of temperatures and using several scales.

Silicon Detector Pyrometer

This pyrometer (Ircon Model 130) employs a silicon, photovoltaic detector. It is of very simple construction, consisting of an optical system for focusing the radiation-silicon chip detector, and an output meter. The raw signal from the detector is used as the output without amplification or modification. It is a single-scale (2000° to 3000°F), single-emissivity, one-color instrument. The intensity of the incident radiation is detected in the range of peak silicon spectral sensitivity of 0.6 to 1.0 micron.

The response of the Model 130 is very fast. The shutter arrangement used for response tests was not fast enough to provide meaningful data. The rotating chopper was used to intercept the beam of radiation periodically, providing an apparent step change in temperature from room temperature to 2500°F. The output signal was fed directly from the sensor to the oscilloscope. The periodic variation of output signal with time was recorded. The photographs for three different chopper speeds are shown in Figure 53. At 380 cycles per second (Figure 53A), the sensor produces a nearly square wave and the output voltage reaches 100 percent of its steady-state value in about 0.55 millisecond; then it remains constant until the disk again begins to block part of the radiation beam. Figures 53B and 53C show the output for chopper speeds of 2600 and 4250 cycles per second respectively. The sensor does not reach its steady-state output (nor zero output at room temperature), and a sinusoidal wave form of smaller amplitude results. Two chopper wheels were used in the experiment: one with 0.5-inch-diameter holes and the other with 0.375-inch notches. The cone of radiation was quite large, making the notch geometry important. Larger amplitudes were observed using the disk with 0.5-inch holes. Temperature was measured using the amplitude of the wave form recorded on the oscilloscope as the measure of sensor output. Since the

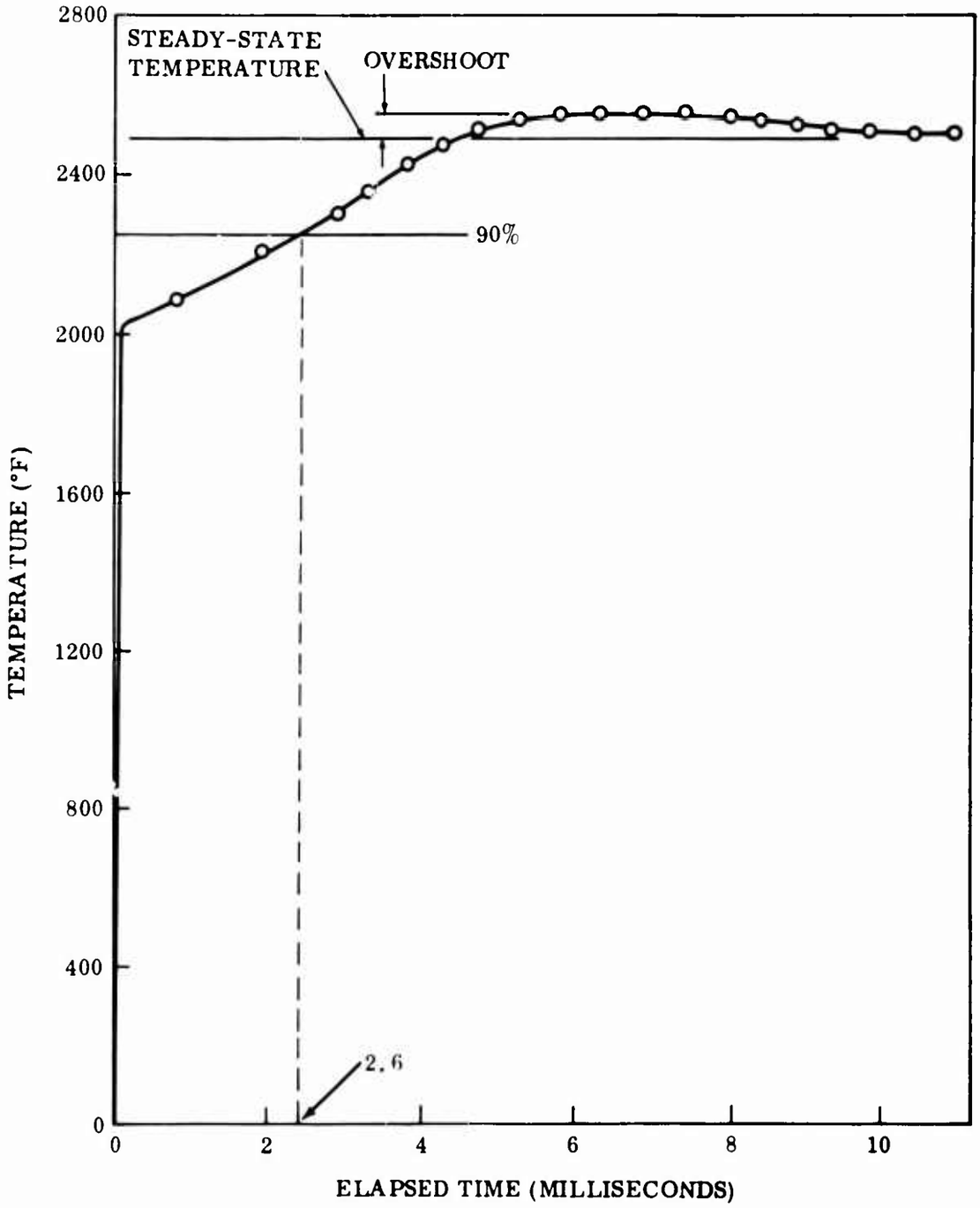

Figure 52. Rise Response Curve for the Two-Color-Ratio Pyrometer.

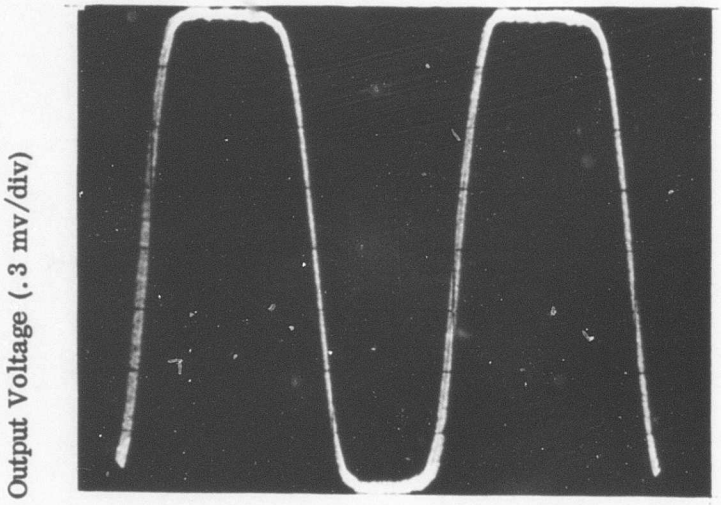

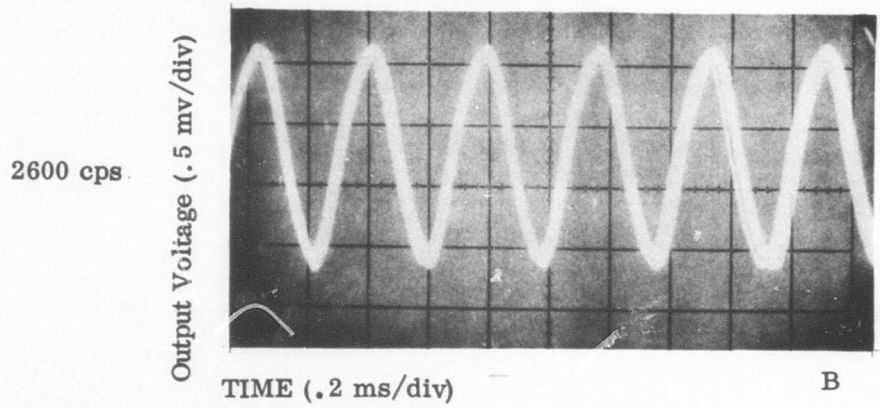

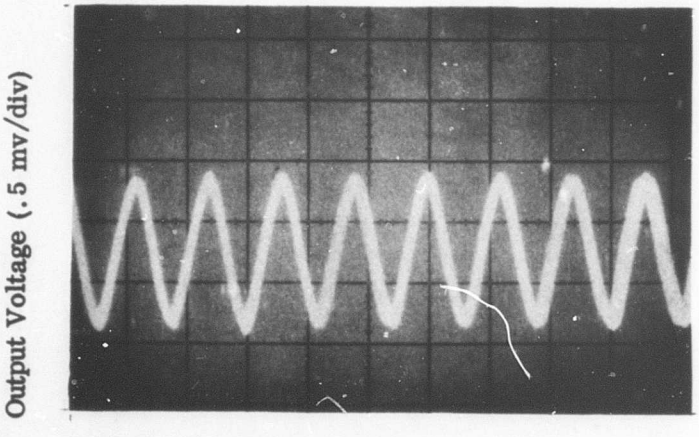

Figure 53. Output of Silicon Chip Pyrometer due to an Oscillating Target Temperature.

signal reaches neither 100 percent nor 0 percent of its nonoscillating output, the indicated temperature dropped as the frequency of oscillation increased. Table XIII indicates the percent of temperature error for increasing frequency of oscillation as well as the percent of the nonoscillating voltage produced by the sensor. The 90-percent response time of this sensor is seen to be less than 0.55 millisecond, an order of magnitude less than the program goals.

The sensor was calibrated and tested for accuracy between 2100° and 2500°F. The data are given in Table XIV and plotted graphically in Figure 54. It can be seen that the experimental calibration agrees very closely with the calibration furnished with the instrument; the error was less than 1.0 percent, even though the temperatures were in the lower one-fourth of the temperature scale.

Signal Transmission

The thermal radiation emitted by the target must pass through the optical system of the sensor. Each lens or window will reduce the signal intensity. The optical materials should be chosen so that the reduction in signal strength is constant over the entire range of conditions encountered by the lens or window and is as small as possible. Several materials offer high transmissibility in the visible to infrared range, as shown by Figure 55. Fused quartz, sapphire and vycor silica glass (#7913) were chosen for study because of good high-temperature properties (Table XV). All have high softening temperatures and high transmissibility over

TABLE XIII. EFFECT OF OPTICAL CHOPPER ON OUTPUT OF SILICON CHIP PYROMETER

Chopper Speed (cps)	Chopper Spacing (inches)	Voltage Amplitude (mv)	Percent of Non-Oscillating Output	Indicated Temperature (°F)	Temperature Error (pct)
380	.5	2.34	100	2500	0
660	.375	2.30	98	2500	0
1700	.5	2.31	98	2500	0
1800	.375	2.05	90	2460	1.6
2000	.375	1.95	85	2450	2.0
2600	.375	1.75	76	2420	3.2
2700	.5	2.0	87	2460	1.6
3300	.375	1.45	63	2370	5.2
3500	.375	1.40	61	2360	5.6
3600	.5	1.80	78	2430	2.8
4000	.375	1.25	54	2330	6.8
4250	.375	1.20	52	2320	7.2

TABLE XIV. TEMPERATURE CALIBRATION OF THE SILICON CHIP DETECTOR

Blackbody Temperature (°F)	Theoretical Detector Voltage (mv)	Actual Detector Voltage (mv)	Indicated Temperature (°F)	Temperature Error (pct)
2140	.59	.66	2160	+ 0.9
2200	.76	.82	2215	+ 0.7
2240	.89	.95	2260	+ 0.9
2300	1.12	1.18	2305	+ 0.2
2320	1.21	1.26	2330	+ 0.4
2360	1.41	1.43	2370	+ 0.4
2400	1.63	1.69	2405	+ 0.2
2420	1.75	1.79	2425	+ 0.2
2440	1.88	1.86	2440	0
2460	2.02	2.00	2455	- 0.2
2500	2.33	2.32	2500	0

the desired spectrum. The thermal expansion coefficient of the material should be low in order to increase its capability to withstand thermal shock and to minimize dispersion of the light caused by distortion of the window or lens.

The transmissibility of the optical materials chosen for study was tested using two different spectral ranges. An Ircon 130 sensor sensitive to radiation of wavelength between 0.6 and 1.0 micron and an Ircon 300 pyrometer with spectral response between 2.0 and 2.6 microns were used to test transmissibility. The sensors were set up with the graphite blackbody as the radiation source. The signal strength through a 0.125-inch-thick sample of the material was compared to the signal strength without the window. A 9-inch-long sapphire "light pipe" was also tested in the same manner. Table XVI gives the results of the tests. All three materials transmitted a large portion of the signal in both spectral regions. Quartz, absorbing 7 percent of the signal, reduced the intensity by the least amount. The fact that the transmissibility of the 9-inch-long light pipe is only slightly less than the 0.125-inch window of the same material demonstrates that the losses are largely at the surface and that absorption in the material is very small.

The three windows were then exposed in air at 2000°F for 100 hours and retested for transmissibility. The quartz and the sapphire did not show any change in transmission characteristics. The vycor silica glass exhibited a fine surface cracking which decreased the transmission to less than 50 percent. Sapphire and

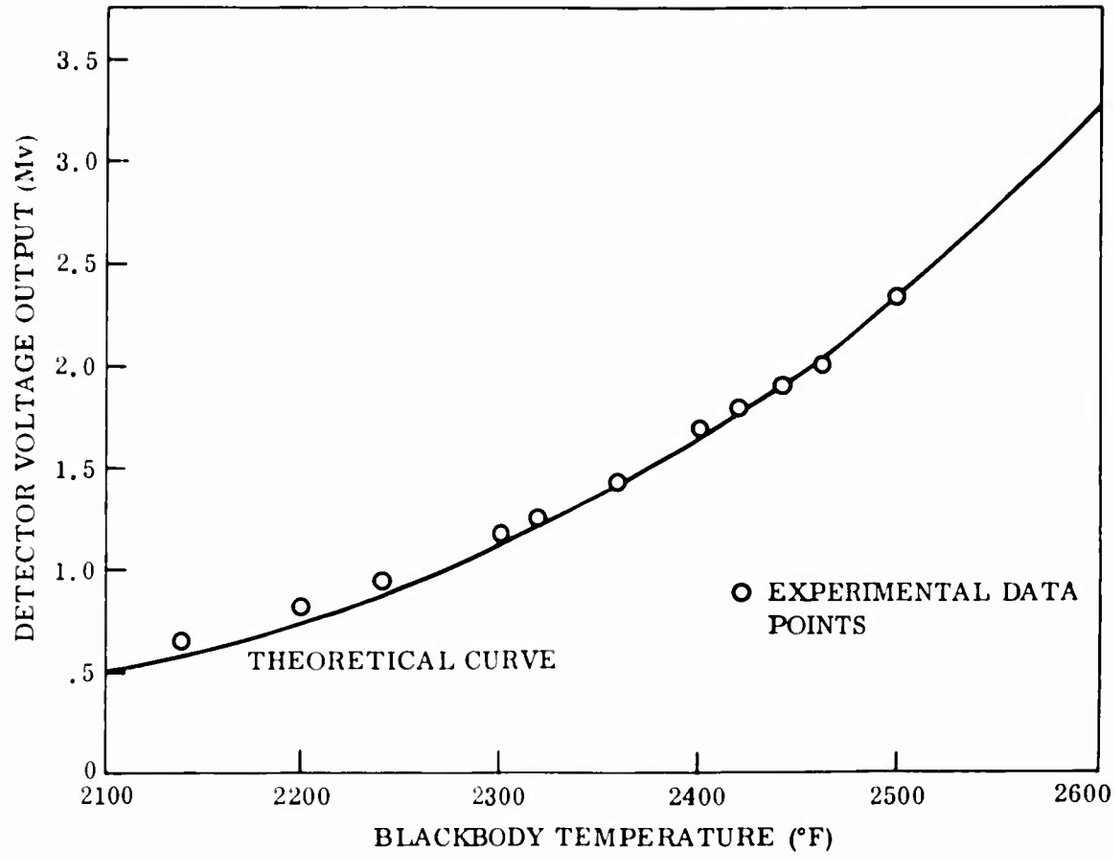

Figure 54. Theoretical and Experimental Calibration for the Silicon Chip Pyrometer.

quartz windows were also tested in the same way while being heated to 500°F. Transmissibility was not decreased over this temperature range. The sapphire light pipe, however, was not able to withstand a thermal gradient and could not be used where such a condition existed.

The conclusions from this series of tests are that sapphire and quartz are the best materials for use with sensors operating in the visible to infrared spectrum. From Figure 55, it can be seen that quartz should not be used at wavelengths longer than about 3 microns and sapphire should not be used above 4.8 microns. Under equal conditions, quartz is preferable due to its better transmissibility and lower cost.

Summary of Laboratory Sensors

Five commercial radiation pyrometers were evaluated for possible adaptation to turbine inlet temperature measurement in a small gas turbine. Laboratory tests were carried out to measure response and accuracy. All of the instruments were designed for the widest possible adaptability and not for one specialized application. Thus, the potential adaptability of the detection system was considered and not the particular model. Consideration was given to size, weight, simplicity, ruggedness and reliability.

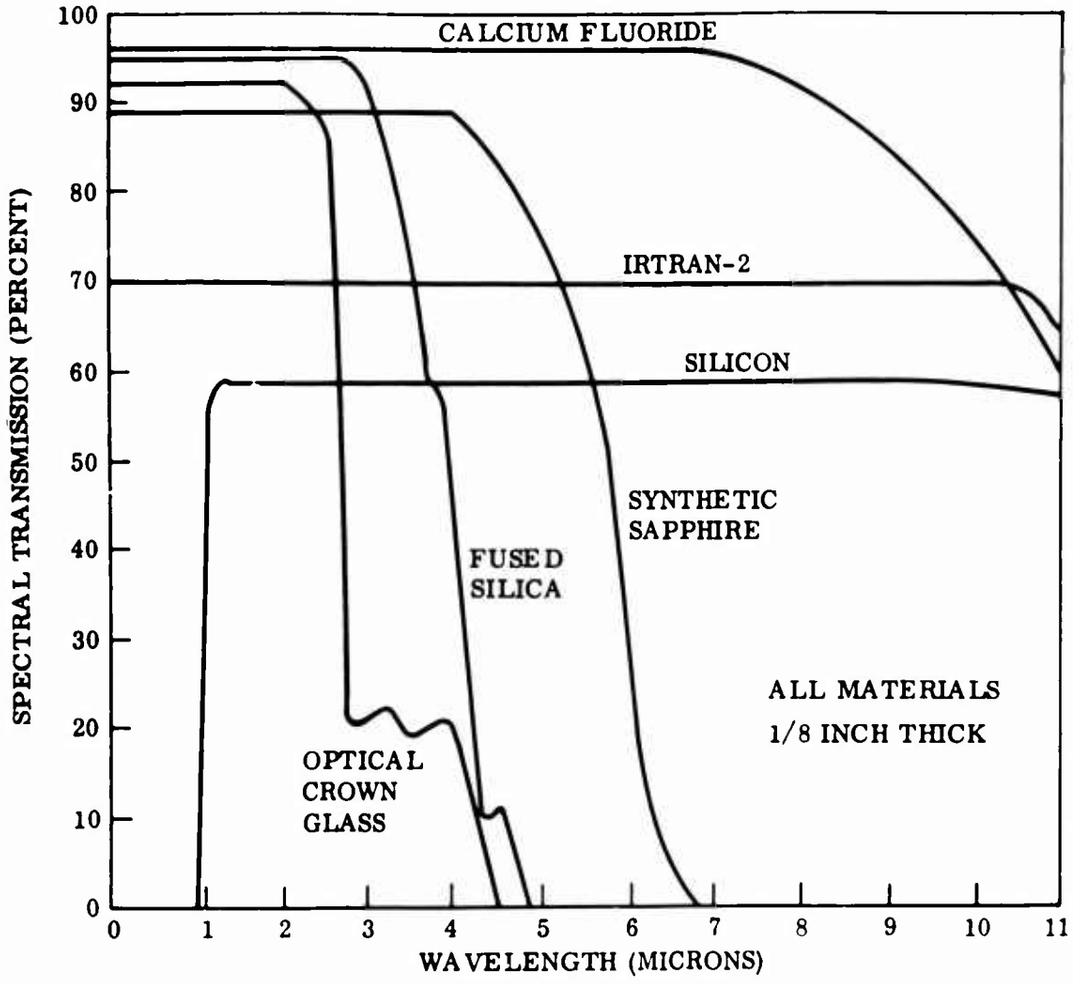

Figure 55. Transmission Characteristics of Several Infrared Optical Materials.

The lead-sulfide detector was judged to be of moderately complicated construction. Modulation and amplification of the detector signal require complicated moving parts, making miniaturization difficult. The accuracy of the tested instrument was poor, but this was not thought to be a characteristic of lead-sulfide detectors in general. The time constant was measured to be 7 milliseconds, indicating a fast response rate. The decay time was slow, however, requiring 22 milliseconds to return to 63 percent of the steady-state temperature.

The single-color photomultiplier tube pyrometer also was of complicated construction. A reference lamp and rotary shutter would make turbine application difficult for durability and reliability reasons. Response was slow, requiring 170 milliseconds to reach 63 percent of the step change and 400 milliseconds to reach 90 percent.

TABLE XV. PHYSICAL AND OPTICAL PROPERTIES OF OPTICAL COUPLING MATERIALS

Material	Index of Refraction	Softening Temperature (°F)	Relative Transmissibility Range (microns)	Thermal Expansion (cm/cm/C)
Calcium Fluoride	1.434	2500	--- to 7.0	--
Fused Quartz	1.544	2800	.24 to 3.4	5.5×10^{-7}
Sapphire	1.77	3700	.15 to 4.7	66.0×10^{-7}
Magnesium Oxide	1.736	4500	--- to 6.0	--
Vycor (#7913)	1.46	2300	.3 to 2.0	8.0×10^{-7}

TABLE XVI. TRANSMISSIBILITY OF OPTICAL COUPLING MATERIALS

Optical Material	Window Thickness (inches)	DETECTOR: IRCON 130 PH* Signal Transmission (pct)	DETECTOR: IRCON 300** Signal Transmission (pct)
Quartz	.125	93	90
Vycor	.125	93	88
Sapphire	.125	86	87
Sapphire Light Pipe 1/4-inch dia.	9.000	74	83

* Wavelength 0.6 to 1.0 Micron
** Wavelength 2.0 to 2.6 Microns

The photoelectromagnetic radiation pyrometer was large and very complicated. Miniaturization would be impossible. A motor-driven chopper and an internal lamp are both heavy and fragile. Fast response was measured, with 90 percent of the step change being recorded in 6 milliseconds.

The two-color radiation pyrometer also had a fast-rise response rate (2.6 milliseconds) but was quite slow (90 milliseconds) in returning to a lower temperature. Accuracy was good but the system was large and very complicated; filters, photomultiplier tubes and an integrating sphere comprised a system that is not easily adaptable to a turbine engine.

It was concluded that the silicon chip photovoltaic pyrometer was by far the best choice. It exhibited the fastest response and the smallest size, and was of simple construction. The ambient temperature characteristics of the silicon detector

were also superior to those of the other pyrometers. The silicon chip detector was completely of solid-state construction without complicated moving parts. This sensor was the only one that offered the potential for a response time (0.55 millisecond) fast enough to allow the use of the rotating turbine blades as targets.

Based on the foregoing reasons, it was decided to purchase a small radiation sensor of the silicon detector type that embodies as many of the desirable features as possible for measuring temperature of rotating turbine blades. Ircon Infrared Controls, Incorporated, of Chicago, Illinois, was selected as the manufacturer, since the miniature sensor would be a package redesign of one of their products. After negotiations with Ircon, a contract was let to build a miniature radiation sensor to specifications tailored to fit turbine inlet temperature requirements.

MODEL T-1 TURBINE RADIATION SENSOR

Operation

The miniature turbine radiation sensor, Model T-1, is shown schematically in Figure 56. The specifications to which it was built are listed in Table XVII. The sensor is exceptionally simple, consisting of a sapphire window, a lens and the silicon detector. Output leads are soldered directly to the silicon chip. There are no moving or fragile parts to be damaged by mechanical vibration or shock loading. The case is of stainless steel and the back is sealed with epoxy resin. No power is required by the sensor and no amplification of the detector output is needed.

A silicon photovoltaic p-n junction serves as the detector element, generating an output current in direct proportion to the intensity of the radiation incident upon its surface (within its spectral response). The incident radiation is directly proportional to the radiance of the target. The intensity of the radiation is decreased by a fixed amount due to passage through the window and lens of the optical system. A voltage is produced across the p-n junction, causing a current to flow in an external circuit proportional to the target radiancy. An element of known resistance is added to the circuit, and the voltage drop across this resistor is measured as the sensor output.

Calibration

The sensor output is a function of the temperature of the target, the target emissivity and the temperature of the detector. The dependence of output on detector temperature will be discussed later. The absolute calibration is fixed by measuring the output current produced in a closed circuit with negligible resistance when the detector (at 100°F) is exposed to a blackbody target at 2000°F. The current I_T produced by this sensor at any other temperature can then be calculated by using Planck's radiation equation (Equa. 45) to find the radiance (R_T). The current (I_T) produced at temperature will be given by

$$I_{(T)} = \frac{R_T}{R_{2000}} I_{2000} \qquad (45)$$

The output current relative to that at 2000°F was calculated in this way and is plotted in Figure 57. This plot is actually the radiance at temperature divided by the radiance at 2000°F.

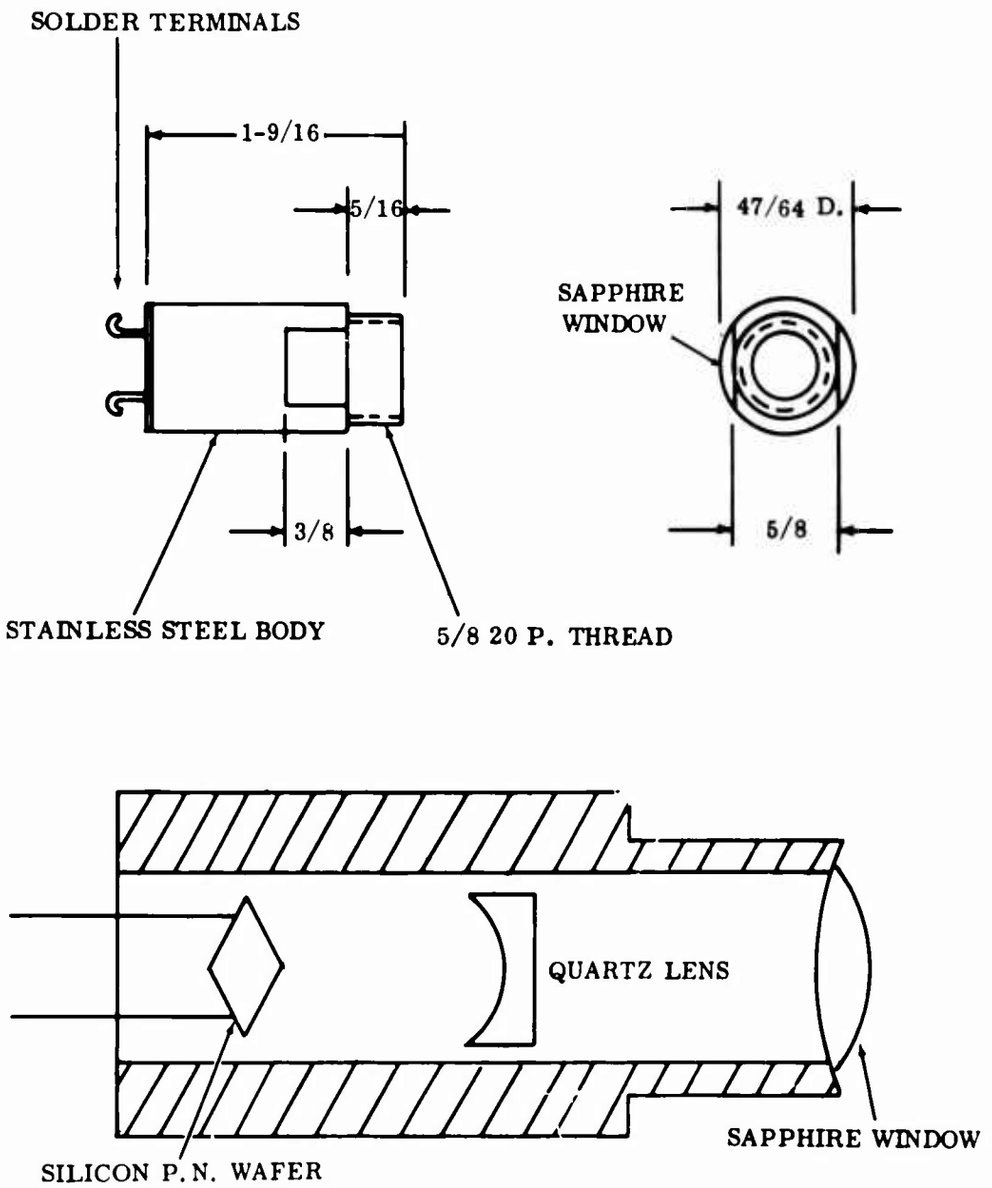

Figure 56. Schematic Diagram of the T-1 Radiation Sensor.

TABLE XVII. SPECIFICATIONS FOR THE T-1 RADIATION SENSOR	
Spectral Range:	0.6 - 1.0 micron
Source Temperature Span:	1400°F to over 3000°F
Spot Size:	5/16 inch
Focal Length:	0 to 5 inches
Output Level:	50mv full scale
Response Time:	Less than 10 microseconds
Operating Temperature, continuous:	to 250°F
Absolute Maximum Temperature:	250°F
Power Requirements:	None

I_{2000} for this sensor was measured to be 4.2 microamperes. This value will vary approximately ± 25 percent from detector to detector so that each sensor of this type must be individually calibrated.

In practice, the voltage drop across a resistor is measured and not the current directly. The value of the resistor is adjusted to give the desired reading over the temperature range of interest. The sensor output current I_T is converted to an output voltage V_T by passing the current through the external calibration resistor R_C:

$$V_T = I_T R_C \tag{46}$$

To preserve the linearity between the target radiance and output current, the voltage should be limited to 50 millivolts and the calibration resistor should not exceed 25,000 ohms. The value of the calibration resistor is fixed by choosing the maximum temperature to be measured and adjusting the resistance to give an output voltage of about 50 millivolts at full scale. A full-scale temperature of 3000°F was chosen and a calibration resistance of 370 ohms was used. This resulted in a full-scale voltage of 48.17 millivolts.

As a check on the calculated values for output current (or voltage) shown in Figure 57, an experimental calibration was carried out using a small platinum-wound resistance furnace to heat a 5/8-inch-long cylindrical graphite, blackbody cavity with a 5/16-inch inner diameter. The emissivity of this cavity was calculated to be 0.95 ± 0.02. The temperature at the cavity was measured by an NBS transfer standard thermocouple inserted into the cavity. The radiation sensor was maintained at 100°F and was calibrated every 100 degrees between 1600° and 2600°F. The results are compared with the calculated values in Table XVIII and are plotted in Figure 58. The experimental calibration agrees quite closely with the values calculated for a perfect blackbody.

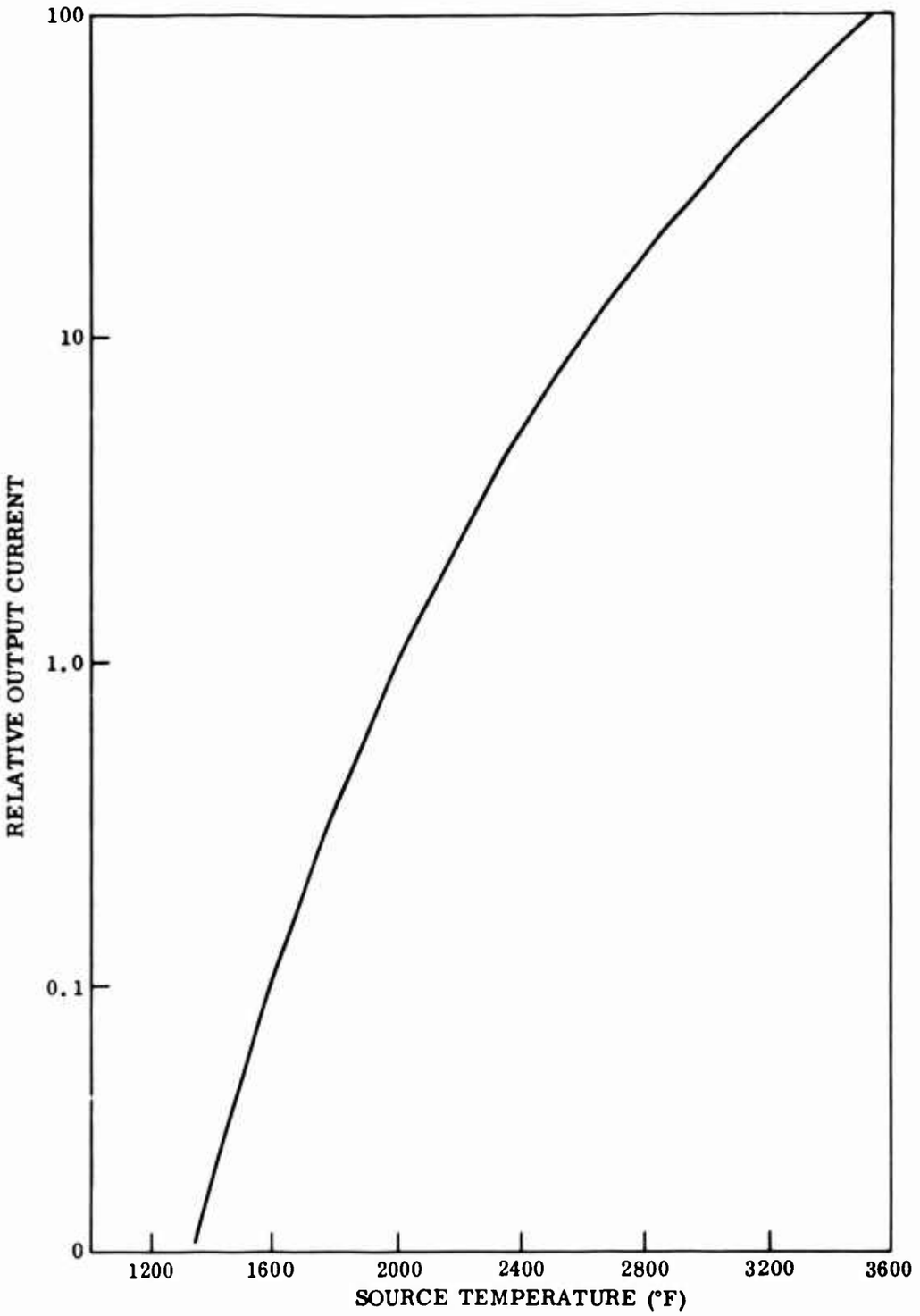

Figure 57. Calculated Calibration Curve for the T-1 Radiation Sensor.

TABLE XVIII. CALIBRATION OF T-1 RADIATION SENSOR

NBS Temperature (°F)	Output of Sensor (mv)	Calculated Blackbody Calibration (mv)	Error (°F)
1600	0.189	0.163	+17
1800	0.605	0.559	+16
2000	1.610	1.55	+ 8
2100	2.48	2.49	+ 1
2200	3.66	3.73	+ 4
2300	5.36	5.59	-12
2400	7.75	8.08	-11
2500	10.66	11.50	-19
2600	14.70	15.54	-15

The sensitivity of the radiation sensor is quite adequate, increasing with increasing temperature. At 1600°F, a change in temperature of 6.5°F corresponds to a change in output voltage of 0.10 millivolt. At 2500°F, a change of only 0.25 degree will cause the same output change.

Detector Temperature Correction

The output voltage of the sensor is dependent upon the detector temperature as well as the source temperature. This is because the detector becomes sensitive to long wavelength radiation as the temperature increases, allowing a wider spectrum of radiation to act upon the detector and thus increasing the output current. The approximate temperature of the detector was measured by measuring the temperature of the stainless-steel case. There is also a maximum temperature to which the sensor may be exposed without damage to the detector. This temperature was originally set by the manufacturer at 300°F, but this has since been lowered to 250°F.

The change in output voltage (or current with changing case temperature) was measured by Ircon, and the data were furnished with the sensor. The tests were made at a constant target temperature of 1800°F. The results were normalized relative to the output at the standard case temperature of 100°F. As a check on these data, similar tests were performed using a different target temperature (2100°F) to verify that the case temperature correction is constant for all target temperatures. The relative output voltage is shown as a function of ambient temperature for both sets of tests in Figure 59. It can be seen that the data are in

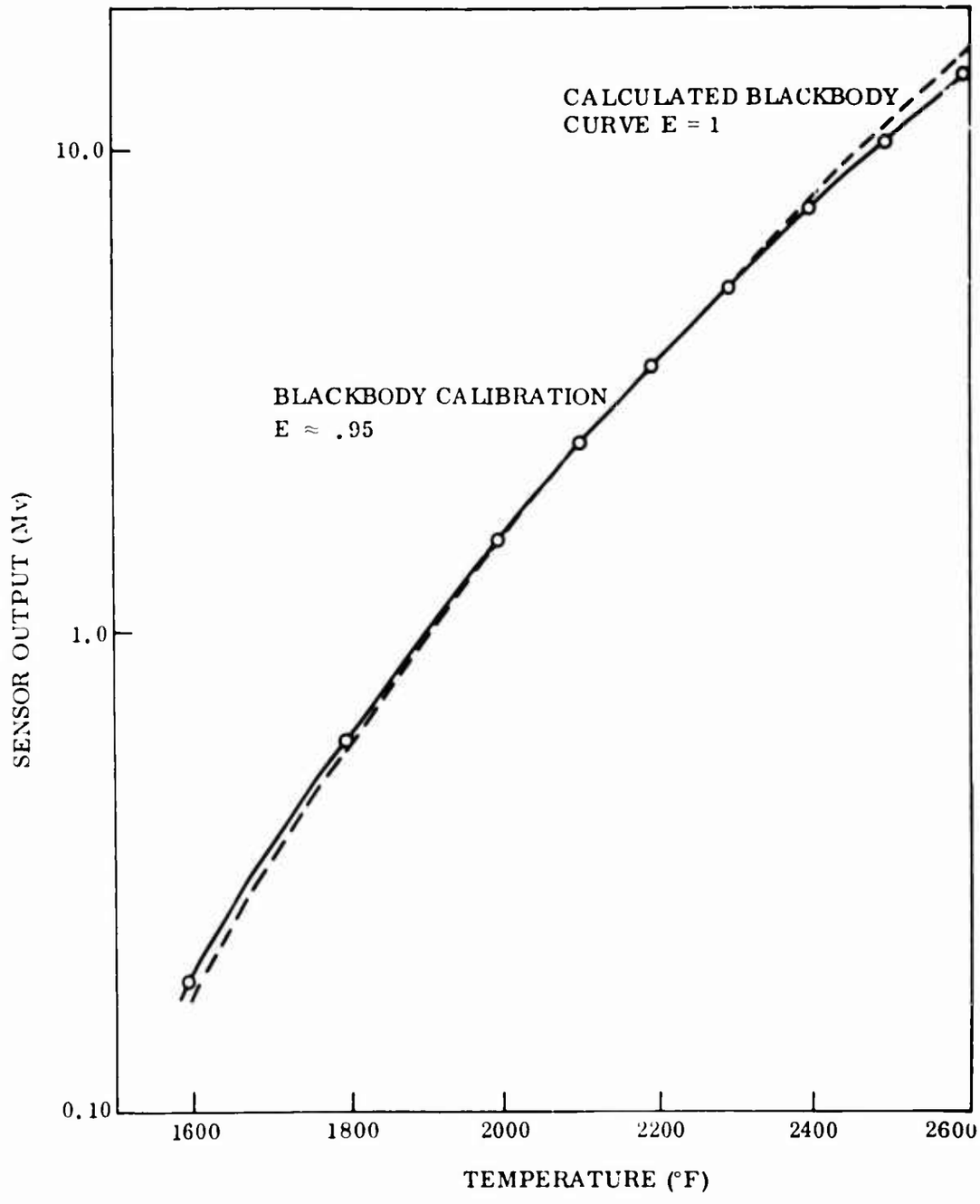

Figure 58. Experimental Calibration Curve for the T-1 Radiation Sensor.

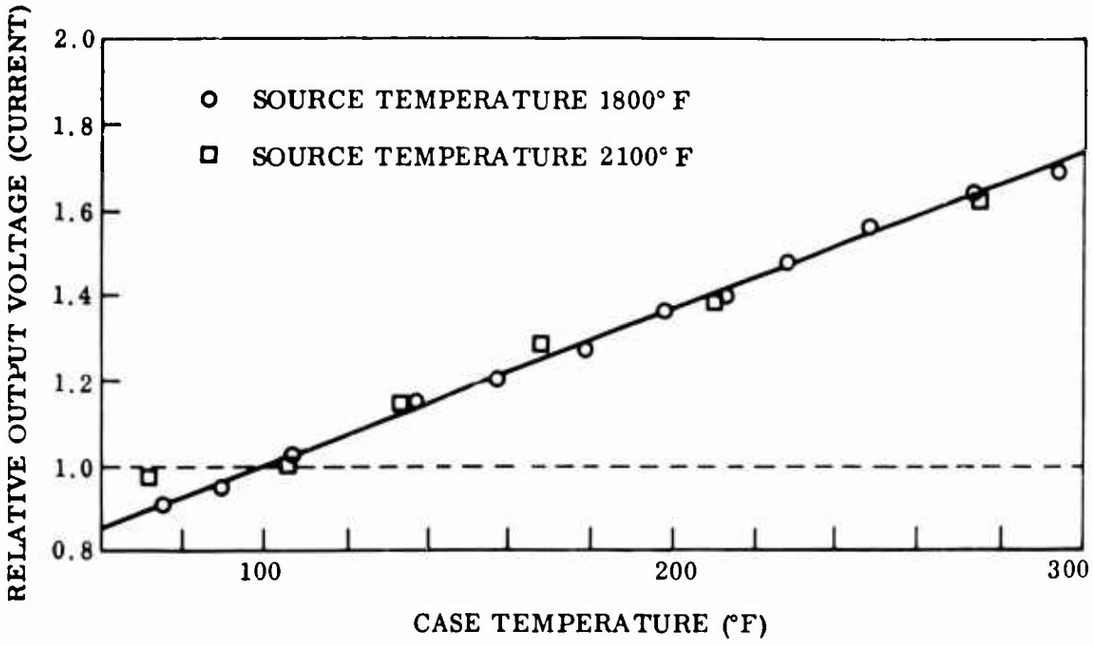

Figure 59. Output as a Function of Ambient Temperature.

very close agreement and that the voltage correction is constant for different target temperatures.

Target Emissivity

A radiation sensor applied to turbine inlet temperature measurement would not have a blackbody target. To study the effect of nonblackbody radiation sources on sensor accuracy, the T-1 radiation sensor was calibrated for two nonblackbody targets. An Inconel 713LC disk was placed in the small tubular furnace in place of the blackbody. The cavity formed by the disk and the furnace tube resulted in an emissivity of approximately 0.8. A resistance heated platinum foil (emissivity ≈ 0.3) was also used as a target. The sensor output as a function of temperature is compared with the blackbody calibration in Figure 60 for both targets. The plots of voltage output versus temperature for all three values of emissivity are nearly parallel. The sensor output can be calculated from the blackbody calibration if the emissivity is known and is constant over the temperature range of interest. If the emissivity changes with temperature, then the sensor can be experimentally calibrated for the particular conditions present. Emissivity changes would not be expected to cause any problem in correct temperature measurement.

Effect of Luminous Gas

The overall effect of luminous gas on the sensor output is to add noise to the signal. If the signal strength is sufficiently large, the noise added by the gas should not have an adverse effect. The color of the flame determines the effect on the T-1 radiation sensor. A blue flame with a short wavelength (0.48 micron) does not fall within the spectral range of the sensor; therefore, changes in intensity do not affect the sensor. Figure 61A shows the output of the sensor viewing a 2255°F

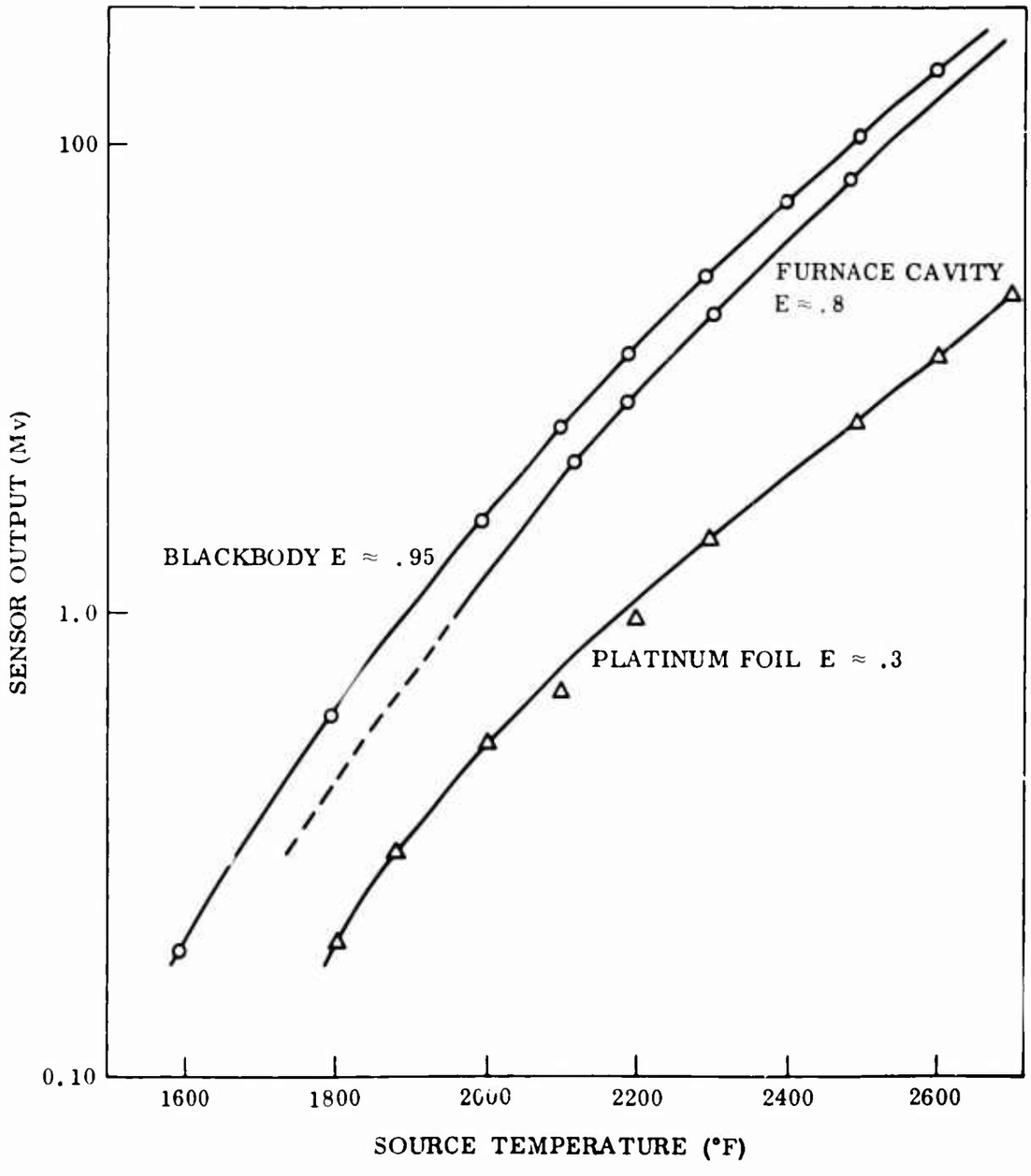

Figure 60. Calibration Curves for the T-1 Radiation Sensor.

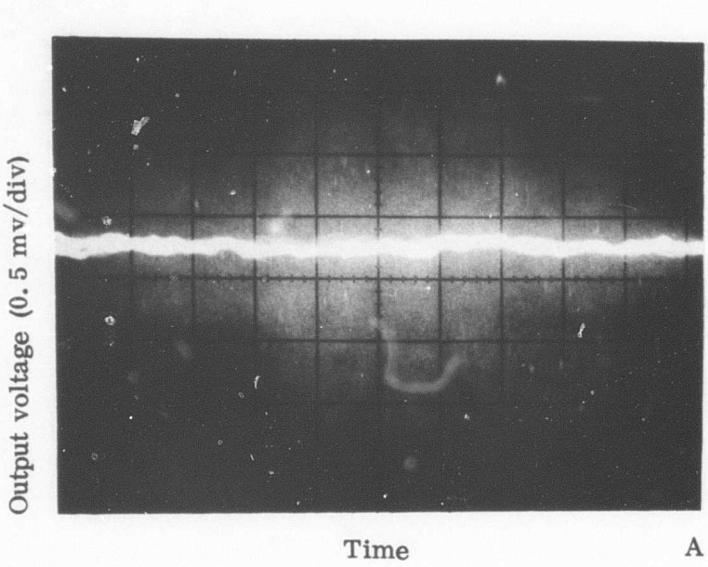

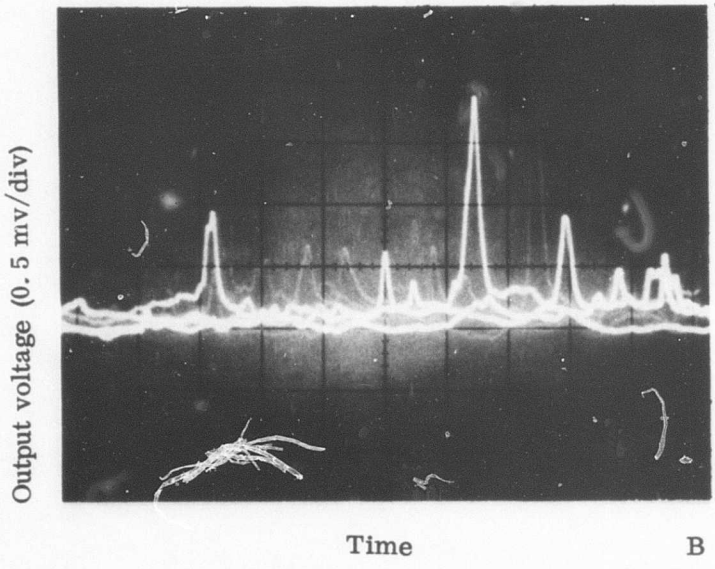

Figure 61. The Effect of Luminous Gas on the Output of the T-1 Radiation Sensor.

target through a blue flame. The total output is 4.2 millivolts, and the deviation from the mean is about ± 0.1 millivolt. The output for the same target at 2370°F viewed through a bright yellow flame with a predominantly longer wavelength (0.6 micron) is shown in Figure 61B. The total signal is 6.7 millivolts, and a deviation of ± 0.2 millivolt with peaks up to 1.75 millivolts is shown. Although the noise created by the luminous gas has greatly increased, the basic signal is still clear. The calibration of the sensor was not affected by the luminous gas, and the added noise could be eliminated electronically.

Response

The rotating chopper described earlier was used to interrupt the beam of radiation to test the response of the T-1 radiation sensor and is shown in Figure 62. The response rate was found to be several orders of magnitude faster than had been measured previously. The disk was rotated at a maximum of 12,500 rpm. Twenty cycles per revolution resulted in 4,160 cycles per second or 240 microseconds per cycle. An oscilloscope trace of the sensor output is shown in Figure 63. It can be seen that even at this frequency, a square wave is produced by the sensor. The time to go from room temperature to 2500°F was about 35 microseconds. This figure does not represent the maximum response rate of the sensor, but only the minimum time that a step change could be effected by method.

Figure 62. Response Time Measurement Equipment for the T-1 Radiation Sensor.

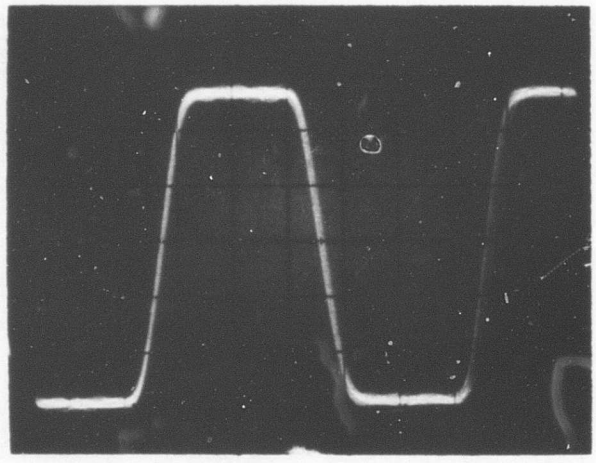

Figure 63. Output of T-1 Radiation Sensor due to an Oscillating Target Temperature.

A faster step change was obtained by using a pellet from an air rifle to momentarily block the beam. A schematic diagram and photograph of the test apparatus are shown in Figure 64. The apparent step change from steady-state signal to room temperature occurred in 20 microseconds, and 90 percent of this change was recorded. The true response rate of the sensor appears to have been approached in this test. The response is adequate to allow a wave form output to be obtained from the sensor using a rotating blade target.

Lens Protection

The reduction in the intensity of the radiation passing through the optical system must be as small as possible and remain constant with time. Any change in the amount of radiation lost in a lens or window will change the calibration of the instrument and cause an error in the indicated temperature. The only place where this is likely to occur is the protective window exposed to the moving gas. Temperature changes have been shown not to change the transmissibility of sapphire windows. Carbon or other combustion products adhering to the window surface will reduce the effective area available for transmission and reduce the signal, causing a negative temperature error. Keeping this window clean is an important and difficult problem. Compressor discharge air could be used to purge the front of the window. A simple configuration, consisting of an air manifold encircling the window and directing air radially in front of the window, has proven ineffective in tests carried out in the turbine simulator shown in Figure 65. It appears that turbulence in the purge airstream picks up carbon from the moving gas and carries it back to the lens, even though the total airflow is away from the lens. This turbulence was eliminated by the insertion of an airflow collimator in the purge airstream in front of the window. The air-lens is designed to produce laminar airflow in all air passages, thus not allowing solid particles to be carried against the bulk flow and deposited on the sensor window. A schematic diagram of this arrangement is shown in Figure 66. Figure 67 shows photographs of a trial collimator and the cooling jacket used to mount the sensor on the atmosphere simulator. Without the collimator, the window of the sensor became covered with carbon particles in 5 minutes. The trial collimator with 0.10-inch diameter air passages was added, and the amount of carbon was considerably reduced. By reducing the size of the air passages to 0.015 inch, the carbon deposition was completely eliminated during more than 3 hours' exposure on the test rig.

The signal intensity was reduced by the insertion of the collimator into the path of the radiation. Alignment of the collimator with the sensor axes was critical,

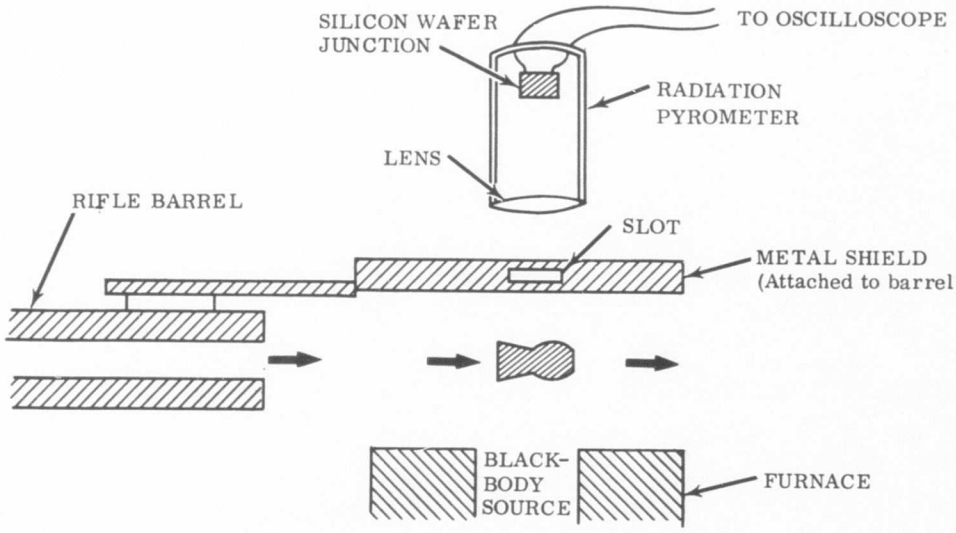

Figure 64. Experimental Setup for Response Tests Using a Ballistic Impact Apparatus.

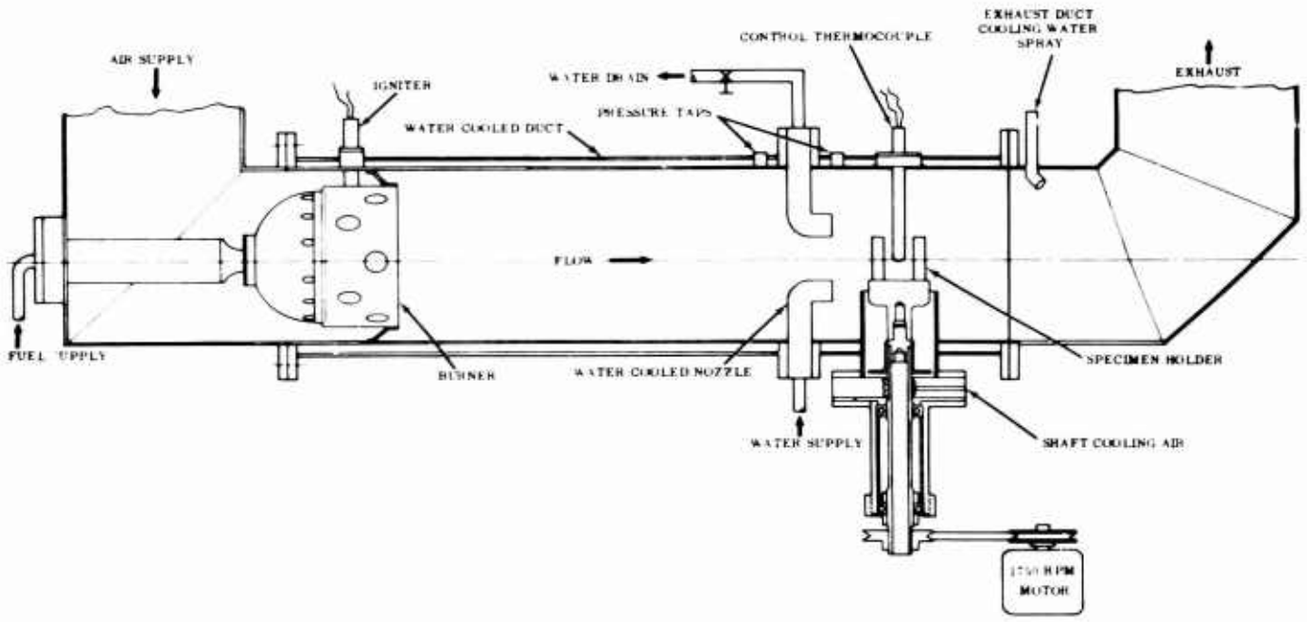

Figure 65. Two-Inch Combustion Rig for Turbine Environment Simulation.

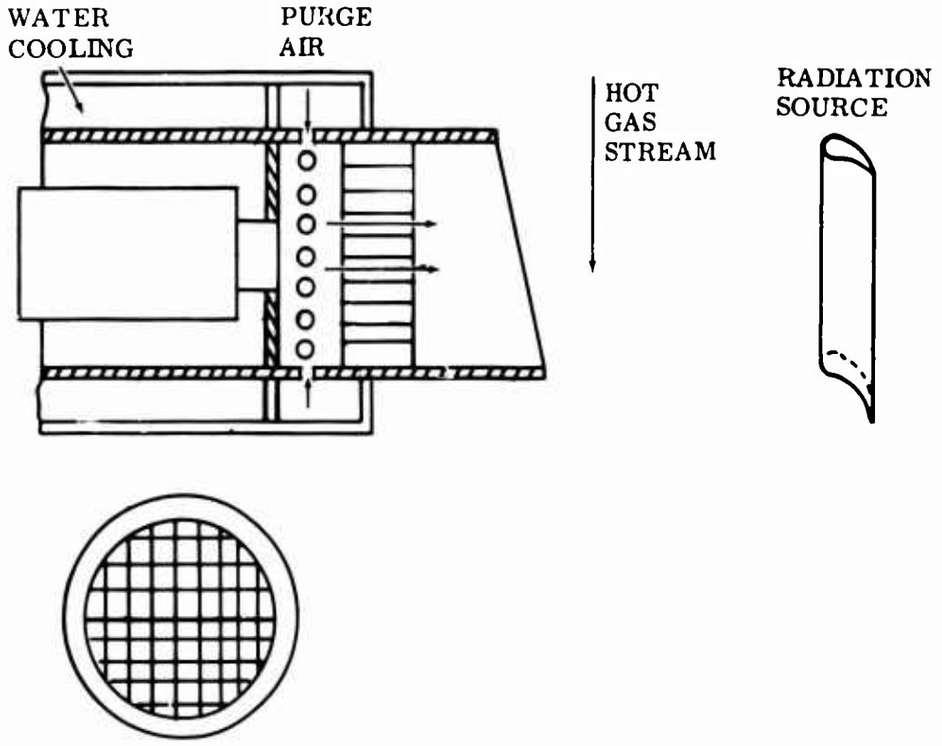

Figure 66. Air-Collimator Lens.

especially for the smaller diameter collimators. Signal reductions of between 5 and 35 percent were measured. No detailed analysis of the maximum diameter air passage able to maintain the clean window was attempted, nor was a relationship between collimator configuration and signal reduction established.

Summary and Projections

The T-1 radiation sensor has proved to exhibit many of the properties necessary for a radiation sensor to be applied to turbine inlet temperature measurement as well as some limitations which must be overcome or minimized. It is small, is of simple, solid-state construction, and has extremely rapid response. The accuracy and sensitivity of the instrument is excellent at high temperature (1800° to 3000°F) and is adequate down to approximately 1500°F. It must be calibrated for the emissivity of the particular target, and changes in that emissivity will cause errors in the temperature reading if the instrument is not recalibrated. The sensor output is directly proportional to the detector temperature, and there is a maximum detector temperature that may not be exceeded without damage to the sensor.

The dependence of sensor output on the detector temperature can be easily compensated for in two ways. One would be to include a temperature sensitive resistor inside the sensor case that would compensate for changes in the detector output. The increased output is caused by the increasing bandwidth of the spectral response at higher temperatures. The second way would be to place a filter in the

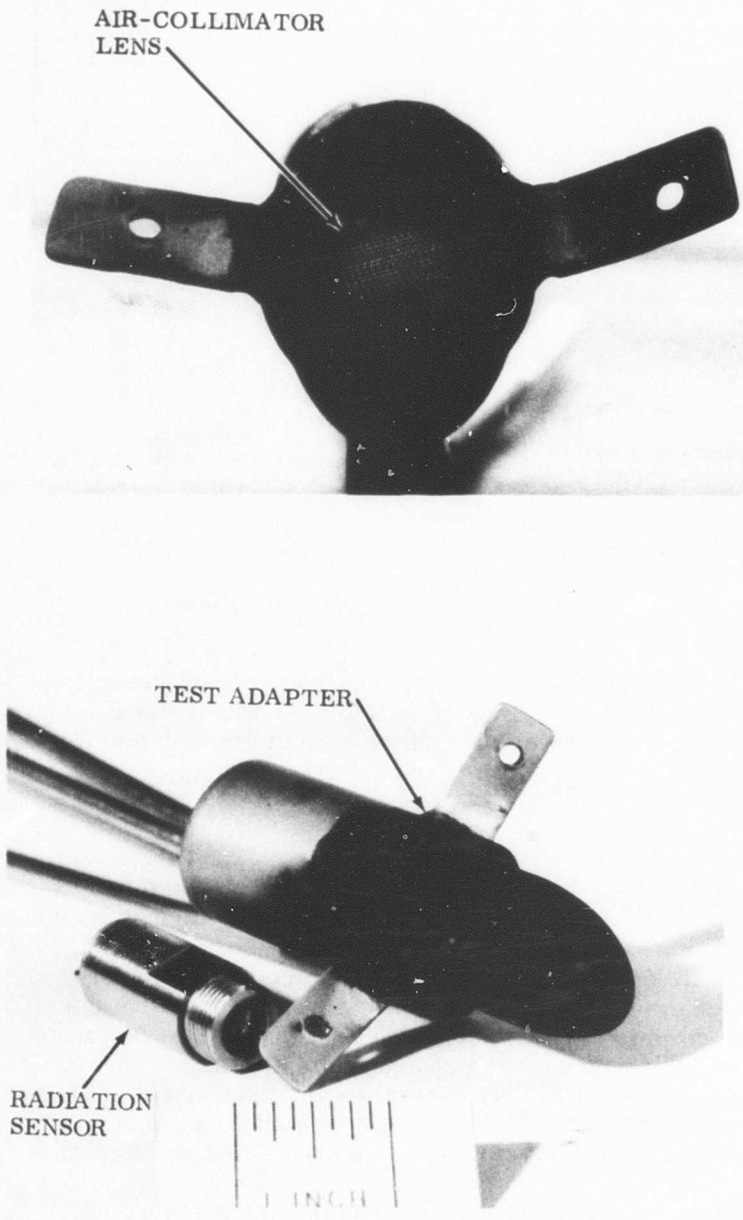

Figure 67. T-1 Radiation Sensor with an Air-Collimator Lens and Test Adapter.

optical system to eliminate the longer wavelengths from the incident radiation. The increased sensitivity would then have no effect on output because the particular wavelengths would not be present in the radiation. The detector must be maintained at less than 250°F, both during operation and after shutdown of the engine. Increasing this temperature limitation must involve changes in the solid-state detector itself.

Further work must also be concerned with adaptation of the optimized sensor to the turbine environment. The temperature limit can be maintained by proper design of the sensor mount. Insulating the sensor from the turbine casing will decrease the heat transfer, and compressor discharge air might be used to cool the sensor during operation. After shutdown of the turbine, the cooling air would not be available and care would have to be taken to assure that the maximum temperature was not exceeded.

Lens protection also is a part of adapting the optimized sensor to the turbine engine. Optimization of the purge airflow collimator will be necessary to maintain a clean optical system and to help keep it cool. The optics must also be designed for the application with the focal length and spot size tailored to the particular engine. The spot size must conform to the size and configuration of the target. In general, a more complicated and larger optical system will allow a smaller target to be viewed and will produce a larger signal by focusing more incident radiation on the detector. Continued work, therefore, can be divided into two problems: optimizing the sensor itself, and then adapting the improved instrument to function as a turbine inlet temperature sensor either by viewing the turbine buckets directly or by inserting an object in the gas flow path.

CONCLUSIONS AND COMPARATIVE EVALUATION

Three types of turbine inlet temperature transducers were considered during the program: thermoelectric, resistive, and radiation sensors. Resistive devices demonstrated the least potential for turbine application and were investigated in less detail than the other two concepts. The ability and potential of the three types of sensors to meet the program goals are discussed in this section and, finally, recommendations are made for continued work toward the development of an effective and reliable turbine inlet temperature sensor.

Two types of thermoelectric devices were considered: exposed and protected hot junction thermocouples. The exposed junction offers fast response to temperature changes but presents difficult design problems to establish sufficient reliability and durability at the turbine inlet. The protected junction is inherently durable but does not offer fast response.

Platinum-rhodium was chosen as the only thermocouple able to operate as an exposed junction in an oxidizing atmosphere. Iridium-rhodium was unacceptable due to the high rate of oxidation of the iridium. Tests at 2500°F showed that several refractory oxides were compatible with platinum-rhodium alloys. Alumina performed as well as, or better than, any other oxide and was chosen for its greater availability and reduced cost. Tungsten-rhenium was also found to be compatible with Al_2O_3 in an inert atmosphere and is suitable for use as a protected junction.

Pt versus Pt10%Rh and Pt6%Rh versus Pt30%Rh are both acceptable junctions; the latter exhibited slightly better oxidation resistance and is the preferable choice.

Five radiation pyrometers were tested. One, the silicon detector pyrometer, was found to have far more potential for turbine application than any other type. It is of simple construction, rugged, easily miniaturized, and accurate, and it has extremely fast response. Even though it had the best ambient temperature capability of all the models tested, it is still limited in this respect. A miniature version was designed especially for the program. Comprehensive tests indicate that this sensor is able to perform most of the tasks outlined in the program specifications.

ABILITY OF THE SENSORS TO MEET PROGRAM GOALS

All of the thermocouples tested possess sufficient temperature capability. The Pt6%Rh versus Pt30%Rh couple is calibrated to 3250°F. W-Re couples are capable of reaching over 4000°F in an inert atmosphere.

The maximum transients, pressures and velocities that a thermocouple can withstand depend, for a large part, on the design of the entire probe. A protected junction would be able to withstand the maximum conditions outlined in the program

goals, but at the expense of response. Exposed junctions are much more susceptible to damage due to these factors. Platinum-rhodium exposed junctions easily sustain temperature transients of 2000°F per minute. Tests showed that velocities of greater than 700 feet per second had only a small effect on the thermoelectric properties during the 30 hours of the test. The strength of Pt-Rh is very low at temperatures above 2000°F, and plastic deformation will take place in a junction exposed directly to the moving gas.

Both types of thermocouples are potentially accurate to within ±15°F. To estimate errors particular to TIT measurement (recovery, radiation and conduction errors), exact design data would have to be obtained for a particular engine and probe design.

Single wire junctions, of 0.010 inch diameter, exhibited 90% response times of 540 milliseconds when tested in a fluidized bed. Wire multijunctions reduced this to 290 milliseconds. Fusion-welded foil junctions made of 0.002-inch foild reached 90% in 430 milliseconds. Testing in a moving gas atmosphere increased the response rate in all cases, dropping response times to 150 for the multijunction and to 230 for the foil single junction. Thermocouples capable of withstanding the turbine environment will not have response time greatly reduced from these figures.

The T-1 radiation pyrometer is not directly affected by gas velocities or pressures at the turbine inlet because the sensor is not immersed in the moving gas. The maximum temperature that can be measured is easily adjustable to fit any particular application. Accuracy is dependent on a knowledge of the emissivity of the target. For a constant emissivity, the sensor may be calibrated to measure the target emperatures to within ±15°F. The sensitivity increases at higher temperatures, allowing increased accuracy.

The radiation sensor possessed extraordinary response rates. Step changes occurring in 35 microseconds were fully recorded. Due to experimental limitations in producing step changes of sufficient rapidity, the 90% response time was approximated at 20 microseconds. This response time would allow the use of turbine blades as a target. If a stationary target were used, the sensor would follow the temperature exactly with no delay time, since the thermal delay of any target is much longer than the response time of the sensor.

COMPATIBILITY WITH SMALL GAS TURBINE ENGINES

The radiation sensor appears to be the most compatible with small gas turbine engines because there is no probe immersed in the flowing gas to cause blockage or other problems associated with decreased flow area. The total weight of the sensor would be small. The amount of bleed air needed for the collimator-air lens is quite small and not likely to affect efficiency to any great extent.

A thermocouple must be immersed in the moving gas, which will cause a loss of efficiency due to gas blockage. Because a number of thermocouples is needed to measure average temperature, further loss of efficiency is encountered. Calculations showed that thermocouples applied to a 2- to 5- pound-per-second engine might cause a significant power loss. As the size of the engine increases, the loss

of efficiency decreases, allowing more probes to be placed in the gas stream. The exact effect will depend upon the design of the engine and the size of the probes.

RELIABILITY AND DURABILITY

The reliability of an exposed junction thermocouple depends upon its thermoelectric stability and mechanical integrity. The thermoelectric stability is affected mainly by contamination by the combustion products and preferential vaporization of one constituent. Tests indicated that sufficient stability can be attained from exposed Pt-Rh thermocouples, but further work must be done to provide definite data. Plastic deformation caused by loading by the moving gas is likely to occur. Overall probe design will be critical in preventing mechanical failure. Protected junctions are less susceptible to contamination and mechanical failure. A trade-off between strength and response must be made.

The reliability of the radiation pyrometer will depend on maintaining the proper ambient temperature and keeping the lens clean. Ambient temperature is limited to 250°F in the present model. The air-collimator lens was shown to be capable of maintaining a clear optical path.

ADAPTABILITY TO MULTISYSTEM FUNCTIONS

Three uses are most often proposed for the signal from the turbine inlet temperature transducer: cockpit indication, overtemperature protection, and full engine control. Overtemperature protection would, of course, be included in a closed-loop control system. A transducer can measure either the gas temperature or the temperature of some portion of the hardware. The hardware temperature may or may not accurately reflect the true gas temperature. Cooled vanes or parts of the casing with large conduction losses would not be an accurate measure of the gas temperature. A transducer that measured average gas temperature would be adaptable to dual system functions. Engine control, hardware protection, and cockpit indication could all be obtained from the same signal. Hardware temperature might not be so easily adapted to engine control due to slow response and poor correlation with the average gas temperature.

Thermocouples demonstrate time constants on the order of 100 to 200 milliseconds. In an overtemperature shutdown system, the transducer would be coupled with a relay and solenoid valve with an action delay of 30 to 45 milliseconds and additional lag in the fuel injector manifold-combustor assembly of 10 to 40 milliseconds. The total response time for the system is the sum for all of the components. The response time of the radiation sensor is several orders of magnitude faster, but the response of the transducer as a whole is limited to that of the target.

The overall adaptability of the transducer signal to dual system function will depend on exactly what temperature is measured and the relationship between the transducer response time and that of the system as a whole.

PRESENT STATUS OF PROGRAM SENSORS

The major effort needed to advance thermocouple probes to the test engine stage is one of design, fabrication, and testing. The fast-response, exposed-junction thermocouples will require testing and design work to demonstrate that this type of probe can withstand the severe conditions of the turbine inlet and provide reliable service. A research program of approximately one man-year could provide the information needed to outline the conditions under which an exposed-junction probe may be applied, and to design a probe ready for testing in a suitable engine.

A thermocouple probe employing a protected junction will be inherently more rugged and durable but will respond more slowly to temperature changes. The advancement of a materials system that will provide both reliable service and an adequate response rate will also require an effort of approximately one man-year. Such a program would include the fabrication and qualification of a grounded thermocouple junction probe in simulated atmosphere tests. Information would then be available on response rates, lifetime, and temperature capability.

Radiation sensors applied to turbine bucket temperature measurement are in an early stage of development. Major problem areas have been surmounted, but much careful design work and testing remains. The silicon detector devices are clearly superior. The problems of vibration, ambient temperature, and lens sooting have been resolved in principle. Design of the three major divisions of the sensor: the air-collimator lens; the optical system; and the detector to combine into a complete system will require a program of one-year duration. Qualification of the optimized system by simulated atmosphere testing would prepare it for application on test engines.

All three concepts require additional work before fully qualified for final testing in turbine engines. Although thermocouple technology is much older and better established than that related to photovoltaic radiation detectors, their state of preparedness for application to turbine inlet temperature measurement is approximately equal. It is very likely that the three sensor concepts found most suitable for inlet temperature measurement during this program will not be ideally suited for application under the same conditions. Gas temperature and velocity, desired lifetime, engine size, and intended utilization of the output signal will determine which transducer will be applied in a given situation. Preflight testing of engines using turbine inlet temperature measurement will occur during the early 1970's.

RECOMMENDATIONS

It is recommended that work be continued in the future on three phases of the present program: exposed junction thermocouples, protected junction thermocouples, and radiation pyrometers. Each concept offers particular advantages and problems with respect to turbine inlet temperature measurement.

An exposed junction thermocouple could be housed in several types of probes ranging from a stagnation probe, designed to slow the gas velocity and thus lessen the mechanical loads on the junction, to aspirated probes that increase the velocity and thus optimize the response. Specific data, based on tests of large numbers of thermocouples, are needed on the effect of velocity and time on the thermoelectric and mechanical stability of Pt-Rh thermocouples in a moving gas atmosphere.

Sheathed probes offer increased reliability and ruggedness. An advanced concept optimizing the temperature capabilities and response of this type of probe consists of a W-Re thermocouple junction grounded to a coated tantalum sheath. Fabrication technology must be advanced, possibly using diffusion-bonding techniques, to join the various components without embrittling the W-Re junction.

Two phases of the work on radiation sensors merit further work: optimization of the optical system including the air-collimator lens, and upgrading the ambient temperature capabilities of the detector. Possible use of fiber optics to allow the placement of the detector in a position more remote from the hot casing would be emphasized.

LITERATURE CITED

1. Bredt, J. H., ed., THERMOPHILE GENERATOR FEASIBILITY STUDY, Part II - Materials Investigations, WADD Technical Report 60-22, AD-265-599, (1960).

2. Dahl, A. I., and Flock, E. F., SHIELDED THERMOCOUPLES FOR GAS TURBINES, Transactions of the ASME, February 1949, pp. 153-161.

3. Turbush, R. K., IMPROVED SONIC PYROMETER, Temperature, Vol. 3, Part 2, Reinhold Publishing Corporation, 1962.

4. Wolfe, H. C., ed., TEMPERATURE, ITS MEASUREMENT IN SCIENCE AND INDUSTRY, Vol. II, New York, Reinhold Publishing Co., 1960.

5. PROCEEDINGS OF AN INTERNATIONAL SYMPOSIUM ON HIGH TEMPERATURE TECHNOLOGY, New York, McGraw Hill, 1959.

6. Krier, C. A., Jaffee, R.I., OXIDATION OF THE PLATINUM-GROUP METALS, Journal of the Less-Common Metals, Vol. 5, 1963, pp. 411-431.

7. Rudnitski, H. A., Tyurin I. I., NEW ALLOYS FOR HIGH TEMPERATURE THERMOCOUPLES, Russian Journal of Inorganic Chemistry, Vol. 5, No. 2, February 1960, pp. 192-196.

8. Sanders, V. D., REVIEW OF HIGH-TEMPERATURE IMMERSION THERMAL SENSING DEVICES FOR IN-FLIGHT ENGINE CONTROL, The Review of Scientific Instruments, Vol. 29, No. 11, November 1958, pp. 917-928.

9. Wimber, R. T., Stetson, A. R., DEVELOPMENT OF COATINGS FOR TANTALUM ALLOY NOZZLE VANES, Solar Division of International Harvester Company; NASA CR-54529, Fort Lewis, Cleveland, Ohio, July 67 NAS 3-7276.

10. Zysh, ed., NOBLE METALS IN THERMOMETRY-RECENT DEVELOPMENTS, Englehard Industries Inc. Technical Bulletin, Vol. V, No. 3, December 1964.

11. Walker, B. E., Ewing, C. T., Miller, R. R., THERMOELECTRIC INSTABILITY OF SOME NOBLE METAL THERMOCOUPLES AT HIGH TEMPERATURES, The Review of Scientific Instruments, Vol. 33, No. 10, October 1962, pp. 1029-1040.

12. Kostkowski, H. J., THE ACCURACY AND PRECISION OF MEASURING TEMPERATURES ABOVE 1000°K, Proceedings of an International Symposium on High Temperature Technology, New York, McGraw Hill, 1959.

13. Toenshoff, D. A., BIRD-CAGE RESISTANCE THERMOMETER, Engelhard Industries Inc. Technical Bulletin, Vol. V, No. 4, March 1965.

Unclassified

Security Classification

DOCUMENT CONTROL DATA - R & D

(Security classification of title, body of abstract and indexing annotation must be entered when the overall report is classified)

1. ORIGINATING ACTIVITY (Corporate author) Solar Division of International Harvester Company San Diego, California	2a. REPORT SECURITY CLASSIFICATION Unclassified 2b. GROUP

3. REPORT TITLE

High Temperature Sensors for Small Gas Turbines

4. DESCRIPTIVE NOTES (Type of report and inclusive dates)

Final Report, Period covered - 1 April 1966 to 7 July 1967

5. AUTHOR(S) (First name, middle initial, last name)

A. Marshall Gaylord
William A. Compton

6. REPORT DATE	7a. TOTAL NO. OF PAGES	7b. NO. OF REFS
April 1968	132	13

8a. CONTRACT OR GRANT NO	9a. ORIGINATOR'S REPORT NUMBER(S)
DA 44-177-AMC-380(T) b. PROJECT NO. c. Task 1M121401D14416 d.	USAAVLABS Technical Report 67-76 9b. OTHER REPORT NO(S) (Any other numbers that may be assigned this report) RDR 1479

10. DISTRIBUTION STATEMENT

This document has been approved for public release and sale; its distribution is unlimited.

11. SUPPLEMENTARY NOTES	12. SPONSORING MILITARY ACTIVITY
	US Army Aviation Materiel Laboratories Fort Eustis, Virginia

13. ABSTRACT

This report describes an experimental program performed to generate technology on high temperature sensor concepts for small gas turbines. Major emphasis was placed on the definition of material systems needed for transducers with long life, good reliability, and fast response for sensing turbine inlet temperatures in the range of 2200°F to 2500°F with transients to 3000°F. The technology related to three types of sensors was considered; thermocouples, resistive devices, and radiation pyrometers. Inherent material problems with resistive devices at temperatures above 1600°F limited the experimental program on this concept. Thermocouple and radiation sensors were studied extensively, resulting in several promising approaches.

Two types of thermocouple probes were found to have potential application to turbine engines. A proposed protected thermocouple junction offers best reliability and durability, but has relatively slow response to changes in gas temperature. A suggested exposed Pt-Rh junction has much improved response rate; however, the reliability and durability are much less than the protected junction.

Five commercial radiation pyrometers were evaluated and one concept chosen as having, by far, the greatest potential for application to turbine engines. The sensor employs a silicon p-n junction photovoltaic detector. The sensor demonstrated microsecond response, good accuracy, and good reliability as long as the environmental temperature for the silicon chip was kept below 250°F and the window was maintained clean. A unique air-collimator lens was devised which acts as an interface between the turbine gas path and the sensor window. An experimental air-collimator lens operating on a turbine simulator was able to keep the sensor window clean after several hours of operation.

DD FORM 1 NOV 68 1473 REPLACES DD FORM 1473, 1 JAN 64, WHICH IS OBSOLETE FOR ARMY USE.

Unclassified

Security Classification

14. KEY WORDS	LINK A		LINK B		LINK C	
	ROLE	WT	ROLE	WT	ROLE	WT
Turbine Controls						
Turbine Inlet Temperature						
Turbine Bucket Temperature						
Thermocouple						
Thermocouple Response						
Fast Response Thermocouple						
Tungsten-Rhenium Thermocouple						
Platinum-Rhodium Thermocouple						
Turbine Gas Blockage						
Total Temperature						
Static Temperature						
Radiation Sensor						
Photo Voltaic Detector						